A FINITE ELEMENT MODEL FOR THE INVESTIGATION OF SURFACE EMG SIGNALS DURING DYNAMIC CONTRACTION

by

Michelle Joubert

Submitted in partial fulfilment of the requirements for the degree

Master of Engineering (Bio-Engineering)

in the

Faculty of Engineering, the Built Environment and Information Technology

UNIVERSITY OF PRETORIA

September 2007

Summary

Title: A finite element model for the investigation of surface EMG signals during dynamic contraction
Author: Michelle Joubert
Supervisor: Prof. T. Hanekom
Co-supervisor: Prof. Dr. D. Farina
Department: Electrical, Electronic and Computer Engineering
Degree: Master of Engineering (Bio-Engineering)

A finite element (FE) model for the generation of single fiber action potentials (SFAPs) in a muscle undergoing various degrees of fiber shortening has been developed. The muscle is assumed to be fusiform with muscle fibers following a curvilinear path described by a Gaussian function. Different degrees of fiber shortening are simulated by changing the parameters of the fiber path and maintaining the volume of the muscle constant. The conductivity tensor is adapted to the muscle fiber orientation. At each point of the volume conductor, the conductivity of the muscle tissue in the direction of the fiber is larger than that in the transversal direction. Thus, the conductivity tensor changes point-by-point with fiber shortening, adapting to the fiber paths. An analytical derivation of the conductivity tensor is provided. The volume conductor is then studied with an FE approach using the analytically derived conductivity tensor (Mesin, Joubert, Hanekom, Merletti & Farina 2006).

Representative simulations of SFAPs with the muscle at different degrees of shortening are presented. It is shown that the geometrical changes in the muscle, which imply changes in the conductivity tensor, determine important variations in action potential shape, thus affecting its amplitude and frequency content.

The model is expanded to include the simulation of motor unit action potentials (MUAPs). Expanding the model was done by assigning each single fiber (SF) in the motor unit (MU) a random starting position chosen from a normal distribution. For the model 300 SFs are

included in an MU, with an innervation zone spread of 12 mm. Only spatial distribution was implemented. Conduction velocity (CV) was the same for all fibers of the MU. Representative simulations for the MUAPs with the muscle at different degrees of shortening are presented. The influence of interelectrode distance and angular displacement are also investigated as well as the influence of the inclusion of the conductivity tensor.

It has been found that the interpretation of surface electromyography during movement or joint angle change is complicated owing to geometrical artefacts i.e. the shift of the electrodes relative to the muscle fibers and also because of the changes in the conductive properties of the tissue separating the electrode from the muscle fibers. Detection systems and electrode placement should be chosen with care.

The model provides a new tool for interpreting surface electromyography (sEMG) signal features with changes in muscle geometry, as happens during dynamic contractions.

Key terms: sEMG, modelling, numerical model, FE modelling, muscle shortening, joint angle, conductivity tensor, SFAP, MUAP, ARV, MNF.

Opsomming

Titel: 'n Eindige-element-model om die invloed van dinamiese kontraksie op oppervlak-EMG-seine te ondersoek
Outeur: Michelle Joubert
Studieleier: Prof. T. Hanekom
Mede-studieleier: Prof. Dr. D. Farina
Departement: Elektriese, Elektroniese en Rekenaar-ingenieurswese
Graad: Meestersgraad in Ingenieurswese (Bio-Ingenieurswese)

'n Eindige-element- (EE) model vir die generasie van enkelvesel-aksiepotensiale (EVAPe) in 'n spier wat deur verskillende grade van verkorting beweeg, is ontwikkel. Die spier word ovaalvormig voorgestel met die spiervesels wat die ovaalvormige kurwe volg. Die kurwes van die spiervesels word deur 'n Gaussiese vergelyking voorgestel. Die verkorting van die spier word voorgestel deur die veranderlikes van die spierveselkurwe te verander terwyl die volume van die totale spier konstant gehou word. Die konduktiwiteitstensor (KT) is afhanklik van die spierveselkurwe en is groter in die rigting van bronbeweging as in die transversale rigting. Die KT is punt vir punt afhanklik van die spierveselkurwe en verander gevolglik saam met die verkorting van die spiervesel. 'n Analitiese afleiding vir die KT word gegee. Die volumegeleier (VG) word bestudeer met 'n EE-benadering terwyl daar gebruik gemaak word van die analties-afgeleide KT (Mesin, Joubert, Hanekom, Merletti & Farina 2006).

Resultate van simulasies gedoen vir EVAPe vir 'n spier wat deur verskillende grade van verkorting beweeg, word getoon. Daar is bevind dat die geometriese veranderinge in die spier, wat dan ook veranderinge in die KT voortbring, 'n belangrike invloed het op die vorm van die aksiepotensiale. Hierdie verandering in AP-vorm beïnvloed ook die amplitude en frekwensie-inhoud van die oppervlak-elektromiogram- (EMG) seine.

Die model is uitgebrei om ook die simulasie van motoreenheid-aksiepotensiale (MEAPe) in te sluit. Om die model uit te brei, is daar aan elke enkelvesel (EV) in 'n motoreenheid

(ME) 'n lukrake beginposisie toegeken. Die beginposisies word gekies vanuit 'n normale distribusie wat 'n motorpunt van 12 mm voorstel. Vir die model bestaan die MEe uit 300 EVs. Slegs ruimtelike distrubisie is gebruik. Geleidingsnelheid is dieselfde vir alle vesels in die ME. Resultate van simulasies gedoen vir MEAPe vir 'n spier wat deur verskillende grade van verkorting beweeg, word getoon. Hiermee saam word ook die invloed van interelektrode-afstand en hoekverplasing ondersoek. Die invloed van die insluiting van 'n KT word ook bespreek.

Daar is bevind dat die interpretasie van die oppervlak-EMG gedurende verkorting van die spier (soos in dinamiese gevalle) 'n komplekse dissipline is. Dit word gekompliseer deur geometriese artefakte bv. die relatiewe beweging tussen die elektrodes op die veloppervlakte en die spier onder die vel. Die verandering in konduktiwiteit van die spiervesels tydens verkorting lewer ook 'n bydrae tot die kompleksiteit van die situasie. Elektrodedeteksie-stelsels en die plasing van elektrodes moet versigtig oorweeg word.

Die model lewer 'n nuwe metode vir die interpretasie van die oppervlak-EMG tydens dinamiese kondisies.

Sleutelterme: oppervlak-EMGs, modellering, numeriese model, eindige-element model, spierverkorting, geometriese verandering, konduktiwiteitstensor, enkelvesel-aksiepotensiale, motoreenheid-aksiepotensiale, gemiddelde gelykgerigte waarde, gemiddelde frekwensie.

LIST OF ABBREVIATIONS

AP - action potential
ARV - average rectified value
AU - arbitrary units
CMAP - compound muscle action potential
CV - conduction velocity
DD - double differential
FE - finite element
IAP - intra-cellular action potential
IB^2 - inverse binomial of order two
IED - interelectrode distance
IZ - innervation zone
LDD - longitudinal double differential
LSD - longitudinal single differential
MDF - median frequency
MNF - mean frequency
MU - motor unit
MUAP - motor unit action potential
NDD - normal double differential
NMJ - neuromuscular junction
RMS - root mean square
SD - single differential
sEMG - surface electromyography
SF - single fiber
SFAP - single fiber action potential

TABLE OF CONTENTS

1. INTRODUCTION

1.1. PROBLEM STATEMENT

Surface electromyography (sEMG) is a non-invasive method to measure the electrical potential field evoked by contracting muscle fibers (Zwarts & Stegeman 2003). SEMG signals are recorded by placing electrodes on the skin interface surface over the muscle in question and recording the potentials produced as the muscle contracts. This can be done either with voluntary contractions or with electrically elicited contractions. The recorded signals are then interpreted and can be used in a number of different applications, including diagnosis of neuromuscular disorders, control of myoelectric prostheses and investigation of the myoelectric manifestation of muscle fatigue. However, interpretation of the electromyographic signal is a difficult and often ambiguous procedure. A number of factors can influence this signal, including different electrode configurations, power line interference, crosstalk from non-activated muscles and muscle morphology (Merletti & Parker 2004). SEMG modelling is used as a means to improve interpretation of electromyographic signals.

A multitude of simulation models has been developed for the study of sEMG, each model attempting to address different aspects of the sEMG problem domain. Volume conduction models form one type of sEMG model that is frequently employed to investigate the effect of the anatomy and geometry of the tissues on the propagation of the EMG signal. Volume conduction models have been developed with source functions at the single fiber (SF), motor unit (MU) and interference pattern levels. Many models attempt to investigate the influence of motor unit action potentials (MUAPs) on the interference pattern (Farina, Merletti & Fosci 2002; Griep et al. 1982; Stashuk 1999). Bottinelli et al. (1999) did an experimental study on the contribution of different fiber types to the overall contractile performance of the human muscle. An sEMG model that describes the interference pattern should consider both the firing behaviour of the action potentials (APs) and the MUAP wave shapes (Stegeman et al. 2000).

The chosen volume conductor has a significant effect on the wave shape of the MUAP. SEMG models can vary with respect to their choice of volume conductor, which is the geometrical description of the tissue separating the muscle fibers and the detecting electrodes (Mesin, Joubert, Hanekom, Merletti & Farina 2006). Models with a more complex description of the volume conductor have recently been developed using numerical methods as an alternative to the traditional analytical method (Farina, Mesin & Martina 2004).

In previous studies models mostly focused on static conditions and left questions about dynamic conditions unanswered. When a human limb is moved to such an extent that the joint angle changes, the muscle fibers will shorten (Schulte et al. 2005) and the volume conductor is geometrically modified. As a muscle fiber decreases in length, the muscle fiber diameter will increase and the fiber direction will change. These are important factors to take into account when modelling sEMG under dynamic conditions.

1.2. RESEARCH QUESTION

Valuable research has been done on modelling sEMG under static conditions and many questions have been answered. For example, it is a well known fact that the recording electrodes should not be placed directly over the innervation zone (IZ), since electromyographic (EMG) signals are small and noisy in this region (Merletti & Parker 2004). The influence of the end-of-fiber effects has also been investigated using sEMG modelling. SEMG modelling on dynamic conditions has only recently been added to the field. Geometrical changes corresponding to a change in joint angle and the subsequent fiber shortening have only been investigated in a small number of models (Farina et al. 2001; Lowery et al. 2004; Maslaac et al. 200; Schulte et al. 2004).

From the deficiencies in the understanding of the influence of joint angle on sEMG modelling the following research gap has been identified: A model is required that can predict single fiber action potentials (SFAPs) at different joint angles taking the non-space-invariance of the volume conductor into account when calculating the conductivity tensor.

1.3. HYPOTHESIS AND APPROACH

The approach followed was to create a numerical model for the generation of SFAPs in a muscle undergoing various degrees of fiber shortening. The numerical model was created using finite element software. In order to approach the simulation of dynamic conditions

the volume conductor is assumed to be fusiform and follows a curvilinear path of which the parameters are changed in order to simulate shortening of the muscle fiber. An analytically derived conductivity tensor is derived from the muscle fiber orientation and included in the model. Including non-homogeneous conductivity allows for the accurate simulation of intracellular action potential (IAP) shape change during geometrical changes i.e. joint angle changes. The model is then used to simulate SFAPs as well as MUAPs at different joint angles using different electrode detection systems.

Previous models have been designed to show the influence of geometrical changes on the frequency and spectral content of the sEMG (Clancy, Bouchard & Rancourt 2001; Farina, Merletti, Nazzaro & Caruso 2001; Maslaac, Parker, Scott, Englehart & Duffley 2001; Rainoldi et al. 2000; Schulte, Farina, Merletti, Rau & Disselhorst-Klug 2004). Few models have included a conductivity tensor to simulate the changes in the conductive properties of the muscle tissue (Farina, Mesin & Martina 2004; Mesin, Farina & Martina 2004).

The aim of the study is to investigate the influence of geometrical changes on the sEMG signal. Geometrical changes imply changes in the conductivity of the simulation model as well as changes in the relative electrode-source distance. The changes in the conductive properties of the muscle tissue are simulated by including a conductivity tensor that relates to the muscle fiber orientation. The hypothesis is that the model will show that these geometrical changes as well as the inclusion of a conductivity tensor will determine important variations in the IAP shape affecting both frequency and amplitude content.

1.4. RESEARCH CONTRIBUTION

The study of sEMG signals under dynamic conditions is becoming increasingly important. In order to understand the influence of geometrical changes because of dynamic-like contractions, a number of sEMG models have been developed (Clancy, Bouchard & Rancourt 2001; Farina, Merletti, Nazzaro & Caruso 2001; Maslaac, Parker, Scott, Englehart & Duffley 2001; Rainoldi, Nazzaro, Merletti, Farina, Caruso & Gaudenti 2000; Schulte, Farina, Merletti, Rau & Disselhorst-Klug 2004). A number of experimental procedures have also been investigated in order to relate parameter change due to dynamic contractions to the sEMG (Christensen et al. 1995; Farina et al. 2004c; Masuda et al. 1999; Potvin & Bent 1997). However, when muscle fibers shorten, their diameter increases and, as a consequence, muscle geometry changes. A fiber at a specific depth within the muscle at resting conditions may be at a larger depth when the overlaying fibers increase their

diameter. Thus in addition to changes in relative location of the tendons and end-plates with respect to the recording electrodes, the surface detected potentials are affected by variations in 1) the conductivity properties of the muscle tissue and 2) the relative electrode-source distance. The simulation of only a geometrical change in the volume conductor leads to a different effect with respect to the inclusion of variations in both geometry and conductivity tensor (Mesin, Joubert, Hanekom, Merletti & Farina 2006).

The research contribution is to create an sEMG model that simulates both variations in geometry and conductivity tensor of the resulting signal. Simulations of MUAPs from different fiber depths at different joint angles using different electrode detection configurations are carefully analysed. The resulting influence on the amplitude and spectral content of these signals is then discussed.

1.5. LAYOUT OF DISSERTATION

The objective of this study is to investigate the influence of different joint angles on the surface EMG signal. This is done by focusing on the inclusion of a complex conductivity tensor and developing a non-space invariant volume conductor with the help of finite element software. The block diagram in figure 1.1 attempts to place the research in context.

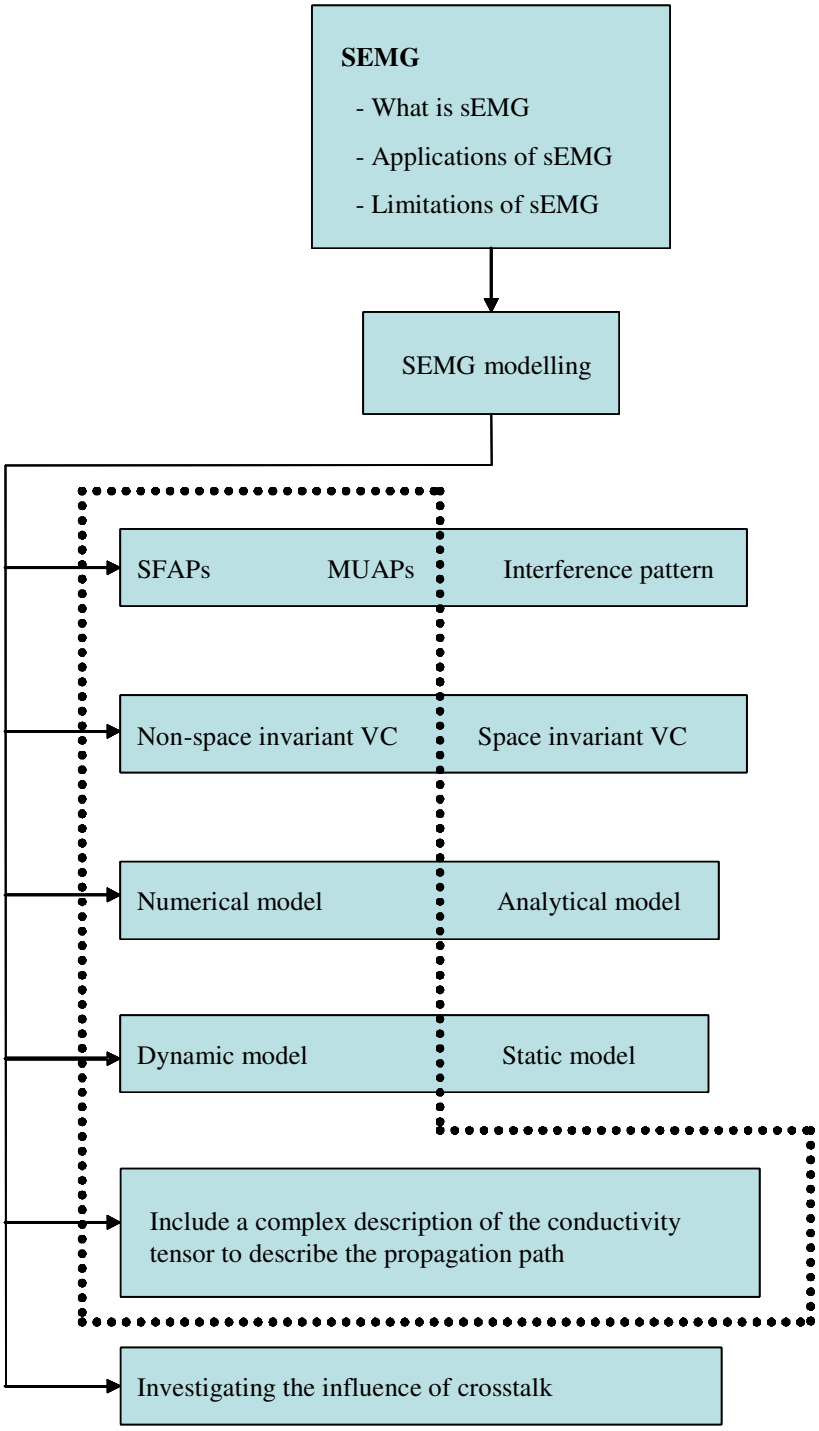

Figure 1.1. A representation of the different factors involved in sEMG modelling. The factors included in the model developed in this dissertation are indicated with the dashed block.

Chapter 2 provides an in-depth literature study in which sEMG, its applications and limitations are discussed. This chapter also includes a description of sEMG modelling, explaining the different focus points of these models, and the issues they address. Chapter

3 explains how the finite element (FE) model was developed, including descriptions of the intra-cellular source, the volume conductor and the conductivity tensor. Chapter 4 provides a summary of the results for the SFAPs obtained with the model. Chapter 5 provides results for MUAPs. Chapter 5 presents results specifically related to the amplitude and spectral changes of the MUAPs when undergoing muscle shortening. Chapter 5 also presents some results on muscle sliding. Muscle sliding is the effect of muscles shifting with respect to the skin and detection electrodes (Rainoldi, Nazzaro, Merletti, Farina, Caruso & Gaudenti 2000). Chapter 6 briefly shows the difference when including a non-homogeneous conductivity tensor as opposed to including homogeneous conductivity in the sEMG model. Chapter 7 provides a general discussion and conclusion.

2. LITERATURE STUDY

A simplistic explanation of EMG is the recording of the electrical activity of muscles, also known as myoelectric or electrophysiological activity (Devasahayam 2000). This myoelectric activity is recorded with electrodes and reflected as an electrical signal of which the amplitude, spectrum and conduction velocity are some of the well known and measurable features (Merletti, Rainoldi & Farina 2001). Myoelectric activity can be recorded using either needle or surface electrodes. SEMG is a non-invasive and inexpensive approach to obtain information about global muscle activity, whereas the use of needle electrodes is an invasive method giving more localised information about the muscle (Merletti & Parker 1994). This study will focus on sEMG. Although it is still a challenge to obtain detailed and repeatable recordings of sEMG waveforms, sEMG has the potential to offer extended insight into basic muscular function (Rau, Schulte & Disselhorst-Klug 2004). SEMG can be used in recognising and diagnosing neuromuscular disease (Wood et al. 2001; Merletti & Parker 1994), understanding the manifestation of muscle fatigue (Merletti & Parker 1994; Merletti & Parker 2004), in the control of myoelectric prostheses, biofeedback and also in occupational medicine, sport (Farina et al. 2002) and ergonomics (Merletti & Parker 1994), to mention just a few disciplines. The challenge in the interpretation of sEMG is to relate measurable variables of the recorded sEMG waveform to anatomical and physiological features of the muscle (Merletti, Rainoldi & Farina 2001).

To meet this challenge better, various sEMG signal models have been proposed in the literature (Farina, Mesin & Martina 2004; Roeleveld et al. 1997a; Kuiken et al. 2001; Farina et al. 2004b). When modelling sEMG signals, the aim is to understand the relationship between the internal physical and biological characteristics and the external information that is extracted from the signal (Duchêne & Hogrel 2000). Since sEMG has

such a large number of possible applications, a variety of sEMG models is used to answer the related questions, each model being suited to a specific type of study.

The objective of this chapter is to explain which sEMG-related issues the model developed in this study will address.

2.1. MUSCLE PHYSIOLOGY AND THE FUNCTIONAL ORGANISATION OF SKELETAL MUSCLE

Muscle covering the human skeleton, also known as skeletal muscle, has three main functions in the human body: to maintain posture, generate heat and procure movement (Marieb 1995). Since sEMG is used in areas of human movement studies and neuromuscular diagnostics, it is important to understand its origins, i.e. the process through which muscles convert chemical energy into mechanical energy to establish contraction (Stegeman, Blok, Hermens & Roeleveld 2000; Merletti & Parker 1994).

2.1.1. Muscle physiology

Muscles consist of cells called fibers. These cells have excitable membranes that maintain a steady electrical potential difference between their internal and external environment. The fiber membrane has a resting potential of approximately -70mV (Merletti & Parker 1994; Zwarts & Stegeman 2003). These muscle fibers can receive and respond to stimuli (Rattay 1990). A stimulus is a change in the fiber environment that can be caused, for example, by a neurotransmitter released by either a nerve cell or by hormones. Local change in pH could also be a stimulus. When the membrane is exited by a stimulus that exceeds the threshold potential of the membrane, the response is the transmission of an electrical current called an AP along the muscle cell membrane. The AP propagates from the generation point to both ends of the fiber simultaneously. The AP generates a current distribution in the surrounding conducting medium, known as the volume conductor, and produces detectable voltages. These voltages can be measured at locations in the volume conductor (using needle or wire electrodes), or at locations on the skin surface (using bar or disk electrodes) (Merletti & Parker 1994). The latter is known as sEMG.

Muscle fibers may differ in size, metabolism, electrical and mechanical behaviour. Muscle fiber diameter can range from 10 um to 100 um, and fiber length from a few millimeters to approximately 300 mm. Two main types of fibers can be identified. They are the fast

twitch-type (white fibers), with high strength capabilities, low fatigue resistance and large diameters, and the slow twitch-type (red fibers), with high fatigue resistance, low strength capabilities and smaller diameters. The natural recruitment order is to activate the red fibers first and, if more strength is required, the white fibers (Merletti, Rainoldi & Farina 2001; Merletti & Parker 1994). These are some of the physiological factors to consider when designing sEMG models.

2.1.2. The functional organisation of skeletal muscle

Skeletal muscle is organised into nerve-muscle functional units called MUs (Marieb 1995; Webster 1998). An MU consists of a motor neuron and all the fibers innervated by the motor neuron. The motor neuron resides in the brain or spinal cord and has long thread-like extensions called axons that establish a connection between the spinal cord and skeletal muscle. When the motor neuron's axon reaches the muscle it branches into a number of smaller axons, each of which forms an electrochemical connection with a muscle fiber. This electrochemical connection is called the neuromuscular junction (NMJ) or is also known as a motor endplate. Activating or firing the motor neuron will result in the activation of all the connected fibers, triggering a mechanical contraction. An MU typically consists of 150 muscle fibers (Marieb 1995), but can have as few as 10 and as many as 2 000 (Merletti & Parker 1994). The smallest observable muscle activity is that of a single MU. When small forces are demanded, only a few MUs will be activated. As the required force increases, more and more MUs will be activated. This is called recruitment. When all the MUs are being used, maximum force can be increased by increasing the firing rate of the MUs.

Electrical stimulation can artificially activate skeletal muscle. The response is known as a compound muscle action potential (CMAPs). A CMAP or M-wave is considered deterministic and quasi-periodic with a period determined by the stimulation frequency (Merletti & Parker 2004). Figure 2.1 is an illustration of a motor unit where a number of muscle fibers are innervated at NMJs by a single motor neuron.

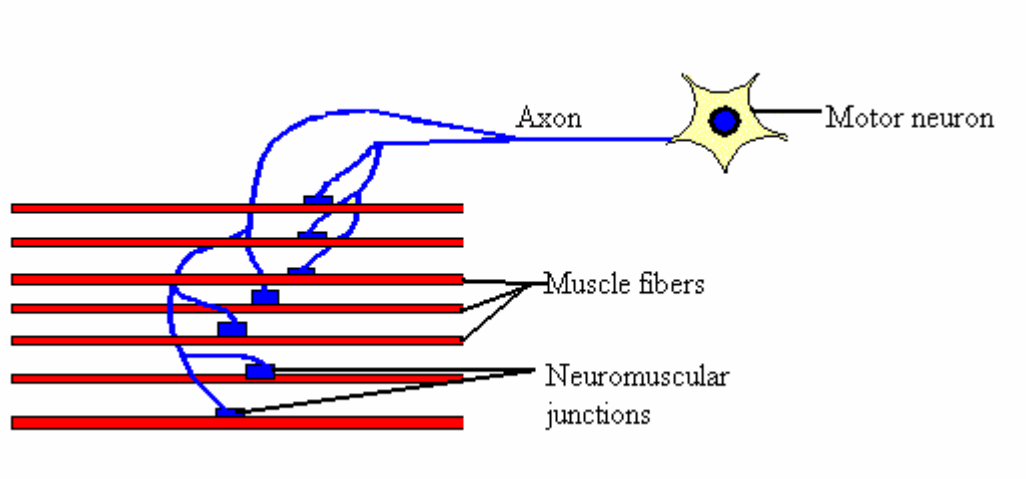

Figure 2.1 Illustration of a single motor unit. A number of muscle fibers are innervated at the NMJ by a single motor neuron

Figure 2.2 represents a longitudinal view of a number of striated muscle fibers with motor endplates (NMJs) and motor neurons.

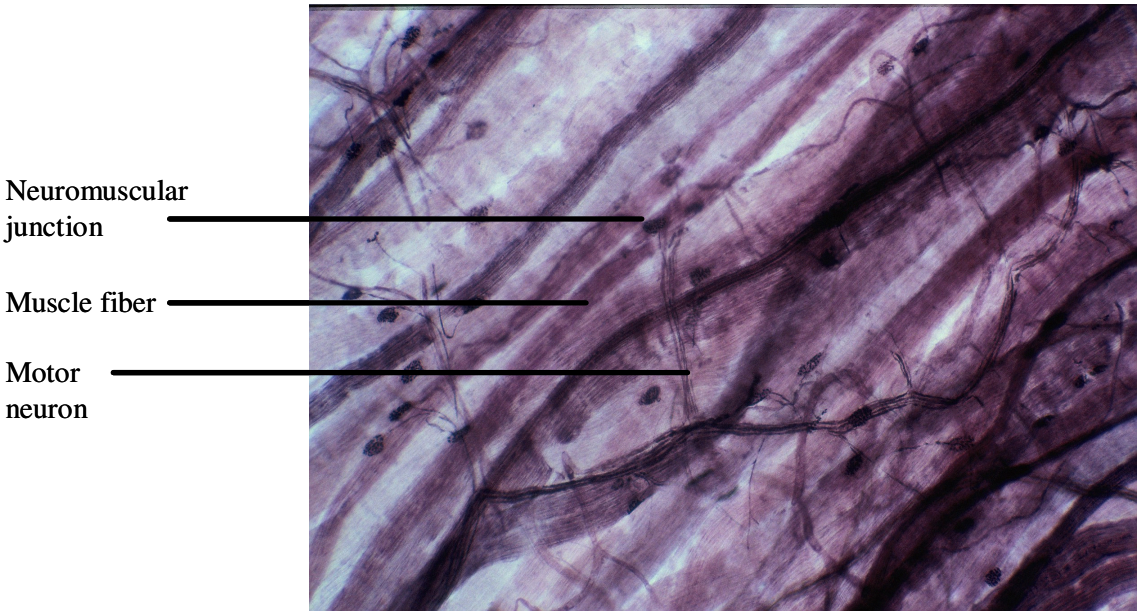

Figure 2.2. Connection of motor neurons to their respective motor units. One motor neuron will branch outwards and connect to a number of different muscle fibers, creating an MU. The motor neuron and muscle fibers connect at the NMJ (slide provided by the University of Pretoria, Faculty of veterinary science, with permission Prof. W. H. Gerneke).

SEMG waveforms are influenced by a number of physiological, geometrical and anatomical factors. It is important to understand the relationship between these factors and

the measured waveform. As mentioned before, sEMG modelling is used in order to understand this relationship better. Some of the more important anatomical factors to consider are:

- muscle fiber conduction velocity,
- number of MUs in the muscle,
- number of fibers in an MU, and
- size and the histological type of the fibers.

When recording sEMG waveforms the following geometrical factors are important (Merletti, Rainoldi & Farina 2001; Duchêne & Hogrel 2000):

- electrode size, shape and interelectrode distance (IED),
- electrode location with respect to the NMJs,
- thickness of the skin and subcutaneous layers, and
- misalignment between muscle fibers and electrodes.

2.2. CHOICE AND IMPLICATION OF ELECTRODE CONFIGURATION

EMG signals can be measured either internally or on the body surface. The invasive measurement of EMG signals can be done with percutaneous needle electrodes or with stainless steel fine wire electrodes (Merletti & Parker 1994; Perry, Schmidt & Antonelli 1981). Invasive EMG measurement is used to monitor the potentials generated by fibers belonging to different MUs. Because of the small surface area of the electrode, this type of EMG measurement provides local information with good morphological details. Another advantage of internal electrodes is that they do not have to contend with the electrolyte-skin interface and its associated limitations (Webster 1998). With needle detection, contributions from the different MUs can be separated and identified. Different shapes of the MUAP can also be recognised. Most of the power contained in needle-detected signals is in the 10 - 1 000 Hz frequency band (Webster 1998). Because the needle electrodes provide EMG signals from which the different MUAP shapes can be identified, they are used for diagnosing neuromuscular disease that modifies the morphology of the MUAP. Information gathered from needle and wire electrodes is different from the information detected with surface electrodes.

One of the most pronounced differences between needle and surface EMG is the low pass filtering effect that surface electrodes have on the EMG waveform. This effect is due to the

tissue layers separating the electrodes from the bioelectric source (muscle fibers) (Farina, Merletti, Indino, Nazzaro & Pozzo 2002).

Most of the power from surface-detected signals falls below 400 Hz (Devasahayam 2000; De Luca 2002). The choice and placement of the electrode detection system for sEMG is a geometrical factor that has a significant influence on the sEMG waveform. Misalignment of electrodes and muscle fibers can lead to misinterpretation and inconsistencies in the detection of signal amplitude and spectral features (Devasahayam 2000). When recording sEMG the following factors relating to the electrodes are important: geometry, size, IED, electrode location and choice of detection system (Merletti & Parker 2004).

Geometry and size

Discs, bars or rectangular-shaped electrodes can be used (Merletti 2004). For a linear array of equally spaced electrodes, silver bar electrodes 1 mm wide and 5 mm long with 10 mm interelectrode spacing are used (Merletti & Parker 1994). The IED can differ from 2-10 mm, depending on whether small (e.g., hand and face) or large (e.g., back) muscles are measured. For a single pair of electrodes, disk electrodes measuring 3-10 mm in diameter are used. However, the choices of geometry and size are directly related to the muscles under investigation, for example, when doing speech research involving the facial muscles, small electrodes are needed with firm fixation of the electrode onto the skin surface. The size of the conductive area of the electrode will have an influence on the amplitude and the spectral components of the EMG signal (Lapatki, Stegeman & Jonas 2004). Smaller electrode surfaces lead to a higher noise level. Larger electrode surfaces will have a smoothing effect on the signal because of the averaging of the potentials (De Luca 2002).

Interelectrode distance

IED is the distance between two electrodes, and is usually chosen between 2 and 10 mm. IED is directly related to the detection volume. If the IED is too large, non-travelling components generated at the innervation and tendon zones will have a greater influence on the EMG waveform (Merletti et al. 1999a). Non-travelling components are high-frequency components that have no relation to the propagating part of the EMG signal. An increase in IED leads to an increase in the number of high-frequency components included in the resultant signal, this may also lead to an overestimation of the conduction velocity (CV) (Merletti, Lo Conte, Avignone & Guglielminotti 1999a; De Luca 2002).

Electrode location

The IZ of a muscle fiber is that part of the fiber where the motor neuron innervates the fiber and an AP is generated. This AP will then travel along the muscle fiber until it reaches the tendon zone and becomes extinct. As the muscle fibers approach the tendon ending, they become fewer in number and thinner (De Luca 2002). Electrodes placed over either the innervation or tendon zones will read small, noisy signals, and will also be highly susceptible to small shifts in electrode location.

When locating the electrode detection system, it should be placed between the innervation and tendon zones. Also, electrodes for surface EMG detection should be placed in the direction of the muscle fibers. Misalignment will lead to over- or under-estimation of amplitude values, spectral information and conduction velocity. Proper alignment is characterised by a symmetric waveform pattern of the AP propagating in two directions between the innervation and tendon zones.

The IZ differs for each person and for each muscle. When an electrode array of 16 bar electrodes is used, they are spaced from one tendon junction to the other, and will include the IZ. If the average values are recorded at different placements of the muscle, and normalised with respect to the largest value, the movement of the IZ can be seen. The average value detected by the electrode situated over the IZ will have a minimum in signal amplitude and phase reversal (Merletti, Farina & Gazzoni 2002), reading small and noisy signals as opposed to the electrodes placed between the tendons and the IZ. Linear electrode arrays can be used for the analysis of the sensitivity of EMG features to electrode placement, and can lead to the standardisation of proceedings related to EMG recording (Merletti, Farina & Gazzoni 2002).

Different detection systems

Conventional bipolar sEMG allows statements about the compound activity of a large number of MUs. Spatial selectivity can be improved by using different spatial filters, allowing for the detection of single MU activity. If the IEDs are small enough, the potentials detected by the electrodes can be regarded as samples containing the complete information for a correct reconstruction of the potential distribution (Disselhorst-Klug, Silny & Rau 1997).

Monopolar detection allows for a single electrode placed over the muscle in question and a reference electrode placed over an electrically unrelated location. Monopolar detection gives global information about superimposed EMG activity. Because of the large detection volume, crosstalk and power-line interference may decrease the fidelity of the signal (Merletti & Parker 1994; Merletti & Parker 2004). The distance between the source and the detection point is also significant, since the tissue separating the source from the electrode has a spatial low-pass filtering effect (Merletti & Parker 2004).

Bipolar or single differential (SD) detection is performed when a differential amplifier is used to detect signals present between two points on the same muscle. The resulting surface signal is a linear combination of the signals recorded from different electrodes. This is the simplest form of spatial filter, and partially compensates for the above-mentioned low-pass filtering effect. Signals detected in the double differential (DD) mode are generated in a local volume smaller than for monopolar or SD detection, leading to better attenuation of the non-travelling components. The DD filter is usually used to estimate muscle fiber conduction velocity (MFCV) because of the greater sharpness in detecting CV differences. Two-dimensional filters like the Laplacian filter can also be used to improve selectivity (Disselhorst-Klug, Silny & Rau 1997). Linear surface electrode arrays provide useful geometric information about individual MUs. Figure 2.3 is a representation of the single and double differential electrode configurations. The weighing factors or filter mask of each configuration is also presented, with each electrode in an electrode array corresponding to a certain weight in the resultant EMG signal (Disselhorst-Klug, Silny & Rau 1997; Merletti & Parker 1994; Devasahayam 2000; Farina, Cescon & Merletti 2002).

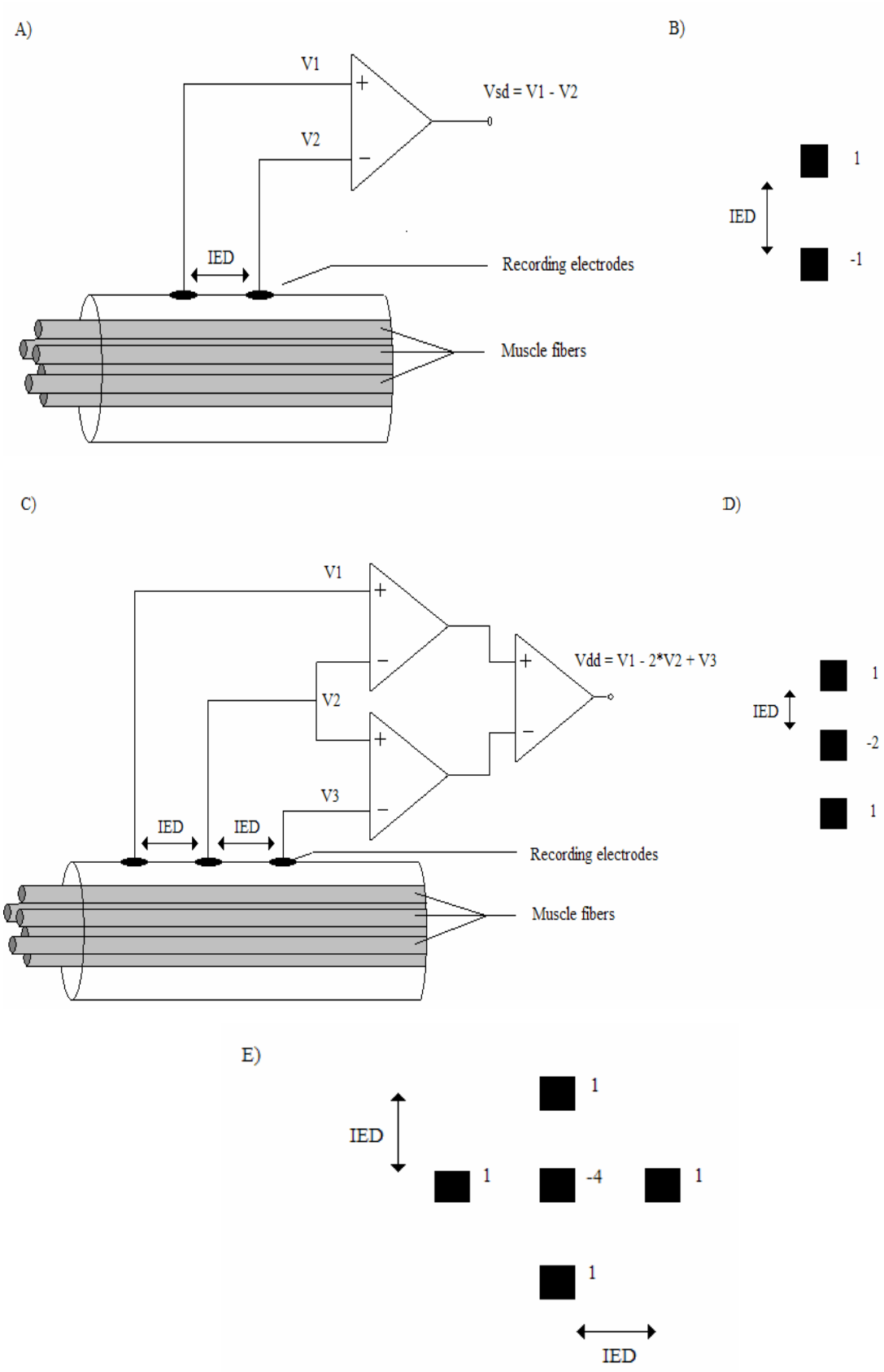

Figure 2.3 Schematic representations of three different electrode configurations. Figure 2.3.A represents the SD configuration and B the corresponding filter mask. Figure 2.3.C represents the DD configuration and D the filter mask. Figure 2.3.E is the filter mask for the Laplacian electrode configuration.

2.3. SEMG WAVEFORMS AND PARAMETERS

A single muscle fiber will, when activated, produce an intracellular action potential (IAP). The potential recorded from a single MU is a combination of the APs from all the muscle fibers. The sEMG signal is the summation of the contributions of all the active MUs within the muscle under investigation (Merletti, Farina & Gazzoni 2002). An sEMG signal can be obtained either by voluntary contraction of the muscles or by electrical stimulation of the muscle fibers. With voluntary contraction, the resulting amplitude of the sEMG signal is stochastic (random), and with evoked contraction, the signal is deterministic (Merletti & Parker 1994). The amplitude of the sEMG waveform is in the region of 10 to 500 uV_{rms} (Webster 1998; Rainoldi, Nazzaro, Merletti, Farina, Caruso & Gaudenti 2000; Merletti, Rainoldi & Farina 2001). The usable energy of the signal is limited to the 10 to 400 Hz-frequency range, with the mean frequency or dominant energy between 70 and 130 Hz (Webster 1998; Rainoldi, Nazzaro, Merletti, Farina, Caruso & Gaudenti 2000). The median frequency is between 50 and 110 Hz. The median frequency is the frequency that splits the spectrum into equal parts containing equal power.

The main measurable variables of an sEMG signal are the amplitude, the spectrum and the CV. These variables are influenced by geometrical, anatomical and physiological factors. Geometrical and anatomical factors include electrode size, electrode shape and IED, electrode placement, skin thickness and subcutaneous layers, and misalignment between muscle fibers and electrodes. Physiological factors include muscle fiber CV as a global average, statistical distribution of muscle fiber conduction velocity, number of MU, number of fibers, fiber size and histological type of each motor unit, blood flow and temperature, rate of metabolic production, intramuscular pH, ion concentration, shifts across muscle cell membrane, and type and level of contraction (Merletti, Rainoldi & Farina 2001; Merletti & Parker 2004).

It is evident that an sEMG signal contains information about many physical and physiological factors whose contributions to the signal are not easily separated. It is important to understand the influence of these anatomical, geometrical and physiological factors on the measurable parameters of the sEMG waveform.

2.3.1. SEMG Amplitude

The amplitude of the EMG signal is related to the force output of the muscle. The force output of the muscle is related to the number of active MUs as well as to the firing rate of

the MUs (Devasahayam 2000). If greater force is required more MUs will be recruited. If all the MUs are active the firing rate will increase to a higher force level. The amplitude of the sEMG signal is stochastic or random, and can be represented by a Gaussian distribution function. The peak-to-peak value of the amplitude is between 0 and 10 mV relating to the root mean square (RMS) value as 0 – 1.5 mV (De Luca 2002).

The following factors can have an influence on sEMG signal-amplitude:

- IED: for larger IED more high-frequency non-propagating components will have a greater influence on the sEMG waveform. For larger IED the amplitude will increase (Farina, Cescon & Merletti 2002).
- Thickness of subcutaneous layers: tissue separating the electrodes from the bioelectric source (muscle fiber) acts as a low-pass filter. As the thickness increases the amplitude will decrease (Farina, Cescon & Merletti 2002).
- Location of electrodes: if electrodes are placed near the innervation or tendon zones, smaller amplitude values will be detected (Merletti et al. 1999b).
- Size of electrodes: larger electrodes will reduce the amplitude. This is because the detected potential equals to the average of the potential distribution under the electrode area on the skin (Farina, Cescon & Merletti 2002; Merletti, Rainoldi & Farina 2001).
- Fiber-electrode misalignment: this can cause either over- or underestimation of amplitude values.
- The amount of muscle shortening and sliding under electrodes: When a high contraction level is reached, there is a large change of muscle shape and a compression of subcutaneous layers, which gives rise to an amplitude change (Farina & Merletti 2000).

When working with the amplitude of an sEMG signal, either the average rectified value (ARV) or the root mean square value (RMS) is computed. Equations 2.1 and 2.2 define these values:

$$ARV = \frac{1}{N}\sum_{i=1}^{N}|x_i| \qquad (2.1)$$

$$RMS = \sqrt{\frac{1}{N}\sum_{i=1}^{N} x_i^{\,2}} \qquad (2.2)$$

with x_i being the signal samples and N the number of samples considered in one time epoch.

One of the driving forces behind the development of sEMG amplitude estimation algorithms have been myoelectrically controlled upper-limb prosthetics. In this application sEMG signals from remnant muscles are used to control the prosthesis. In order to control the prosthesis successfully, input signals from two remnant muscles are monitored. The difference in amplitude between these two muscles are then determined. For example, if this difference is positive, extension could occur i.e. the hand opens. In the other case, if the difference is negative, flexion occurs and the hand closes (Merletti & Parker 2004).

2.3.2. Spectral features

Spectral features relate to the power spectrum of the sEMG signal and are important estimators in the observation of biochemical muscle fatigue. During a sustained contraction the observed spectral content will shift towards the lower frequency range. Since the shape of the spectrum does not change, this phenomenon is described as compression of the spectrum. The variables obtained from the sEMG signal are not related to any one physiological reason, but are sensitive to many. For this reason the shift towards lower frequencies does not reflect one physiological explanation but rather a combination of many. Examples of these physiological effects include MU firing rates having an influence on the low-frequency region of the sEMG power spectrum, IAP shape changes over time as well as MU recruitment (Merletti & Parker 2004). The power of the sEMG signal is contained in a frequency range of 5 to 500 Hz, with the dominant energy between 50 and 150 Hz (De Luca 2002; Merletti 2004).

The spectral variables commonly used are the mean and the median frequencies (MNF and MDF). They are defined by Equations 2.3 and 2.4:

$$f_{mean} = \frac{\sum_{i=1}^{M} f_i P_i}{\sum_{i-1}^{M} P_i} \qquad (2.3)$$

$$\sum_{i=1}^{f_{med}} P_i = \frac{1}{2}\sum_{i=1}^{M} P_i \qquad (2.4)$$

where P_i is the ith line of the power spectrum and M is the highest harmonic considered (Farina, Mesin & Martina 2004). These two variables provide basic information about the spectrum of the sEMG signal.

The MDF refers to the frequency value that splits the spectrum into two parts containing equal power (Farina & Merletti 2000). The MDF and MNF will coincide if the spectrum is symmetric with respect to its centre line and will be different if the spectrum is skew.

Spectral measurements are strongly influenced by electrode location, thickness of subcutaneous layers, fiber misalignment, the depth of the source within the muscle, fiber length, the spatial filter used, electrode size and shape and IED. The following observations can be made:

- IED: a change in IED will change the spatial transfer function of the detection system and affect the signal properties. For larger IED more high-frequency non-propagating components will be included in the computation of the mean frequency.
- Thickness of subcutaneous layers: since the subcutaneous layers separating the electrodes from the muscle fibers act as a low-pass filter, MNF will decrease with increasing thickness. This is also true for the dept of the MU within the muscle. The MNF for a deeper MU will be subject to a stronger low-pass filter effect (Farina, Cescon & Merletti 2002; Merletti & Parker 2004).
- Location of electrodes: frequency content is highest near the innervation and tendon zones, and decreases with distance from these zones. This is again because of the influence of high-frequency non-propagating components (Merletti, Lo Conte, Avignone & Guglielminotti 1999a; Roy, De Luca & Schneider 1986).
- Fiber-electrode misalignment: the effect of the inclination of the muscle fibers with respect to the detection system is difficult to predict. This effect is also dependent on electrode size and shape, as well as which detection system is used.
- Spatial filter: the spatial filter used determines the attenuation of the end-of-fiber component. At the same time it also acts as a high-pass filter for the travelling

components. When high selective spatial filters are used, the frequency content is increased (Merletti & Parker 2004).

Observation of spectral content can be used in sports training. A subject can learn how to control optimal endurance muscle activity through real-time feedback of the frequency shift during sustained contraction (Devasahayam 2000). However, most research on the spectral analysis of the sEMG signal is towards the study of muscle fatigue. Muscle fatigue in itself is not a variable associated with the sEMG signal and its assessment requires the definition of indexes based on physical variables that can be measured, such as firing rates, conduction velocity, amplitude or spectral estimates.

2.3.3. Conduction velocity

The CV of a fiber is an indication of the muscle's functional state. CV is between 3 and 6 m/s, with an average of almost 4 m/s. To measure CV the variables needed are the IED and the delay between two detected signals. The two signals need to be identical and time-shifted. That means there has to be such a degree of similarity between the two signals that an applied time-shift will minimise the mean square error of the one signal with the other (Farina & Merletti 2000). For sEMG detection of CV, either the cross-correlation function or the linear system impulse response has to be used. When these approaches are used, there is a confounding factor to keep in mind. In the signals obtained, coherent nondelayed EMG components are present. This is because of the termination of fibers at the tendon-endings. This effect will give rise to a positive bias in the conduction velocity estimate, and can be reduced by using the DD electrode configuration (Merletti, Roy, Kupa, Roatta & Granata 1999b; Merletti & Parker 2004; Merletti & Parker 1994).

An important fact to remember when calculating the CV is that the electrodes have to be aligned with the muscle fibers; misalignment will lead to electrical noise caused by shape changes to the IAP as well as influences from the non-travelling components (Merletti, Rainoldi & Farina 2001). This is more apparent in anisotropic systems where the anisotropy has a significant effect on the shape of the detected IAPs.

2.4. APPLICATIONS OF SEMG

In the past decade needle EMG has been seen as the more reliable diagnostic tool. However, sEMG has been studied extensively, and now shows considerable potential as a diagnostic tool in human movement studies, neuromuscular disease, clinical neurophysiology and electrodiagnostic medicine (Stegeman, Blok, Hermens & Roeleveld 2000). SEMG is a non-invasive, inexpensive application giving global information about muscle physiology and can be used separately or complementary to needle EMG (Zwarts, Drost & Stegeman 2000; Perry, Schmidt & Antonelli 1981). SEMG is convincingly used in the kinesiological disciplines, which include rehabilitation science, ergonomics, exercise and sports physiology (Stegeman, Blok, Hermens & Roeleveld 2000). In addition sEMG provides an application with which to measure MU location, direction of muscle fibers, endplate position and fiber-tendon transition and is successfully used in the following applications:

Myoelectric manifestation of muscle fatigue

Investigating the myoelectric manifestation of muscle fatigue is important in sport, rehabilitation and occupational medicine. It is also useful in the analysis of back muscle impairment to solve back problems and lower back pain (Merletti & Parker 1994). Muscle fatigue produces changes in the characteristics of the sEMG signal (Dimitrova & Dimitrov 2003). After a prolonged isometric contraction, changes in muscle fiber membrane excitability and in MUAP propagation are detected. If the contraction is maintained, the muscle metabolic conditions are altered, and if conditions are still maintained, this will lead to failure of excitation-contraction coupling. This is called mechanical failure (Merletti, Rainoldi & Farina 2001). Muscle fatigue can be measured with sEMG and is characterised by a decrease in CV and spectral variables and an increase in amplitude (Stegeman, Blok, Hermens & Roeleveld 2000; De Luca 2002; Merletti, Rainoldi & Farina 2001; Zwarts, Drost & Stegeman 2000; Zwarts & Stegeman 2003; Roeleveld, Blok, Stegeman & Van Oosterom 1997a). Muscle fatigue is easier to detect when contractions are electrically elicited. This implies that the detected signal will be deterministic and not stochastic.

Estimation of fiber type distribution

Determining fiber types within a muscle is usually investigated with histochemical analysis or biopsies. The high cost and ethical problems related to this technique of fiber typing is an excellent reason for exploring non-invasive sEMG as a method for fiber typing. As

mentioned before, muscles consist of two types of fibers. Type 2 fibers have a higher CV, which will decrease faster during sustained contraction. CV and the spectral features of sEMG are good variables to use for fiber typing. They are related to the pH decrease due to the increment of metabolites produced during fatiguing contractions (Merletti & Parker 2004). Although more research is needed sEMG can be used as a non-invasive tool for fiber typing (Merletti, Rainoldi & Farina 2001; Merletti & Lo Conte 1997). This information is important in sport and geriatric medicine (Merletti et al. 2002), as well as where fiber type modifications due to diseases or natural adaptation are encountered (Merletti & Parker 2004).

Measurement of changes induced by training, disuse and aging

Amplitude measurement in sEMG is a reliable variable to use when observing changes in force output before and after a training session. Changes in the size of MUs are also reflected in amplitude measurements and can reveal loss of muscle fiber or reinnervation. The onset of atrophy with aging can also be observed (Merletti, Rainoldi & Farina 2001; Zwarts & Stegeman 2003; Merletti, Farina, Gazzoni & Schieroni 2002).

Biofeedback

The onset of muscle fatigue is characterised by a shift in frequency of the sEMG signal. This is due to various physiological effects. Allowing for real-time feedback, it should be possible to control muscle force at optimal endurance by stabilising the frequency of the contraction. This allows for the possible enhancing of the voluntary control of muscles.

Gait analysis and muscle activation intervals

With sEMG, complicated movement patterns can be observed. The activation of different muscle groups during gait analysis can be observed. This information is very useful in movement disorders such as dystonia and tremor (Zwarts, Drost & Stegeman 2000; De Luca 2002; Stegeman, Blok, Hermens & Roeleveld 2000; Zwarts & Stegeman 2003). The relevance of sEMG in kinesiology applications also includes the study of motor control strategies, the investigation of the mechanics of muscle contraction and the identification of pathophysiological factors (Merletti & Parker 2004).

Myopathies characterised by membrane disturbances

Abnormal muscle fiber CV is indicative of myopathies characterised by membrane disturbances. These disturbances occur because of functional disturbances in the ionic

channels (Stegeman, Blok, Hermens & Roeleveld 2000; Zwarts, Drost & Stegeman 2000; Zwarts & Stegeman 2003).

Control of myoelectric prosthesis

The motors of artificial limbs (hands, wrists, elbows) may be controlled by sEMG signals detected from muscles above the level of amputation (Merletti & Parker 1994).

Occupational medicine and ergonomics

SEMG is used in ergonomic studies to evaluate how workplace factors such as tasks, posture, tool design and layout influence the activity of a set of muscles (Merletti & Parker 1994).

2.5. LIMITATIONS OF SEMG

Despite increasingly complex sEMG array designs, sEMG still presents some limitations. SEMG is limited to signal detection of superficial muscles with parallel fibers. Some other limitations are:

- SEMG is not particularly successful when measured for muscles with pennated fiber architecture or curved fibers or when multiple IZs are measured (Zwarts, Drost & Stegeman 2000).
- SEMG detection is sensitive to crosstalk. Crosstalk refers to interference from muscles other than those containing the electrodes.
- SEMG is also sensitive to other artefacts, for example artefacts due to relative movement between the electrodes and the skin, or artefacts due to changes in electrode contact impedance (Merletti & Parker 1994).
- The different design consideration for electrodes can lead to amplitude and spectral variance in the recording of sEMG signals.
- Tissue filtering attenuates the shape differences of the sEMG signals. Morphological features have a smaller relevance as classification criteria (De la Barrera & Milner 1994).

Geometrical factors also have some relevance when evaluating the success of sEMG measurements. When working under dynamic conditions, the muscles in question will shift with respect to the skin. This will cause an amplitude change, which can be attributed to geometrical reasons and not to a different level of muscle activation. This change in amplitude is mostly because IZ shifts with respect to the skin surface. Little movement of

the IZ will provide great amplitude differences in electrodes placed near the IZ. A 1 cm shift can cause an increase in amplitude of up to 200%, and a 90° change in angle can cause a 50% change in amplitude (Martin & MacIsaac 2006). Differences caused by geometrical factors have to be evaluated. The standard deviation of the measured ARV values is an indication of residual error and defines the resolution one can reach in the evaluation of geometrical factors. Differences in amplitude can only be attributed to geometrical factors if they are sufficiently larger than the resolution defined by the standard deviation (Merletti, Farina & Gazzoni 2002).

2.6. SEMG MODELLING

The most significant reason for sEMG modelling is to establish an approach through which muscle properties can be related to the measurable variables of the sEMG signal (Merletti, Lo Conte, Avignone & Guglielminotti 1999a; Farina, Mesin & Martina 2004; Stegeman, Blok, Hermens & Roeleveld 2000; Farina, Merletti, Nazzaro & Caruso 2001; Rau, Schulte & Disselhorst-Klug 2004). Signal modelling is also important for understanding the bio-electric signal generation mechanism, for the testing of processing algorithms, for detection system design and for the teaching of muscle electrophysiology (Merletti, Lo Conte, Avignone & Guglielminotti 1999a; Farina, Mesin & Martina 2004). Since sEMG attempts to answer a number of different questions related to muscle properties, neuromuscular disorders or even to the control of myoelectric prosthesis, sEMG models are being developed with increasing complexity and accuracy (Farina, Mesin & Martina 2004). A great number of analytical models are found in literature and more recently also a variety of numerical models. Recent numerical models were developed by Lowery, Stoykov, Dewald and Kuiken (2004), Schneider, Silny and Rau (1991), Kuiken, Stoykov, Popovic, Lowery and Taflove (2001) and Lowery et al. (2002).

SEMG models range from models predicting the behaviour of single muscle fibers to models producing complete EMG waveform simulations. Different designs of the volume conductor are used, ranging from infinite flat planes to cylindrical designs. The recent addition of numerical modelling resulted in more complex volume conductor designs (Kuiken, Stoykov, Popovic, Lowery & Taflove 2001; Mesin, Farina & Martina 2004). The electrode detection system has also been redesigned a number of times, leading to a number of different models. The basic building blocks of sEMG modelling comprise the source function, the volume conductor and the electrode detection system. Further model characteristics such as fiber type, number of fibers, tendon and endplate distribution,

subcutaneous layers, recruitment and MU firing rate, to name only a few, can further complicate and enhance sEMG models (Stegeman, Blok, Hermens & Roeleveld 2000).

Generally, sEMG models have been developed for testing sEMG under static isometric conditions. However, some clinical evaluations, for example gait analysis, can be understood better if dynamic conditions are incorporated. Recent models have begun to focus on modelling muscle contractions at different joint angles. This is already a step closer to dynamic sEMG modelling. When including muscle shortening in an sEMG model, consideration should be given to geometrical artefacts, for example geometrical modification of muscle due to fiber shortening and the effect of muscle sliding under the skin (Farina, Merletti, Nazzaro & Caruso 2001; Schulte, Farina, Merletti, Rau & Disselhorst-Klug 2004).

This section will explain the different building blocks and characteristics of the sEMG model. Figure 2.4 is a representation of the possible elements of an sEMG model (Stegeman, Blok, Hermens & Roeleveld 2000). The model developed in this study includes some but not all of these building blocks. The black line represents the blocks included in this study.

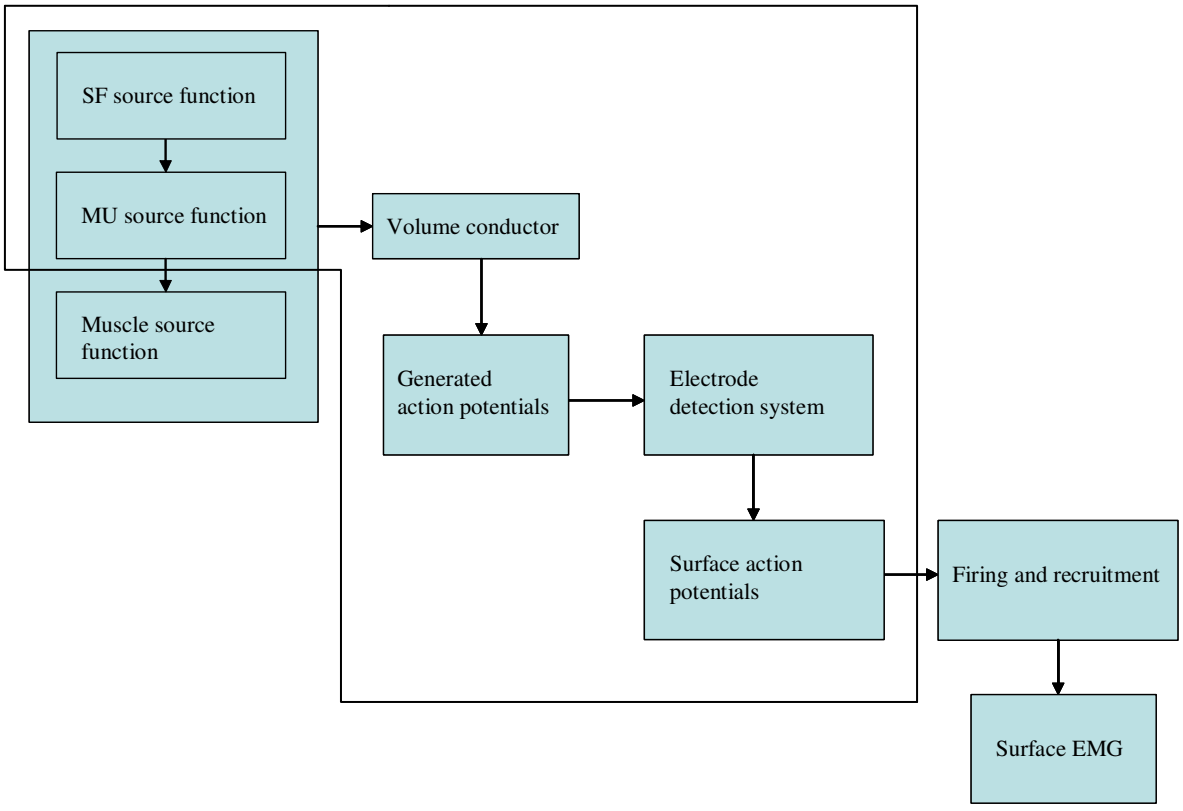

Figure 2.4. Schematic representation of the possible elements of an sEMG model

Each of the elements in figure 2.4 has a number of different design considerations that relate directly to the type of questions the model under consideration will attempt to answer.

2.6.1. Source function

The bio-electric source of all neuromuscular activity is found in the outer membrane of a single muscle fiber. In order to find a definition for the source contained in a single fiber two assumptions are made. The first assumption implies that the measured potential field is the linear summation of the potential fields of the contributing muscle fibers. The second assumption implies that from an sEMG point of view each muscle fiber can be considered as a line source, thus neglecting its diameter. These two assumptions imply that describing the IAP wave shape suffices as a source definition (Stegeman, Blok, Hermens & Roeleveld 2000). Equation 2.5, along with its derivative, is a mathematical description often used for describing the IAP wave shape.

$$Vm(z) = Az^3 e^{-\lambda z} - B \tag{2.5}$$

V_m is the membrane voltage and z the distance along the fiber. Parameters A, B and λ are responsible for the shape of the IAP. Common values are A = 96 mV for the amplitude of the action potential and B = -90 mV for the resting membrane potential. λ is a scale factor expressed in mm^{-1} , z is the length along the muscle fiber. The membrane current distribution shown in Equation 2.5 has a triphasic shape and can be simplified to a tripole source description, which becomes valid for sufficiently large observation distances. To approximate the tripole, each region of the current source is collapsed into a single equivalent point source, the sum of which is zero. It is important to know that the tripole length and intensities are not independent variables and must guarantee physiological values for the transmembrane action potential amplitude. Thus, if it is assumed that each active muscle fiber is rectilinear with uniform properties along its length, two tripoles travelling in the opposite direction can be used as a legitimite source function for generating measurable action potentials (Merletti, Lo Conte, Avignone & Guglielminotti 1999a; Stegeman, Blok, Hermens & Roeleveld 2000; Farina & Merletti 2001; Rosenfalck 1969). The triangular IAP estimate and the connected tripoles are shown in figure 2.5.

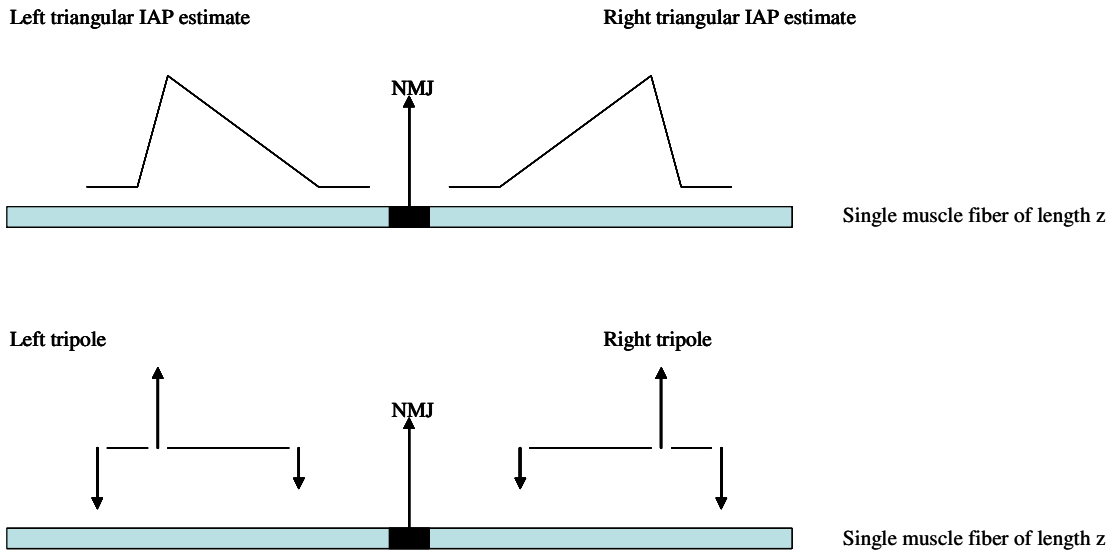

Figure 2.5. The triangular estimate of the IAP and the corresponding tripole

Another important consideration in describing the source function is the generation and extinction of the AP at the NMJ or motor endplate and at the tendon endings. It has to be taken into account that with extinction the tripole becomes a dipole and finally a monopole. These effects greatly influence the sEMG signal.

There are sEMG models that only focus on SFAP generation. Muscle fatigue has often been investigated on this level, resulting in a finding that prolonged repetitive stimulation of muscle fibers leads to a decrease in CV (Rau, Schulte & Disselhorst-Klug 2004). However, it is necessary also to have a description of the collective activity of muscle fibers in an MU. An MU can be modelled by superimposing *N* single fibers. SEMG models at this level are different from one another with regard to the variations of fiber properties they incorporate. Some of the possible variations in properties of single fibers included in an MU are the following (Merletti, Lo Conte, Avignone & Guglielminotti 1999a; Stegeman, Blok, Hermens & Roeleveld 2000):

- Distribution of motor endplates and of tendon endings. Used in models investigating neuromuscular disease, optimal electrode placement, size of MUs and crosstalk.
- Different CVs. Used in models investigating neuromuscular disease, size of MUs, the calculation of CV from the sEMG interference pattern and muscle fatigue.
- Different fiber types. Used in models investigating questions on the influence of muscle composition.

- Relative position of muscle fiber within an MU. Used in models investigating the position in the muscle from where sEMG signals originate.
- Number of fibers in an MU. Used in models investigating neuromuscular disease, the number of active MUs for a specific task, muscle forces, positions of tendon endings and motor endplates.

It can be seen that studies performed at the MU level provide valuable information on neuromuscular disorders and also on muscle physiology. SEMG is commonly used in applications in biomechanics, ergonomics and rehabilitation (Rau, Schulte & Disselhorst-Klug 2004). It is valuable to understand how the sEMG interference pattern is generated.

The modelled surface signal is the superposition of the contributions from *M* MUs (Rau, Disselhorst-Klug & Silny 1997). As with the transition from SFs to MUs, there are also a number of variations that can be included in a model of sEMG generation. These include:

- Number of MUs. Used in models investigating how many MUs are active in a specific task, influence of muscle composition, muscle fatigue and which central drive changes can be estimated from the sEMG.
- MU radius. Useful in investigating neuromuscular disorders.
- MU location. Used in models investigating muscle force, sEMG origination, neuromuscular disorders and the influence of muscle composition.
- Distribution of motor endplates and of tendon endings of the MU. Used in models investigating how many MUs are active for a specific task.
- CV. Used in models investigating muscle fatigue, calculating CV from an interference pattern and the influence of muscle composition.
- Force prediction per MU. Used in models investigating muscle force prediction.

When considering the sEMG interference pattern an important aspect to include in the modelling thereof is the recruitment and firing behaviour of the different MUs. The recruitment of different MUs during a muscle contraction is directly related to the task at hand. Movement, speed and direction are task requirements that influence the recruitment pattern. The size and composition of the muscle will also have an influence on the recruitment pattern. The firing rate of different MUs is usually chosen between 10 and 50 Hz (Viljoen 2005) and described in terms of the interpulse intervals. MU firing rate in most cases are activated with a Gaussian distribution (Stegeman, Blok, Hermens & Roeleveld 2000).

2.6.2. Volume conductor

Human tissue acts as a volume conductor, conducting APs from the bioelectric source to the skin surface. The shape of these APs is greatly influenced by the choice of volume conductor parameters. The most straightforward description of a volume conductor is to assume that it is infinite, isotropic, homogeneous and purely resistive. However, in order to investigate MUAPs accurately at the skin surface it is necessary to include a more complex volume conductor (Roeleveld, Blok, Stegeman & Van Oosterom 1997a; Stegeman, Blok, Hermens & Roeleveld 2000).

Anisotropic muscle tissue

Muscle tissue is anisotropic with higher conductivity in the axial direction (the direction of source propagation) than in the radial direction (the direction perpendicular to the fibers) (Roeleveld, Blok, Stegeman & Van Oosterom 1997a; Stegeman, Blok, Hermens & Roeleveld 2000). Although different values for the axial and radial conductivities have been reported in the literature (Gabriel & Gabriel 2007; Kuiken, Stoykov, Popovic, Lowery & Taflove 2001), the values are widely accepted as $\sigma_r = 0.1\ \Omega m^{-1}$ and $\sigma_z = 0.5\ \Omega m^{-1}$ (Lowery, Stoykov, Dewald & Kuiken 2004; Roeleveld, Blok, Stegeman & Van Oosterom 1997a; Lowery, Stoykov, Taflove & Kuiken 2002). In more recent studies a conductivity tensor has been introduced to determine the local electrical properties of the volume conductor. The inclusion of a conductivity tensor requires a numerical approach. Since the conductivity of the muscle tissue depends on the direction of the muscle fiber, the conductivity tensor of the tissue should depend point-by-point on the fiber orientation (Farina, Mesin & Martina 2004; Mesin, Farina & Martina 2004).

Finite volume conductor

In sEMG models the muscle fibers are modelled as finite length fibers. This is necessary to explain the characteristic end-of-fiber effects in the sEMG waveform. The influence of the finite fiber length is accentuated by the finite dimension of the volume conductor [47]. As an AP propagates along a path of excitable tissue, the well-known triphasic waveform is recorded. When the AP encounters the termination of excitable tissue at the tendon endings, a phenomenon known as the far-field will contribute to the action potential waveform (Stegeman et al. 1997; Roeleveld, Blok, Stegeman & Van Oosterom 1997a).

Inhomogeneity of the surface layers

Since sEMG is recorded on the skin, both a subcutaneous fat layer and the resistive skin layer can be included in a volume conduction model. Subcutaneous fat layers have low conductivity and if included in the volume conductor will enhance the amplitude of the surface action potentials. However, if a better conducting skin layer is also included in the model, the potential profile is largely averaged out (Roeleveld, Blok, Stegeman & Van Oosterom 1997a).

Except for the different subcutaneous layers, inhomogeneities are also found within the excitable tissue. Examples are narrowing and expansion of muscle fiber diameter and a change in muscle fiber direction. These inhomogeneities are generally found in pinnated muscles, and have recently been investigated by sEMG models (Mesin, Farina & Martina 2004).

Including capacitive effects

It is generally accepted that volume conductors are quasi-stationary, implying that the potential field at any moment is determined by the sources at that particular instant only. This requires that inductive and capacitive effects be ignored, and that the volume conductor be purely resistive (Lowery, Stoykov, Taflove & Kuiken 2002; Stegeman, Blok, Hermens & Roeleveld 2000). However, the question of the frequency dependence of EMG signals caused by the presence of capacitive effects in layered muscle tissue has often reappeared. In a recent study (Lowery, Stoykov, Dewald & Kuiken 2004), capacitive effects have been included and this was found to have a noticeable effect on the AP waveform.

Finite element modelling

SEMG models have predominantly been based on an analytical solution for muscle fibers located in either finite or infinite volume conductors. Including some of the above mentioned corrections, for example capacitive effects, in an analytical model complicates the analytical calculations and the mathematical description becomes extremely difficult to handle. In order to simulate more complex geometries or include inhomogeneous effects, numerical methods such as the FE method has been implemented.

Sufficient FE analysis software is available. For sEMG modelling, software with an efficient geometry modelling ability should be chosen. FE models yield only an

approximation to the exact solution of the underlying boundary value problem. When FE modelling is used the geometry of the volume conductor is discretised into mesh elements. The potential generated by the electric source is then calculated at each node of the mesh. Accuracy depends on the size and order of the FE mesh. Fine discretisation of regions with high intensity of the electric field is necessary. A limitation of numerical modelling is the computational time; a finer mesh implies greater computational time (Kuiken, Stoykov, Popovic, Lowery & Taflove 2001; Lowery, Stoykov, Taflove & Kuiken 2002; Zhang, Mak & Roberts 1998). Figure 2.6 is a representation of a spherical geometry discretised into an FE mesh.

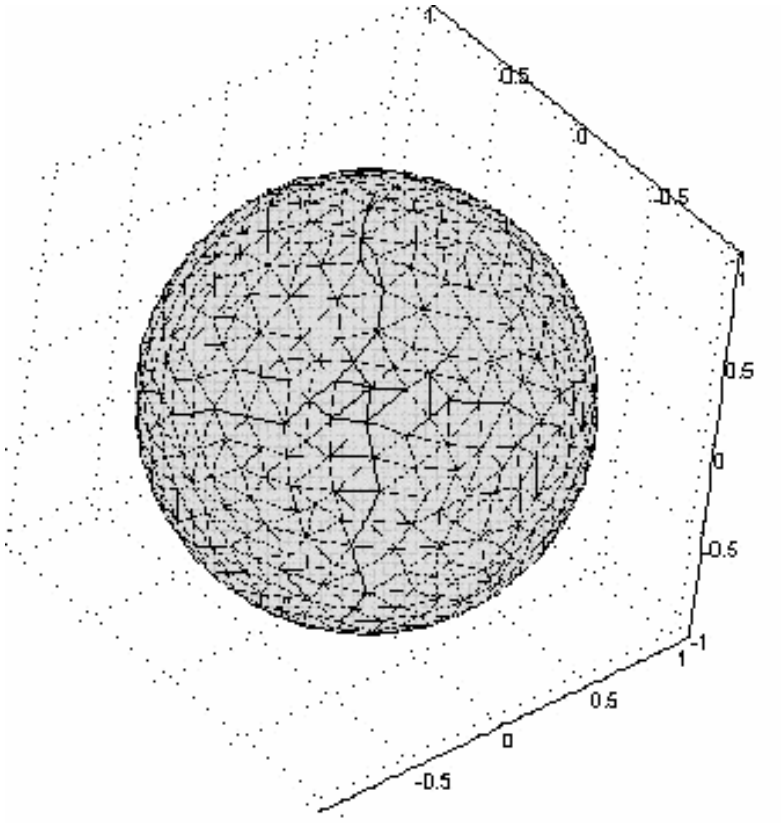

Figure 2.6. A three-dimensional illustration of a spherical geometry discretised into an FE mesh

2.6.3. Electrode detection system

The electrode geometry and recording configuration have a significant effect on the detected surface potential. Except for the monopolar recording configuration, all other configurations perform spatial filtering on the sEMG signal by a linear combination of the signals detected by the different electrodes (Merletti & Parker 2004). A computationally effective way of simulating different electrode configurations is to incorporate the specified spatial filter with the transfer function of the volume conductor. The fourier

transform of the detected potential can then be found by multiplying the fourier transform of the source by the transfer function of the volume conductor and by the transfer function of the electrode detection system.

The transfer function of the electrode detection system is linked to the filter mask, which represents the weighing factors of each electrode. Figure 2.3 E shows a representation of a Laplace filter. Equation 2.6 shows the filter mask for this electrode configuration

$$M_{NDD} = \begin{pmatrix} 0 & 1 & 0 \\ 1 & -4 & 1 \\ 0 & 1 & 0 \end{pmatrix} \tag{2.6}$$

with M_{NDD} the normal double differential (NDD) Laplace filter mask. The weighted average of the signals detected by the point electrodes can be viewed as the application to the potential in spatial domain of a finite impulse response. The spatial transfer function depends on the number of electrodes, the IED and the weights given to the electrodes. Equation 2.7 defines the transfer function

$$H_{SF}(k_x, k_z) = \sum_{i=-m}^{n-1} \sum_{r=-w}^{h-1} a_{ir} e^{-jk_x id_x} e^{-jk_x rd_z} \tag{2.7}$$

where $(w+h)$ is the number of rows in the matrix, $(m+n)$ is the number of columns, a_{ir} the weights given to the electrodes, d_x the IED in the x direction and d_z the IED in the z direction and k_x and k_z are the spatial angular frequencies (Merletti & Parker 2004).

Commonly used detection systems in sEMG modelling are the longitudinal (L) SD, LDD, NDD and inverse binomial of order inverse two (IB^2) detection systems (Farina, Cescon & Merletti 2002).

2.6.4. Dynamic modelling

SEMG modelling has mostly been used when investigating isometric contractions during static conditions. However, there are some clinical applications in which the investigation of muscle contraction during dynamic conditions could be valuable. These applications include clinical gait analysis, isokinetic assessment, cyclic movement and estimating the torque produced about a joint (Clancy, Bouchard & Rancourt 2001; Farina, Merletti,

Nazzaro & Caruso 2001; Farina et al. 2004a). The definition of dynamic muscle contraction is a contraction involving changes in muscles force and/or joint angle as the contraction progresses (Maslaac, Parker, Scott, Englehart & Duffley 2001). Thus, models of dynamic sEMG involve the modelling of isometric contractions at different joint angles (Farina, Merletti, Nazzaro & Caruso 2001; Schulte, Farina, Merletti, Rau & Disselhorst-Klug 2004; Maslaac, Parker, Scott, Englehart & Duffley 2001). SEMG at different joint angles is greatly affected by geometrical artefacts related to the fiber shortening, sliding of the muscle under the skin during movement, changes of the relative location of the muscle fiber with respect to the detection system and variations in muscle and subcutaneous layer thickness (Schulte, Farina, Merletti, Rau & Disselhorst-Klug 2004).

Dynamic sEMG modelling is needed to explain which of the above-mentioned artefacts influences the variables selected as indicators of muscle activation level or muscle fatigue.

3. METHODS

A numerical model for the generation of SFAPs in a muscle undergoing various degrees of fiber shortening is developed. The muscle is assumed to be fusiform with muscle fibers following a curvilinear path described by a Gaussian function. Different degrees of fiber shortening are simulated by changing the parameters of the fiber path and maintaining the volume of the muscle constant. The conductivity tensor is adapted to the muscle fiber orientation. In each point of the volume conductor, the conductivity of the muscle tissue in the direction of the fiber is larger than that in the transversal direction. Thus, the conductivity tensor changes point-by-point with fiber shortening, adapting to the fiber paths. An analytical derivation of the conductivity tensor is provided. The volume conductor is then studied with an FE approach using the analytically derived conductivity tensor. The model is extended to simulate MUAPs and results are obtained to show the effects of geometrical changes on the AP shape and on AP amplitude and spectral content.

The muscle chosen for this sEMG model is the *biceps brachii* muscle. The muscle fibers of the *biceps brachii* run parallel to one another and the muscle is situated near the skin surface. Muscle or fiber shortening is achieved by varying the joint angle of the elbow. Five stages of fiber shortening are simulated.

A complex geometry is chosen and to include the conductivity tensor as well as simulate shortening, a numerical solution is implemented. The model is developed using FEs. The software used is FEMlab 3.0.

Figure 3.1 presents an overview of the sEMG model developed for this study.

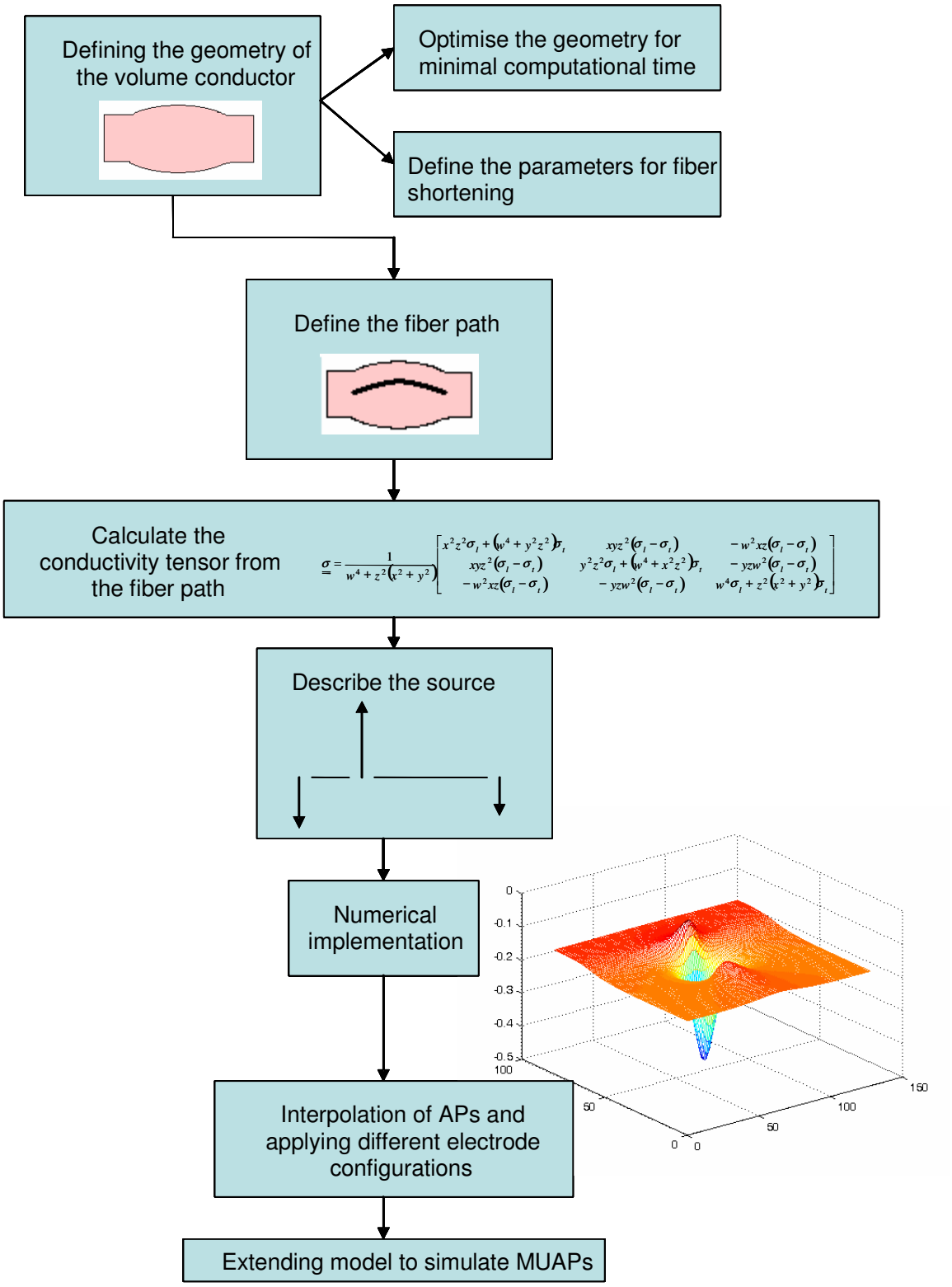

Figure 3.1. A block diagram illustrating the development of the sEMG model

3.1. MODEL GEOMETRY

The *biceps brachii* muscle is modelled as a fusiform volume conductor. For this study the volume conductor comprises muscle and tendon only. Subcutaneous layers i.e. skin and fat layers, are ignored.

When muscle contraction is initiated an AP causes depolarisation of a segment of muscle fiber. This depolarised zone is the source of a potential distribution detectable on the skin surface (Merletti, Lo Conte, Avignone & Guglielminotti 1999a). For the model developed in this study a tripole approximation of the source propagates along the fiber path to create the depolarisation of the muscle fiber and the simulated surface potential. To define the fusiform geometry of the muscle, the fiber paths are described by means of the following cylindrical curves:

$$\gamma(z) = \begin{pmatrix} r(z)\cos(\theta) \\ r(z)\sin(\theta) \\ z \end{pmatrix}, \tag{3.1}$$

where θ identifies the radial location of the muscle fiber, and r(z) is the distance of the fiber from the z-axis (central axis of the muscle).

Since the model used in this study ignores the outer skin or fat layers, the external-most fibers also create the outline of the fusiform volume conductor. The external-most fibers or basic muscle form is then characterised by a radius $r(z) = f(z)$.

Equation 3.2 defines $f(z)$:

$$f(z) = \mathrm{Re}^{\frac{-z^2}{2w^2}}, \tag{3.2}$$

where R is the maximum radius of the muscle tissue. $f(z)$ is illustrated as the outline of the muscle shown in figure 3.2.

The function $f(z)$ is limited to the interval $z \in [-d, d]$, such that the minimum muscle radius, shown in Equation 3.3,

$$R_0 = \mathrm{Re}^{\frac{-d^2}{2w^2}}, \tag{3.3}$$

corresponds to the chosen tendon thickness. d is the half-length of the muscle as illustrated in figure 3.2. The parameters R and w determine the geometry of the muscle. For example, increasing w will increase the muscle length, implying a more relaxed muscle. Decreasing w will lead to a larger muscle radius and a shorter muscle length, implying a more contracted state. This description allows for a change in muscle geometry by varying only two parameters. Figure 3.2 is a two-dimensional representation of the muscle geometry as defined for the simulation model.

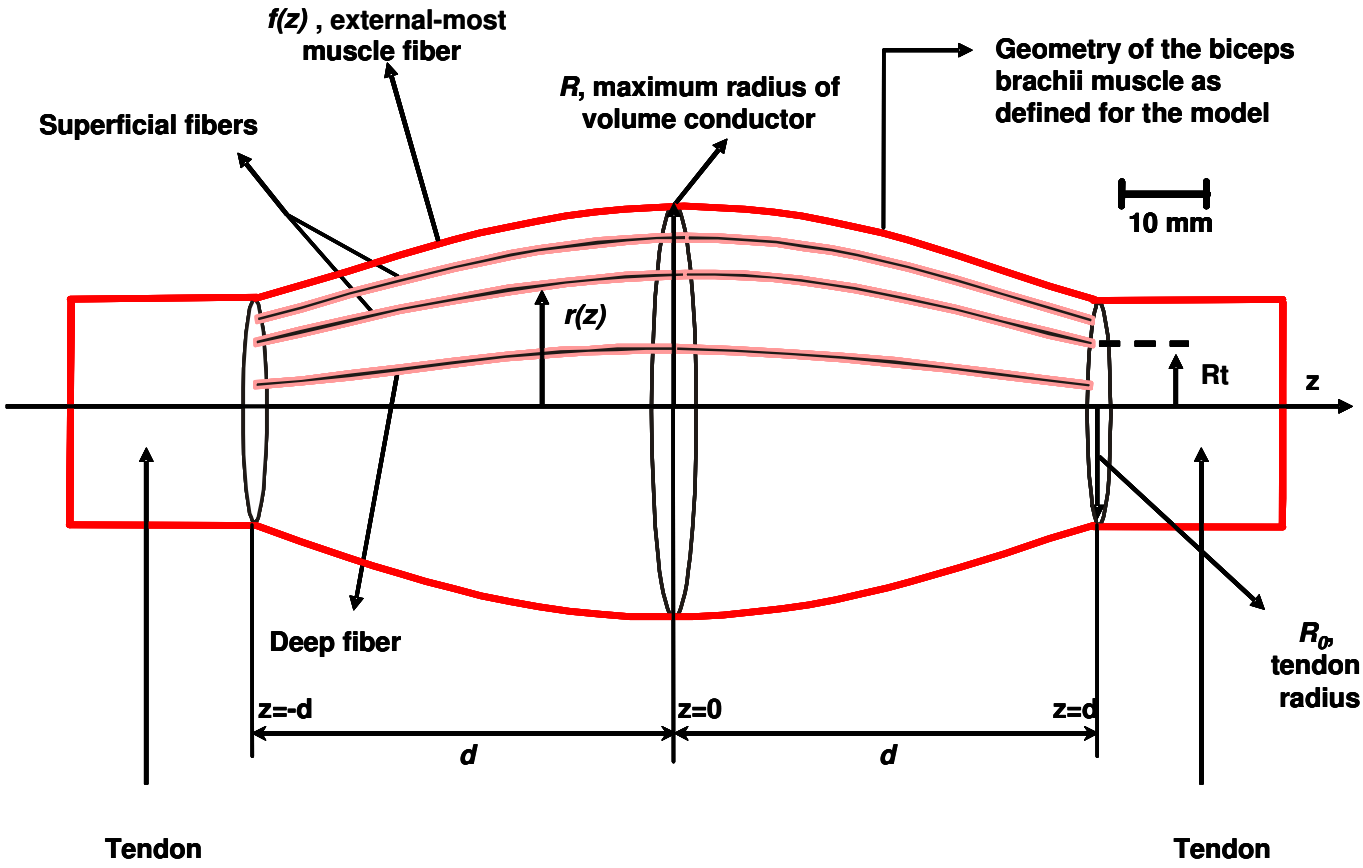

Figure 3.2. A two-dimensional view of the volume conductor's geometry. The muscle geometry has a tendon radius R_0 of 10 mm and a maximum radius R of 18.5 mm. R_t is the distance of the fiber from the z axis at the tendon level. Both superficial and deep fibers are shown. As per definition, the superficial fibers are more curved than the deep fibers.

Figure 3.2 also shows the geometrical difference in superficial and deep fibers. Superficial fibers are more curved than deep fibers. The conductivity tensor depends point-by-point on the curvature of the fiber. This implies that not only is there a difference in the electrode-source distance but also in the conductive properties of superficial and deep fibers. These

details are illustrated in chapters 4 and 5, where the results of the simulations are discussed.

As the joint angle of the elbow is decreased, the *biceps brachii* muscle shortens. To simulate muscle shortening only two parameters, the width w and the radius R have to be changed. To represent the *biceps brachii* muscle accurately at five different stages of shortening, the values for w and R have to be calculated. In order to calculate these values two constraints are imposed:

1) the volume V of the muscle has to remain constant,
2) the minimum radius, R_0 (the radius of the tendon), has to remain constant for each shortening condition.

Equation 3.4 imposes the first constraint:

$$V = \int_{\Omega} dV = \pi \int_{-d}^{d} r^2(z)dz = wR^2\pi^{\frac{3}{2}} Erf\left(\frac{d}{w}\right) = constant, \tag{3.4}$$

with

$$Erf(z) = \frac{2}{\sqrt{\pi}} \int_{0}^{z} e^{-\lambda^2} d\lambda \tag{3.5}$$

The second constraint imposes $f(d)=R_0$, leading to the relation shown in Equation 3.6:

$$d = w\sqrt{2\ln\left(\frac{R}{R_0}\right)}. \tag{3.6}$$

Substituting Equation 3.6 into Equation 3.5 one obtains Equation 3.7:

$$V = R^2\pi^{\frac{3}{2}} \sqrt{\frac{d^2}{2\ln\left(\frac{R}{R_0}\right)}} * Erf\left(\sqrt{2\ln\left(\frac{R}{R_0}\right)}\right). \tag{3.7}$$

Given the volume of the muscle V, the length of the muscle d and the radius R_0 of the tendon, the value of R can be calculated from Equation 3.7. This is a numerical calculation. When R is determined the parameter w is obtained by Equation 3.6. The parameter w is the same for all fibers. The maximum distance $R_d \leq R$ of each fiber from the z axis is computed by assuming the ratio R_d / R constant in each shortening condition. In this way, fiber density is the same in each point of the muscle section. Table 3.1 gives the calculated simulation parameters for the five stages of shortening.

Table 3.1. Model parameters

Model Parameter	Stage 1	Stage 2	Stage 3	Stage 4	Stage 5
R_0	10 mm	10 mm	10 mm	10 mm	10 mm
R	15 mm	16.5 mm	18.5 mm	21 mm	23 mm
L	150 mm	130 mm	110 mm	90 mm	80 mm
w	83.29	64.95	49.58	36.94	30.99
V	83.2 cm^3	83 cm^3	83.4 cm^3	83 cm^3	85.1 cm^3
CV	4 m/s	4 m/s	4 m/s	4 m/s	4 m/s

Stage 1 assumes a relaxed muscle condition. This stage is the reference. The percentage shortening for the other stages are computed with respect to the reference stage. For the reference stage a maximum radius R of 15 mm was chosen based on anatomical data from the literature (Viljoen 2005). The *biceps brachii* muscle has a limited range of fiber lengths over which the muscle can operate effectively. The optimal muscle fiber length is chosen as $d = 150\ mm$ (Garner & Pandy 2003). Since muscle tissue cannot generate active muscle force beyond 0.5 times the optimal length (Garner & Pandy 2003), the four remaining stages of shortening were chosen within this constraint. The volume for the relaxed stage was calculated and kept constant for the following stages. The volume conductor for five stages of shortening is shown in figure 3.3.

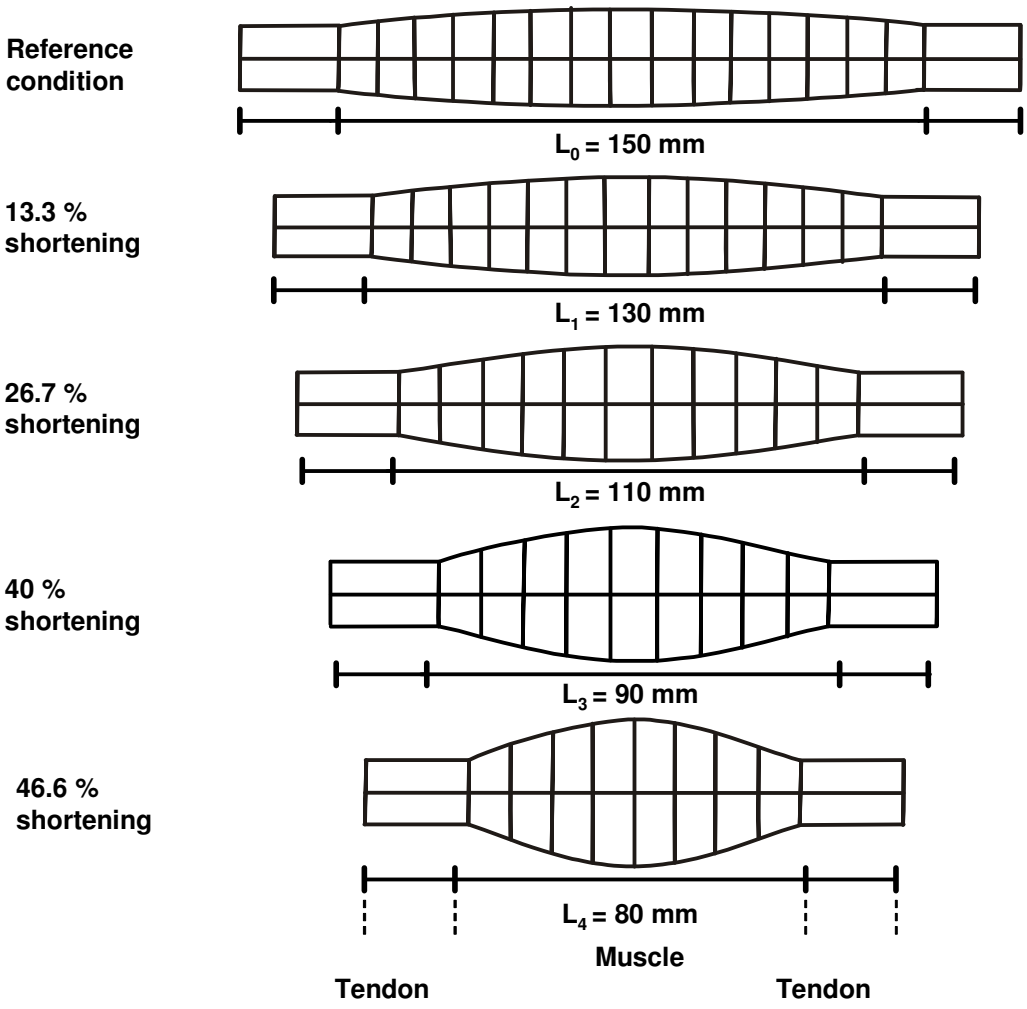

Figure 3.3. A two-dimensional view of the volume conductor for five stages of shortening. As the muscle geometry shortens, the volume increases. The tendon regions remain of the same length and diameter for all conditions.

3.2. CONDUCTIVITY TENSOR

In less complex models the conductivity of muscle tissue was described using constant values for the longitudinal and transversal conductivities (Lowery, Stoykov, Taflove & Kuiken 2002). The model presented in this work attempts to simulate changes in the surface potential representative of a change in the electrical properties of the muscle tissue. To integrate this change with the geometrical changes due to muscle shortening, the local electrical properties of the volume conductor are fully determined by its conductivity tensor. The conductivity tensor has to be related to the curve describing the fiber path. A general conductivity tensor is described in Equation 3.8. The conductivity tensor of Equation 3.8 procreates with the vector describing the fiber path in order to produce a new

vector, which is linearly related to the old one, but now points in the direction of source propagation (2004).

In order to have an advanced numerical description of the volume conductor, an accurate description of the conductivity tensor for the muscle tissue is required. Since the conductivity of the muscle tissue depends on the direction of the muscle fibers, the conductivity tensor of this tissue should depend point-by-point on the fiber orientation (Farina, Mesin & Martina 2004).

A general conductivity tensor for muscle tissue is expressed in Equation 3.8:

$$\underline{\underline{\sigma}} = \sigma_l \hat{v}_l \hat{v}_l + \sigma_t \hat{v}_{tn} \hat{v}_{tn} + \sigma_t \hat{v}_{tb} \hat{v}_{tb}\,, \tag{3.8}$$

where the subscript l stands for longitudinal and t for transversal coordinates with respect to fiber direction. Thus $v_l, v_{tn},$ and v_{tb} are the longitudinal, normal and binormal versors relative to the fiber orientation, respectively. Such versors are functions of the position in case of curvilinear fibers (Farina, Mesin & Martina 2004; Mesin, Joubert, Hanekom, Merletti & Farina 2006).

Since the bioelectrical problem of EMG simulation can be considered quasi-statical, implying that the potential field at any moment is determined by the sources at that same instant (Merletti & Parker 2004), the Poisson equation holds. Poisson's equation is shown in Equation 3.9:

$$\begin{cases} -\nabla \cdot (\underline{\underline{\sigma}} \nabla \varphi) = g & \Omega \\ \underline{\underline{\sigma}} \nabla \varphi = 0 & \partial\Omega \end{cases}, \tag{3.9}$$

where $\underline{\underline{\sigma}}$ is the conductivity tensor, φ the electric potential, g the source term (which is a current density travelling along the fiber and inducing its contraction), Ω and $\partial\Omega$ the volume conductor domain and its boundary, respectively. Poisson's equation links potentials directly to the sources producing them (Plonsey & Barr 2000).

Different volume conductors can be modelled by choosing a conductivity tensor that is related to the volume conductor shape (Mesin, Farina & Martina 2004). Since the fiber

path is given in cylindrical coordinates, translation is necessary. Poisson's equation, in a Cartesian system for the general conductivity tensor introduced above, can be obtained by introducing the Cartesian representation of the curvilinear differential operators (gradient and divergence). This is represented by Equation 3.10:

$$\nabla \cdot \left(\underline{\underline{\sigma}} \nabla(\bullet)\right) = \begin{pmatrix} \partial_x & \partial_y & \partial_z \end{pmatrix} \left[\left(\sigma_l \hat{v}_l \hat{v}_l + \sigma_t \hat{v}_{tn} \hat{v}_{tn} + \sigma_t \hat{v}_{tb} \hat{v}_{tb} \right) \begin{pmatrix} \partial_x \\ \partial_y \\ \partial_z \end{pmatrix} \right], \tag{3.10}$$

where ∂_x, ∂_y and ∂_z indicate the partial derivative operators in Cartesian coordinates. Equation 3.10 can be used in general to determine the conductivity tensor given the propagation path of the source (Farina, Mesin & Martina 2004). For the propagation path given in Equation 3.1, the longitudinal versor $\vec{v}_l$ is calculated by taking the first derivative with respect to z. The binormal versor $\overrightarrow{v_{tb}}$ is calculated by taking the first derivative with respect to θ, and the normal versor $\overrightarrow{v_{tn}}$ is calculated by taking the cross product of the longitudinal and binormal versors. For the fusiform muscle introduced, the longitudinal, normal, and binormal vectors translated into Cartesian coordinates become:

$$\hat{v}_l = \begin{pmatrix} \dot{x}\cos(\theta) \\ \dot{x}\sin(\theta) \\ 1 \end{pmatrix} = \begin{pmatrix} -\frac{zx}{w^2} \\ -\frac{zy}{w^2} \\ 1 \end{pmatrix};$$

$$\hat{v}_{tn} = \begin{pmatrix} \cos(\theta) \\ \sin(\theta) \\ -\dot{x} \end{pmatrix} = \begin{pmatrix} \frac{x}{\sqrt{x^2+y^2}} \\ \frac{y}{\sqrt{x^2+y^2}} \\ \frac{z}{w^2}\sqrt{x^2+y^2} \end{pmatrix};$$

$$\hat{v}_{tb} = \begin{pmatrix} -\sin(\theta) \\ \cos(\theta) \\ 0 \end{pmatrix} = \begin{pmatrix} -\frac{y}{\sqrt{x^2+y^2}} \\ \frac{x}{\sqrt{x^2+y^2}} \\ 0 \end{pmatrix} \tag{3.11}$$

where the point over a symbol indicates the first derivative with respect to z. Using their normalised versions in the general expression for a conductivity tensor described in Equation 3.10, calculations yield the following expression (Equation 3.12) of the conductivity tensor in a Cartesian system for the fusiform muscle defined by the fiber orientation of Equation 3.1.

$$\underline{\underline{\sigma}} = \frac{1}{w^4 + z^2\left(x^2 + y^2\right)} \begin{bmatrix} x^2 z^2 \sigma_l + \left(w^4 + y^2 z^2\right)\sigma_t & xyz^2\left(\sigma_l - \sigma_t\right) & -w^2 xz\left(\sigma_l - \sigma_t\right) \\ xyz^2\left(\sigma_l - \sigma_t\right) & y^2 z^2 \sigma_l + \left(w^4 + x^2 z^2\right)\sigma_t & -yzw^2\left(\sigma_l - \sigma_t\right) \\ -w^2 xz\left(\sigma_l - \sigma_t\right) & -yzw^2\left(\sigma_l - \sigma_t\right) & w^4 \sigma_l + z^2\left(x^2 + y^2\right)\sigma_t \end{bmatrix} \tag{3.12}$$

Equation 3.12 is the tensor to be used in an FE model for describing the conductivity properties of the muscle tissue point-by-point under different degrees of fiber shortening.

Equation 3.10 provides a general way to compute the conductivity tensor, given the direction of the muscle fibers. In general, given the parametric representation of the curve defining the muscle fiber, it is possible to compute the corresponding normal, binormal and longitudinal versors, and from there the determination of the conductivity tensor (Farina, Mesin & Martina 2004).

The specific muscle shape and the way to simulate shortening are not a constraint of the proposed model. By deriving the Cartesian representation of the conductivity tensor starting from the analytical description of the fiber orientation, the concepts proposed in this study can be applied to generic muscle shapes and fiber orientations.

3.3. SOURCE DESCRIPTION

The modelling of the generation, propagation, and extinction of the IAP has been extensively addressed in the literature (Dimitrov & Dimitrova 1998; Duchêne & Hogrel 2000; Lowery, Stoykov, Taflove & Kuiken 2002; Griep, Gielen, Boon, Hoogenstraten, Pool & Wallinga de Jonge 1982). The general assumption is that the integral of the current density over the muscle fiber length is zero in each instant of time. For volume conductors that are not space-invariant in the direction of propagation, as the one studied in this work, the response of the system to an impulsive current depends on the position of the current (thus, it is not an impulse response in the sense of linear and space-invariant spatial

filtering). The source function should be sampled and viewed as a multi-pole. In sEMG modelling it is accepted that the detection electrodes are a sufficient distance from the source and that the AP voltage $V_m(z)$ described in Equation 2.5 can be approximated as a tripole (Merletti & Parker 2004). For the field source implemented in this model the tripole approximation of the transmembrane current density was used (Mcgill & Huynh 1988). The tripole equations connected to Equation 2.5 are defined in Equations 3.13 and 3.14:

$$I_1 + I_2 + I_3 = 0 \tag{3.13}$$

$$I_2 a + I_3 b = 0 \tag{3.14}$$

I_1, I_2, and I_3 represent the values for the three current impulses. a and b are the distances between impulses. For the source implemented in this work the values for Equations 3.13 and 3.14 are given in table 3.2.

Table 3.2. Current source parameters

Model parameters	Values
I_1	24.6
I_2	-35.5
I_3	10.8
a	2.1
b	6.9

Generation (at the NMJ) and extinction (at the tendon) of the IAPs have very important implications for the resulting simulations. For the tripole approximation the three poles are coincident at the NMJ at the moment of excitation. The first pole then moves in discrete steps for distance a, the second moves with the first for distance b until finally the tripole propagates as a unit along the fiber path. For the extinction at the tendon ending, the opposite effect takes place. The first pole reaches the ending and stops, leaving the second and third poles to form a dipole moving towards the tendon. Finally the three poles overlap and cancel out. Figure 3.4 is a three-dimensional FE representation of the movement of the tripole towards the tendon ending.

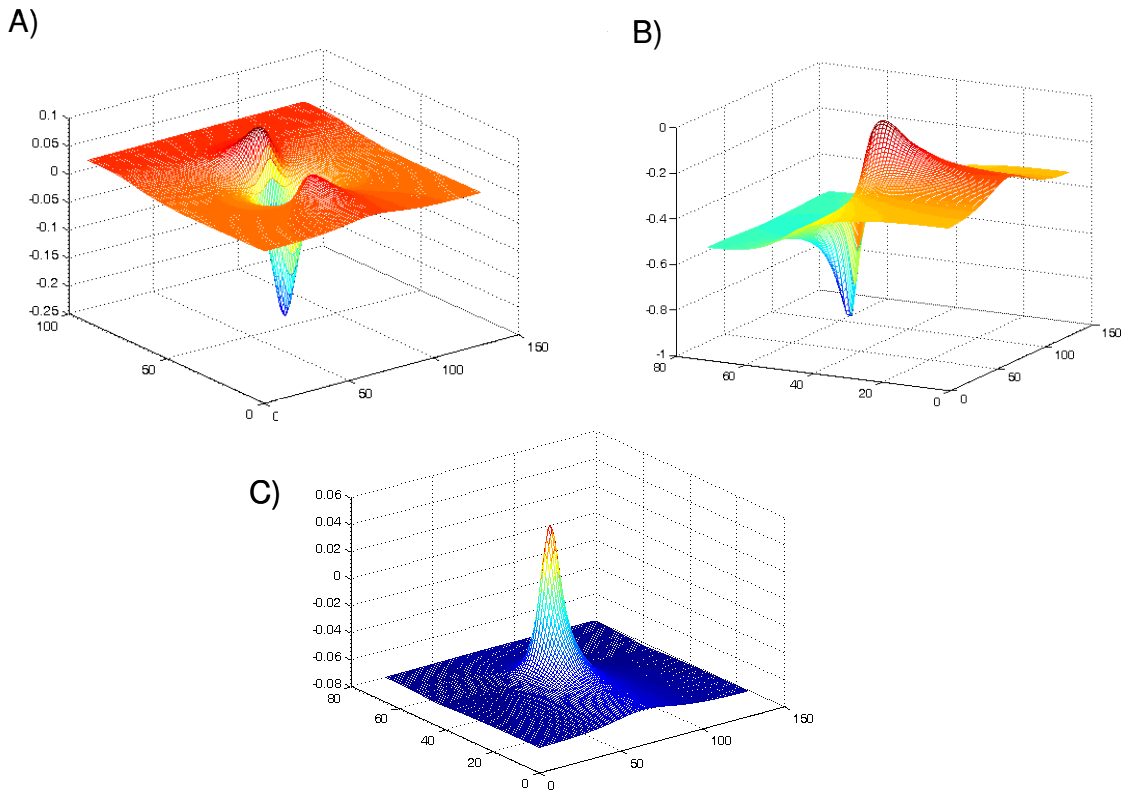

Figure 3.4. A) The tripole is propagating along the fiber path. B) The first pole is at the tendon ending, leaving the second and third poles to propagate as a dipole. C) Extinction of the tripole

The path of propagation of the transmembrane current was defined by the curve γ in Equation 3.1, which also determined the conductivity tensor. The arch length of γ was used as the coordinate to locate the tripole source within the muscle and to describe its propagation (Farina, Mesin & Martina 2004).

3.4. NUMERICAL IMPLEMENTATION

The numerical approach applied was based on FEs and implemented by the software package FEMLAB (version 3.0a). The boundary conditions for the muscle were homogeneous Neumann conditions (Silvester & Ferrari 1983). A Neumann boundary (also referred to as natural boundary) condition specifies the value of the normal flux across the boundary. By the image theorem, Neumann boundary conditions lead to periodicity (Silvester & Ferrari 1983). A sub-domain representing the tendon ending was added to the muscle geometry (Figure 3.1) in order to reduce aliasing. The periodicity given by the Neumann boundary conditions can be used to reduce computational time. From image theory, cutting the muscle geometry in two halves, it is possible to study two propagating

tripoles by simulating only one (the second is an image of the first). Thus, in order to save computational time, only half of the original volume conductor can be described (the halved volume conductor is presented in figure 3.5), imposing the Neumann boundary conditions at $z = 0$, which account for the second half of the volume conductor (image of the first half). This approach is valid only for symmetric muscle fibers, with the end-plate in the middle of the volume conductor. If the muscle fibers are asymmetric, the entire volume conductor and the two tripoles should be studied.

The tendon ending was considered isotropic (conductivity 0.3 S/m), while the muscle tissue was electrically described by the conductivity tensor in Equation 3.12 (in-homogeneous and anisotropic), with σ_l and σ_t 0.5 S/m and 0.1 S/m, respectively.

To calculate the surface potential, the source was moved step-wise along the fiber path described by Equation 3.1. Given the conduction velocity v of the IAP and the sampling rate f_s in the time domain, v/f_s is the step by which the source is moved between two sampling instants. For each sampling instant, the potential distribution over the entire muscle surface was computed by meshing the volume conductor using tetrahedral elements. This is shown in figure 3.5.

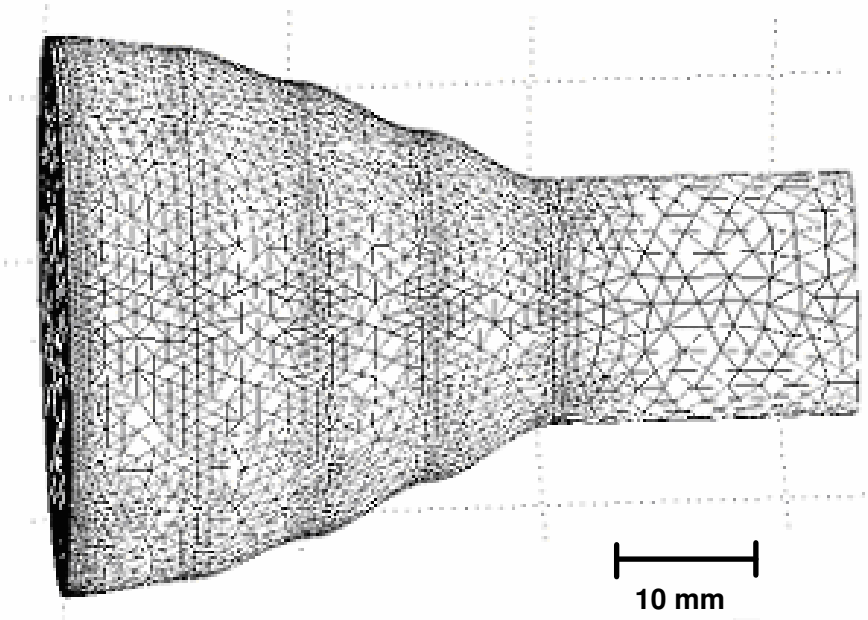

Figure 3.5. A three-dimensional view of the volume conductor described by finite elements. Because of image theory, the muscle geometry has been halved (see text for details). The volume conductor (muscle and tendon) is meshed into approximately 100 000 tetrahedral elements.

The elements surrounding the source were smaller than the others (maximum diameter of these elements 0.1 mm), to improve accuracy. The potential was calculated at the nodes located at the vertices of the tetrahedral elements (Lowery, Stoykov, Taflove & Kuiken 2002). Point electrodes were simulated. To obtain the potential at the muscle surface corresponding to the exact location of the electrode, the potential values at the four nodes nearest to the detection point were interpolated. This was done by calculating the distance of each node from the electrode and summing the potentials at the nodes by a convex linear combination (i.e., with unitary sum of the weights) with weights proportional to the inverse of the distances (which is the rate of decrease of the free-space potential in the three-dimensional space, neglecting the effect of anisotropy within the specific element). Figure 3.6 shows the solution obtained with FEMLAB for the geometry of figure 3.5 when the source of section 3.3 propagates along the fiber path.

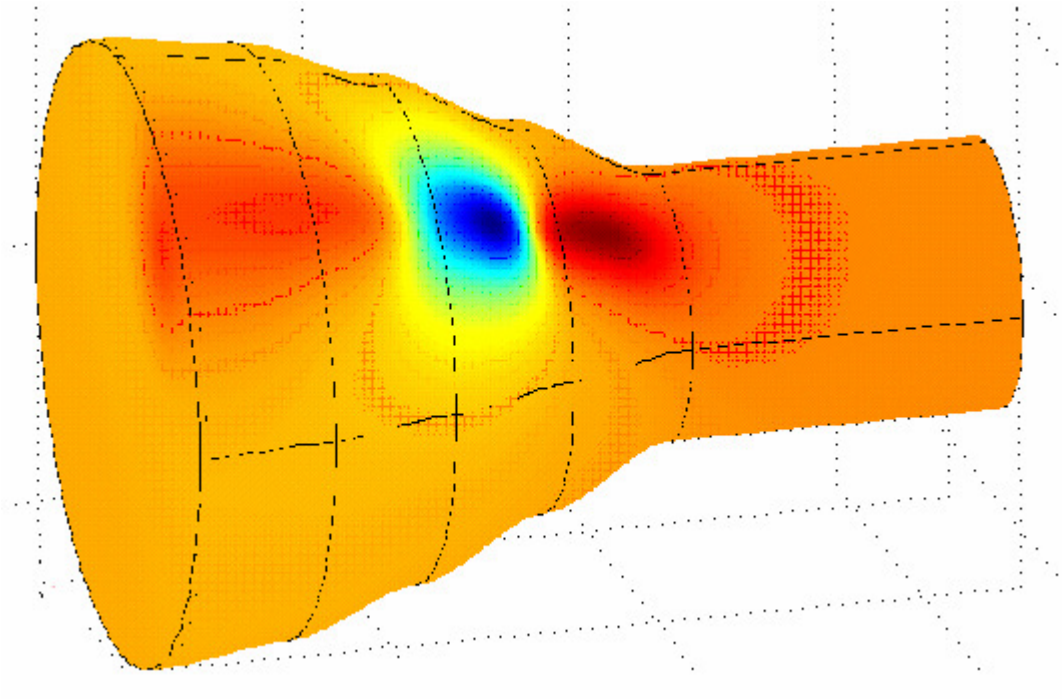

Figure 3.6. Solution obtained with FEMLAB for the tripole source propagating along the volume conductor. The darker red patches represent the positive poles of the tripole, and the blue patch represents the negative pole.

3.5. ANALYTICAL GENERATION OF MUAPS

The model created in this work was used to create libraries of extracellular potentials for SFs. These libraries consist of potentials calculated at 2 mm steps along the fiber path. Seven different fiber depths are simulated and, for each fiber depth, potentials are obtained for five different muscle shortenings. These libraries are then used to expand the model and include the simulation of MUAPs. An MU is modelled as the summation of N parallel fibers uniformly distributed inside a cylinder of radius R (Merletti, Lo Conte, Avignone & Guglielminotti 1999a). For the model expansion it is assumed that all fibers in the MU are located at the same cross-sectional location and are of equal CV (4 m/s). These assumptions were also used in previous works (Lowery, Stoykov & Kuiken 2003). The number of fibers inside a single MU of the *biceps brachii* muscle is found to vary significantly. Numbers of between 50 and 700 have been reported in the literature (Viljoen 2005). It was decided to use 300 fibers in each of the MUs. Before the single fibers are summed into the MUs, the NMJ or end-plate of the indivivual fibers are uniformly distributed throughout a zone of 12 mm. This uniform distribution is repeated at the tendon

junction. MUs are now created at seven depths and for five muscle shortenings. Representative results for the MUAPs are shown in chapter 5.

4. RESULTS: EFFECT OF MUSCLE SHORTENING ON SFAPS

4.1. OBJECTIVE

Chapter 3 describes the FE model developed in this study. The aim of this study is to develop a simulation model, which could bring to light the influence of muscle shortening when a complex analytical conductivity tensor is included.

The results obtained from simulations prepared with this model are presented in chapter 4. Simulations were prepared to generate SFAPs on the muscle surface at five stages of shortening. SFAPs were generated for fibers situated at seven different depths. The parameters related to the five geometries are reported in Table 3.1. The APs were recorded using monopolar, SD and DD detection systems. The objective is to validate the model at a single fiber level as well as to highlight the geometrical artifacts brought about by muscle shortening as well as changes in the electrical properties of the muscle tissue. The muscle modelled is the *biceps brachii* muscle.

An analytical expansion of the model is used to generate MUAPs. Since MUs comprise single fibers with uniformly distributed NMJs, it is important to validate the model at the single fiber level. Results for simulations prepared for MUAPs are shown in chapter 5.

4.2. METHODS

To generate the APs the tripole source was moved along the propagation path using 2 mm steps. The surface potential at the recording electrode was then calculated by interpolating the four surface potentials nearest to the detection point. This was done by calculating the distance of each node from the electrode, and summing the potentials at the nodes by a convex linear combination with weights proportional to the inverse of the distances. The recording electrode system was placed over the surface of the muscle between the fiber end-plate and the tendon ending in all conditions. The longitudinal muscle shift with respect to the electrodes, which probably occurs in experimental recordings, was not considered in the simulation results shown in this chapter. The muscle shift, however, is included in the simulation of the MUAPs that follow in chapter 5. Monopolar, SD, and DD recording systems are simulated. For single and double differential detection, the IED is 5 mm and the electrode detection system is placed directly over the fiber.

Except for the surface potentials shown for the three recording systems, two other processing techniques known as the ARV and the MNF are used to interpret results on the amplitude and spectral content of the potentials. The ARV is an amplitude estimator and can be calculated with Equation 2.1 shown in chapter 2. The MNF is a variable that provides information on the spectral content of the signal and can be calculated with Equation 2.3 shown in chapter 2.

4.3. RESULTS

4.3.1. SFAPs detected over the muscle surface

Figures 4.1 - 4.3 show the SF surface potentials detected by the different electrode configurations for the five stages of muscle shortening. Figure 4.1 presents the monopolar detection system. Figure 4.2 presents the SD detection system and figure 4.3 the DD detection system. Each figure represents the surface potentials measured for fibers at two depths. The two depths presented are located within the muscle corresponding at the tendon location to a distance of R_t = 6.25 mm (representing deep fibers) and R_t = 8.75 mm (representing more superficial fibers). The IED for the SD and DD detection systems is 5 mm. The electrodes are placed directly over the fiber.

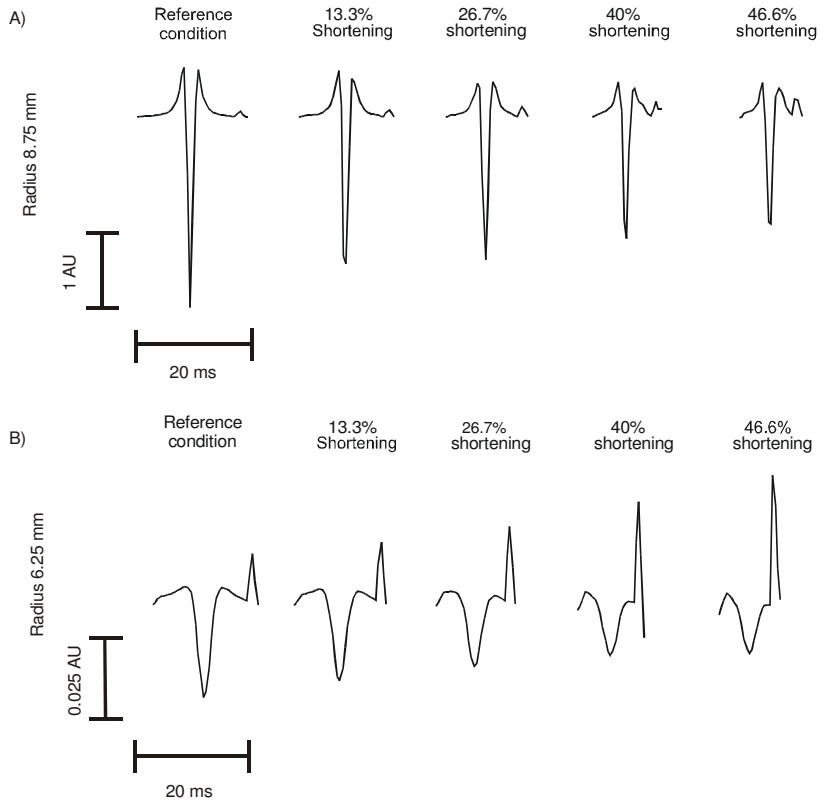

Figure 4.1. Monopolar detected surface potentials generated at five stages of shortening. Potentials are shown for a superficial and a deep fiber. AU stands for arbitrary units.

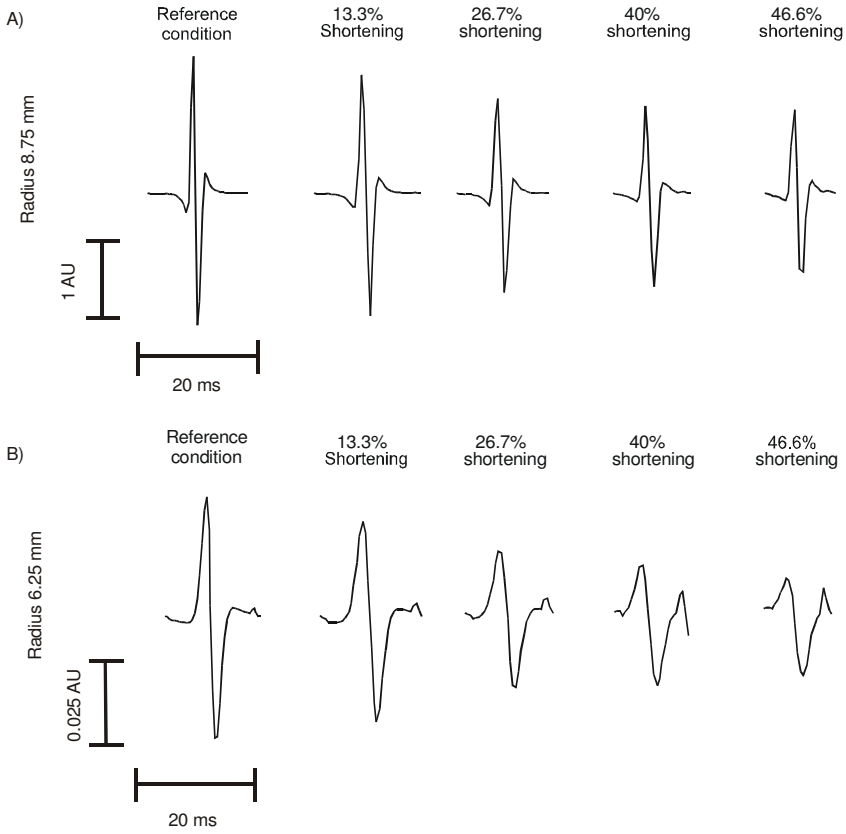

Figure 4.2. SD detected surface potentials generated at five stages of shortening. Potentials are shown for a superficial and a deep fiber. AU stands for arbitrary units.

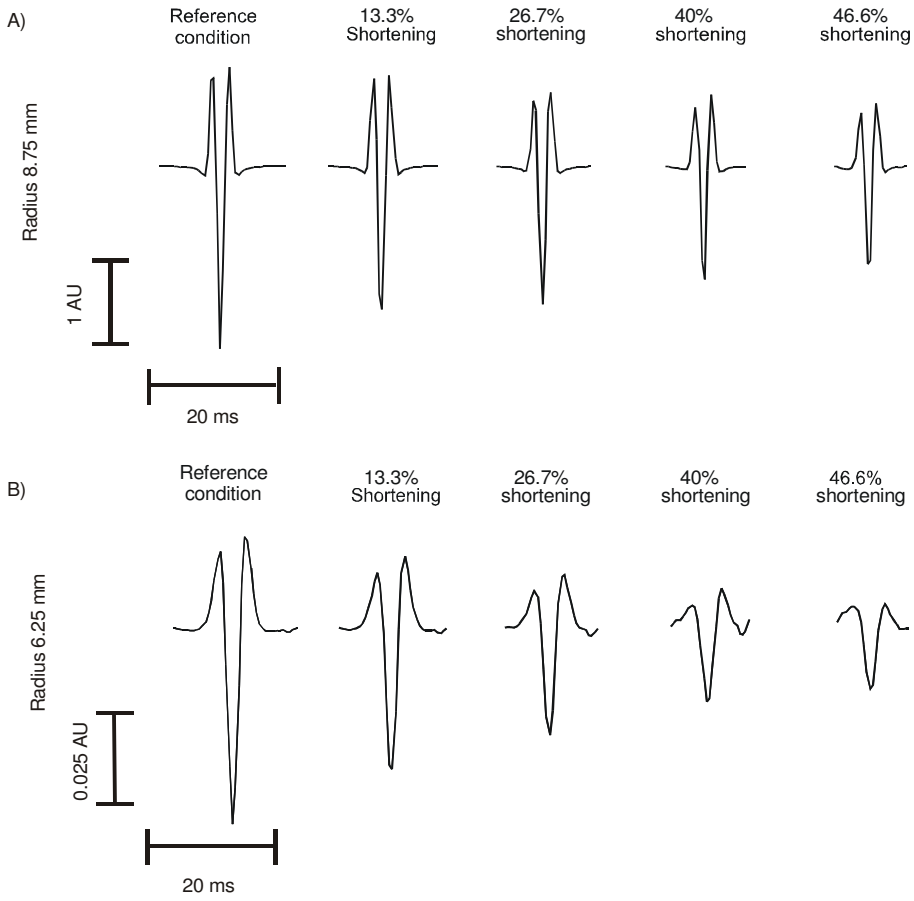

Figure 4.3. Double differential surface potentials generated at five stages of shortening. Potentials are shown for a superficial and a deep fiber. AU stands for arbitrary units.

Discussion

For the surface potentials shown in figures 4.1 to 4.3, a noticeable difference can be seen between potentials detected for a deep fiber and potentials detected for a superficial fiber. The influence of muscle shortening is clearly identifiable, and in all probability enhanced by the inclusion of a conductivity tensor. The amplitude of the propagating part of the potential significantly reduces while that of the non-propagating part clearly increases. The difference for potentials detected with different electrode detection systems is also clear. The DD detection system is more selective than both the SD and monopolar systems. The DD detection system also reduces the end-of-fiber effects more successfully.

4.3.2. MNF and ARV as estimators for amplitude and spectral content

Figures 4.4 and 4.5 show the ARV and MNF computed at seven different fiber depths and for the five stages of shortening shown in figure 3.3. Three detection systems are compared: monopolar, SD and DD. Both the ARV and MNF values are recorded at 0° from the fiber and normalised with respect to values obtained for the relaxed muscle

condition. The fiber is located within the muscle at seven depths, corresponding at the tendon location to a distance R_t from the z axis (see figure 3.1). R_t is in the range 1.25 mm – 8.75 mm (1.25 mm increments). A small R_t implies a deep fiber. Electrodes are located in the middle between the end plate and the tendon in all conditions. Again, for single and double differential detection, the IED distance was 5 mm.

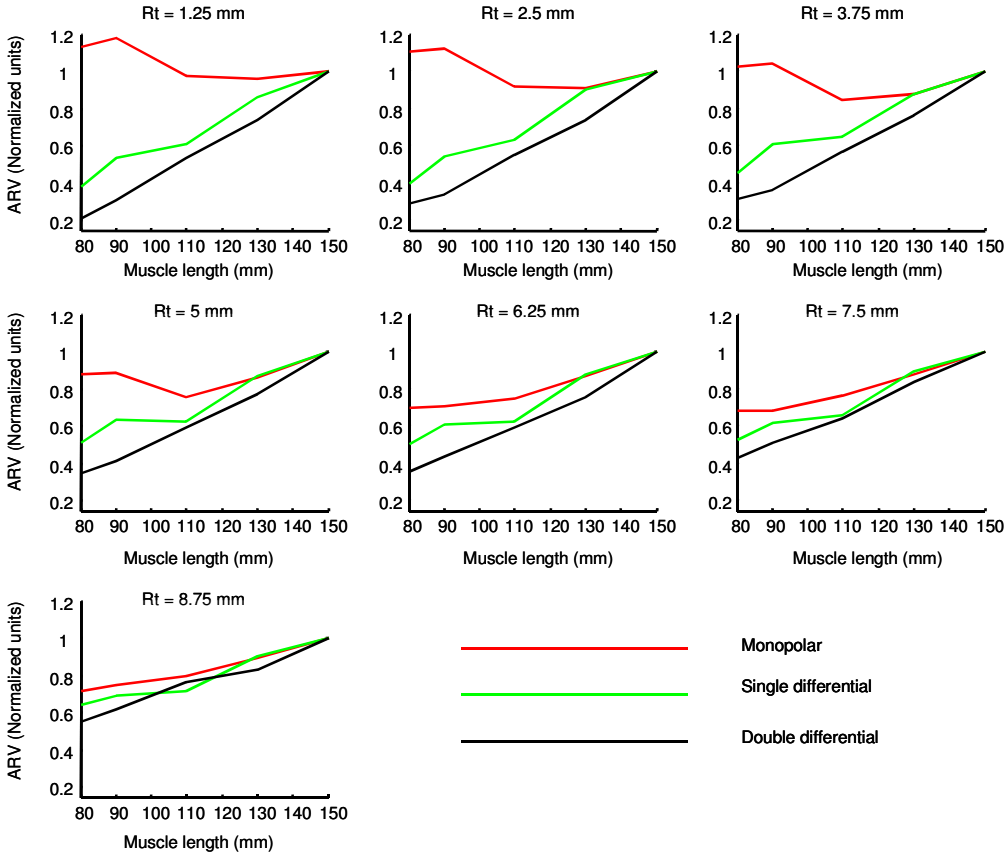

Figure 4.4. ARV computed from simulated muscle fiber APs for seven different depths and for the five muscle lengths given in table 3.1. Monopolar, single and double differential detected potentials are shown. R_t = 1.25 mm represents the deepest fiber.

Discussion

The ARV estimator shown in figure 4.4 is normalised with respect to stage 1, the relaxed muscle. It is clear that the amplitude decreases as the muscles shortens. This effect is more noticeable for deeper fibers, especially for the DD detection system. The monopolar detection system seems to be less affected by a change in muscle length, especially for the deeper fibers. This might be unexpected, but is easily explained if the influence of the non-propagating part of the signal (see figure 4.1) is kept in mind. For superficial fibers the influence of the type of detection system used is less. This can be seen from the graph for

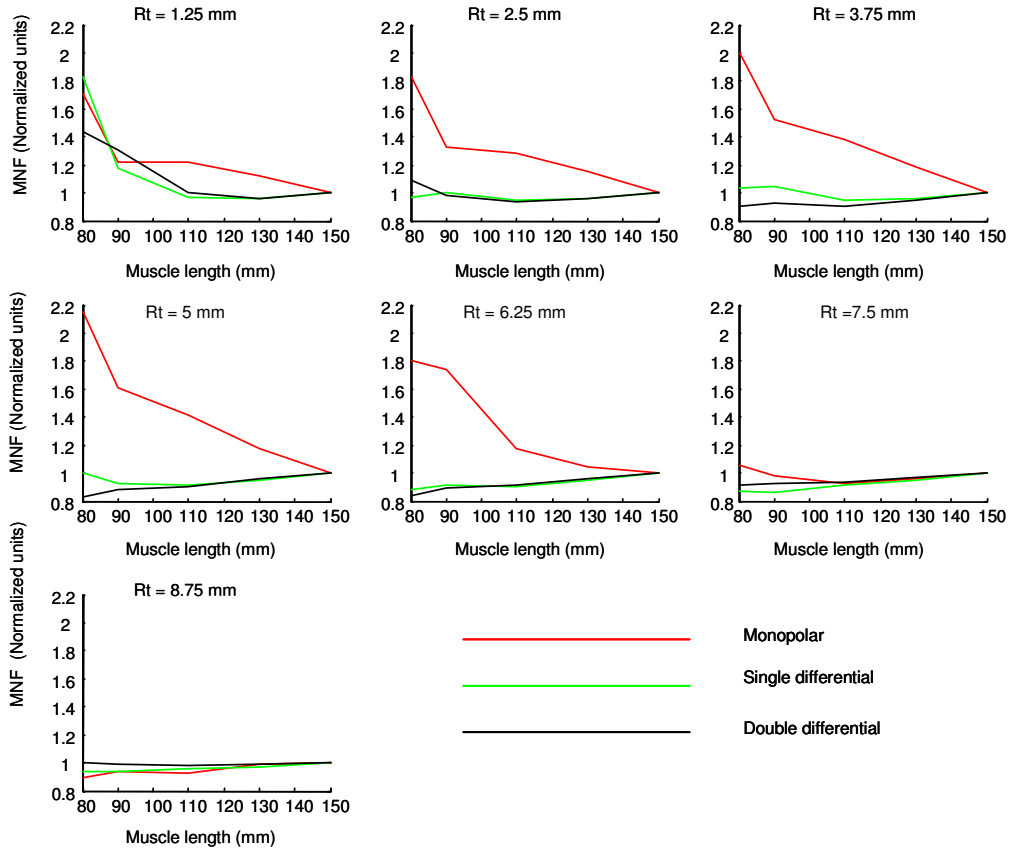

Figure 4.5. MNF computed from simulated muscle fiber APs for for seven different depths and for the five muscle lengths given in table 3.1. Monopolar, single and double differential detected potentials are shown. R_t = 1.25 mm represents the deepest fiber.

R_t = 8.75 mm, which is the most superficial fiber, where the different potentials seem almost to merge into one line.

The MNF estimator shown in figure 4.5 is normalised with respect to stage 1, the relaxed muscle. The general trend for this figure is that the frequency content seems to increase as the muscle shortens. This effect is clear for the three deepest fibers, R_t = 1.25 mm, R_t = 2.5 mm, R_t = 3.75 mm, and is also true for all three the detection systems. For the remaining, more superficial, fibers and for only the SD and DD detection systems the MNF remains more monotonous. For these fibers and detection systems there seems to be a slight decrease in MNF for the muscle in its most contracted state. This effect is only true for the monopolar detection system for the most superficial fiber R_t = 8.75 mm. Again, for superficial fibers the influence of the type of detection system used is less.

4.4. CONCLUSION

When muscle fibers shorten, their diameters increase and, as a consequence, muscle geometry changes. A fiber at a specific depth within the muscle in resting conditions may be at a larger depth when the overlaying fibers increase their diameter. In the work done in this study specifical emphasis was placed on this effect by simulating five stages of muscle shortening (as shown in figure 3.3). Thus, in addition to changes in the relative location of the tendons and end-plates with respect to the recording electrodes (Schulte, Farina, Merletti, Rau & Disselhorst-Klug 2004), the surface-detected potentials are also affected by variations in 1) the conductivity properties of the muscle tissue and 2) the relative electrode-source distance. These changes are reflected in the amplitude and frequency variables extracted from sEMG signals (Figures 4.4 and 4.5). The non-constant conductivity tensor included in this model introduces an in-homogeneity in the volume conductor in the direction of source propagation, in addition to the in-homogeneity due to geometry. The simulation of only a geometrical change in the volume conductor leads to a different effect with respect to the inclusion of variations in both the geometry and the conductivity tensor. These effects are discussed in Chapter 6.

The representative simulations shown provide an indication of the effect of changes in the conductivity tensor accompanying muscle shortening on the properties of the surface-detected potentials. These effects are complex to predict without a numerical model, since shortening implies a number of changes in the system. There are two main signal components that contribute to the sEMG potentials, the propagating and the non-propagating components. The propagating component is generated during the travelling of the IAP along the fiber, while the non-propagating component originates when the IAP is generated and extinguished at the end-plate and tendons, respectively. With muscle shortening the fiber changes position within the muscle. As the fiber length decreases, the end-plate and tendon endings move closer to each other, as well as to the detection electrodes. This implies that the sources of the non-propagating and propagating signal components change their relative distance with respect to the detection electrodes as the muscle shortens. In addition, the electrical properties and geometry of the tissue separating sources and electrodes also change. This complex set of electrical and geometrical modifications affects the surface-detected AP in a way that is dependent on the specific detection system.

As a consequence of muscle shortening, the ARV of SFAPs may be reduced by up to approximately one third of its initial value when muscle length is reduced to approximately 50% and the signals are detected with a bipolar system (Figure 4.4). The effect is smaller for superficial than for deeper fibers since the distance of superficial fibers from the electrodes changes less with shortening than that of the deep fibers. Since most of the sEMG signal power is due to the activity of superficial fibers, the changes in ARV of the interference EMG signal are more limited than those obtained for deeper single fibers, but remains significant in practical applications. The effect on ARV depends on the detection system. While single and double differential systems lead to similar sensitivities to muscle shortening, monopolar recordings are much less sensitive to it. This is due to the relative weight of non-propagating potentials, which is larger for monopolar than for differential recordings. The weight of the non-propagating potentials for the monopolar detection system can be seen clearly in the potentials obtained from R_t = 6.25 mm shown in figure 4.1. As the muscle shortens, the fibers increase their distance from the detection point but the end-plate and tendon endings approach the electrodes, thus the propagating component decreases and the non-propagating one increases in amplitude, counteracting each other. This effect is less evident for single and double differential systems since these systems largely reduce the non-propagating components.

As for ARV, the effect of shortening on MNF depends on the depth of the fiber and on the detection system (Figure 4.5). The APs generated by superficial fibers are less affected by shortening than those from deep fibers, as discussed for ARV. In general, MNF tends to increase with shortening for the monopolar recording, while this is less evident for the other two detection systems. The increase in MNF reveals the well-known larger frequency bandwidth of the non-propagating signal components with respect to the propagating parts of the signal (Farina, Merletti, Indino, Nazzaro & Pozzo 2002). As muscle shortens, the relative weight of end-plate and end-of-fiber components increases, especially for the monopolar recording, as discussed above and shown in figure 4.1. However, the effect on the spectral content of the surface signal is also significantly altered by the change in the geometry and conductivity tensor of the system, which may lead to an opposite trend of MNF with shortening, i.e., to a decrease, which is observed for superficial fibers. Figure 4.1 shows the potentials obtained for two fiber depths from the monopolar detection system. It is clear that for the deeper fiber the non-propagating potential overshadows the propagating potential as the fiber length decreases, explaining the increase for MNF. For

the more superficial fiber the influence of the non-propagating potential is not so intense and explains the decrease in MNF.

Although no movement was included in the model (i.e., the volume conductor geometry did not change during the propagation of each IAP), the model proposed can be used to simulate sEMG signals detected during a dynamic task, assuming that the changes in muscle geometry occur in a time interval much longer than that needed for the propagation of the AP along the muscle fiber. Since the interval of time between generation and extinction of an AP is 20-30 ms, this constraint is not critical. To simulate signals during dynamic contractions, the muscle length (i.e., the shape of the volume conductor) can be specified for each activation of a specific muscle fiber. The length will be the same during the interval of time needed for the complete generation of the surface AP but may change for each discharge of each muscle fiber. This provides the means for assessing the effect of geometrical factors on the features of sEMG signals detected during movement, an issue on which many past works have focused with simpler models (Schulte, Farina, Merletti, Rau & Disselhorst-Klug 2004; Rainoldi, Nazzaro, Merletti, Farina, Caruso & Gaudenti 2000; Maslaac, Parker, Scott, Englehart & Duffley 2001; Farina, Merletti, Nazzaro & Caruso 2001). The representative results on SFAPs presented in this chapter underline that amplitude and spectral content of the signal may change significantly owing to changes in muscle length, independently of the intensity of muscle activation or of the population of active MUs (Mesin, Joubert, Hanekom, Merletti & Farina 2006).

4.5. GENERAL CONCLUSION

For the validation of the model the simulations have to be compared to results obtained from experiments. This is a difficult task, since the activation strategies of the MUs at different joint angles in experimental conditions cannot be controlled. However, significant changes in sEMG amplitude with muscle shortening, depending on the location of the electrode, have been reported (Rainoldi, Nazzaro, Merletti, Farina, Caruso & Gaudenti 2000). Similar considerations hold for frequency variables (Farina, Merletti, Nazzaro & Caruso 2001).

In conclusion, this study proposes an approach for precise simulation of sEMG signals as generated by a muscle at different lengths. The model is innovative with respect to previous approaches since it provides, for the first time, the description of the muscle conductivity tensor according to the orientation of the muscle fibers during shortening.

This model constitutes an important tool for interpreting sEMG signal features in dynamic tasks. The model is expanded analytically to include the simulation of MUAPs. Representative simulations will be shown in the next chapter.

5. RESULTS: EFFECT OF MUSCLE SHORTENING ON MUAPS

The objective of this chapter is to investigate the influence of muscle shortening on the MUAP waveform. Results for the effect of muscle shortening on the SFAP waveform were shown in chapter 4. The MU can be seen as the functional unit of the muscle and the MUAP can be seen as the basic building block of the sEMG (Roeleveld et al. 1997b). Understanding the MUAP is a basis for understanding sEMG.

It is important to understand the influence of geometrical changes on the surface signal as it happens during dynamic or dynamic-like contractions. The model used in this study also simulates a conductivity change with the shortening of the muscle. The conductivity becomes a function of the curvilinear fiber path. Together with the inhomogeneity due to the change in geometry one also has an inhomogeneity in the volume conductor in the direction of source propagation.

As mentioned before, the MU comprises a number of single fibers. Investigating both SFAPs and MUAPs is important, since the translation from SF to MU holds variation in end-plate position, fiber endings, position of muscle fibers within an MU and position of MUs within a muscle (Stegeman, Blok, Hermens & Roeleveld 2000). The MUAP contains information concerning the length, depth and orientation of the muscle fibers, the width of the innervation and termination zones and information on the MU territory (Merletti, Roy, Kupa, Roatta & Granata 1999b).

The shape of a MUAP is dependent on geometrical factors such as the position of the MU relative to the detecting electrodes as well as the size, shape and orientation of the

detection electrodes (Stashuk 1999). Muscle shortening amplifies the influence of these geometrical effects. With joint angle changes or muscle shortening the muscle might slide underneath the skin, changing the relative position of the electrodes with respect to the innervation and extinction zones (Farina, Merletti, Nazzaro & Caruso 2001; Rainoldi, Nazzaro, Merletti, Farina, Caruso & Gaudenti 2000; Maslaac, Parker, Scott, Englehart & Duffley 2001; Schulte, Farina, Merletti, Rau & Disselhorst-Klug 2004). This implies that changes in amplitude and frequency during dynamic conditions may wrongly be attributed to different levels of muscle activation rather than to the influence of geometrical artefacts.

In this chapter the influence of fiber location, electrode position, IED and the detection system used during contractions at different joint angles will be investigated. MNF and ARV estimated from the simulated MU surface potentials are used as the comparative estimators.

5.1. METHOD

To include results on MUAPs the model was expanded by the summation of a number of spatially distributed SFAPs. Results obtained for these MUAPs show differences from results for SFAPs since the temporal variation in the triphasic propagating wave of the different SFAPs causes phase cancellation (Roeleveld, Stegeman, Vingerhoets & Van Oosterom 1997b; Roeleveld & Stegeman 2002).

Since the potential contribution of an SF is known, it is used to find the surface potential of the MU. An MU consists of a number of SFs. When an MU contracts, each of these SFs provides a path for a travelling tripole. The MU potential is a spatial and temporal summation of the potentials resulting from the SFs of that MU (Roeleveld, Stegeman, Vingerhoets & Van Oosterom 1997b; Griep, Gielen, Boon, Hoogenstraten, Pool & Wallinga de Jonge 1982). There is some temporal variation at the end-plate from where the tripole initiates; this variation is also present at the corresponding tendon ending.

Expanding the model was done by assigning each SF in the MU a random starting position chosen from a normal distribution. For the model 300 SFs are included in an MU, with an IZ spread of 12 mm. Only spatial distribution was implemented. CV was the same for all fibers of the MU.

This chapter will show that the end-plate position, in combination with the moment of activation, influences the MUAP shape considerably, mainly with respect to the muscle fibers close to the electrode. This effect was also noted by Griep, Gielen, Boon, Hoogenstraten, Pool and Wallinga de Jonge (1982).

Figure 5.1 represents a simplified version of constructing the MUAP.

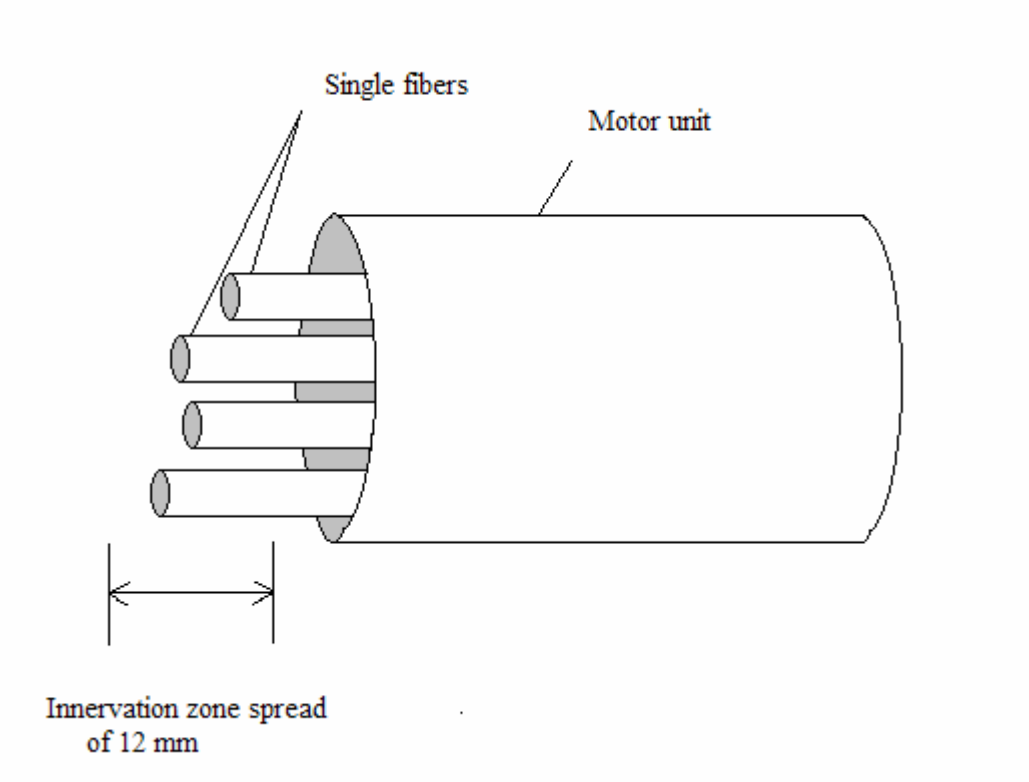

Figure 5.1. An MU constructed from SFs with spatial variation at the IZ

The expanded model used to generate the results in this chapter is based on the superposition of the muscle fiber potentials for the SFs in that MU. This assumption has also been used by Dimitrov and Dimitrova (1998) and Griep, Gielen, Boon, Hoogenstraten, Pool and Wallinga de Jonge (1982).

5.2. RESULTS WHEN USING MNF AS AN ESTIMATOR

As in chapter 4, the changes in frequency content are quantified using MNF as the spectral descriptor.

5.2.1. MNF for different muscle lengths and different fiber depths

Figure 5.2 is a combined representation of MNF computed at seven different MU depths. Each graph represents a depth specified by the variable R_t. R_t = 1.25 mm represents the

deepest fiber. For each depth the MNF for five different muscle lengths is presented. The MNF in each instance was computed using three different detection systems: monopolar, single and double differential electrode systems. An IED of 10 mm was used and 0° angular displacement. The MNF values are normalised with respect to the values obtained at the longest muscle length.

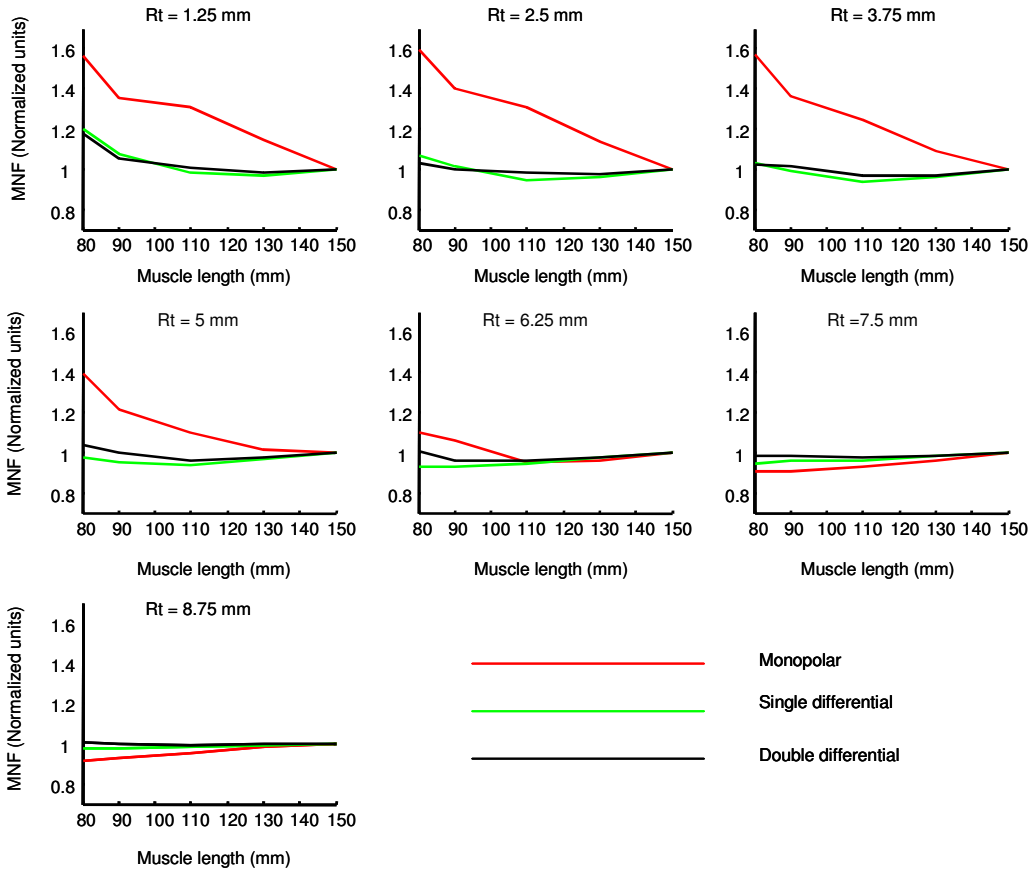

Figure 5.2. MNF computed at seven fiber depths, for five different muscle lengths using three different detection systems

Discussion

From figure 5.2 it can clearly be seen that even though the intensity of muscle activation is not modelled, muscle shortening has a significant effect on MNF. It is also clear that deeper MUs are more affected by muscle shortening than superficial MUs. Furthermore, the monopolar detection system shows a steeper decline towards the relaxed position than the other two detection systems.

Conclusion

When a muscle shortens, the diameter of the muscle fiber, and therefore the overall diameter of an MU, increases. This results in a change in geometry, implying that if an MU were considered at a specific depth before contraction it will be at a deeper depth after contraction because the overlaying MUs increased their diameter. A change in depth means that the relative distance between the source of the MUAP and the detection system has now changed. MNF will theoretically increase with an increase in fiber diameter. Fiber diameter increases with shortening, implying that MNF will increase with shortening (Roy, De Luca & Schneider 1986).

For every MUAP there are two main components contributing to the signal, namely the propagating and the non-propagating parts of the AP. As mentioned before in chapter 2, the propagating component of the signal is generated during the travelling of the IAP along the fiber. The non-propagating component stems from the origination of the AP at the IZ and its extinction at the end-plate.

In effect the surface-detected potentials are then affected by variations in 1) the conductivity properties of the muscle tissue, 2) the relative electrode-source distance and 3) the location of innervation and tendon zones.

The general effect is that MNF tends to increase as the muscle contracts, reaching a peak when the muscle is almost half its original length. From the above comments this can be attributed to the high-frequency non-propagating component of the AP. As the muscle contracts the IZ, the end-plates and the detection system change their relative position with respect to one another. For a more contracted muscle the non-propagating components at the innervation and tendon zones are closer to the detection system, influencing the resulting signal as seen in figure 5.2. The monopolar detection system is more sensitive to non-propagating components and shows a larger MNF than the single and double differential detection systems at the most contracted position. Single and double differential detection systems largely reduce the non-propagating components. As can be seen from figure 5.2 they are less affected than the monopolar system. For the more superficial MUs the MNF is almost equal at all shortenings, although a slight decrease can be seen for the monopolar detection system at R_t = 8.75 mm. This is almost in direct contrast with the rest of the results and can be attributed to spectral content being

significantly altered by the change in the geometry as well as the change in the conductivity tensor of the system.

5.2.2. MNF at different IEDs

Figure 5.3 presents the MNF computed for the five muscle lengths obtained with three different electrode distances. Results were obtained for IED = 4 mm, IED = 10 mm and IED = 16 mm. Results are again shown for five different MU depths and for the three detection systems used before. Results are normalised with respect to MNF computed at the most relaxed position.

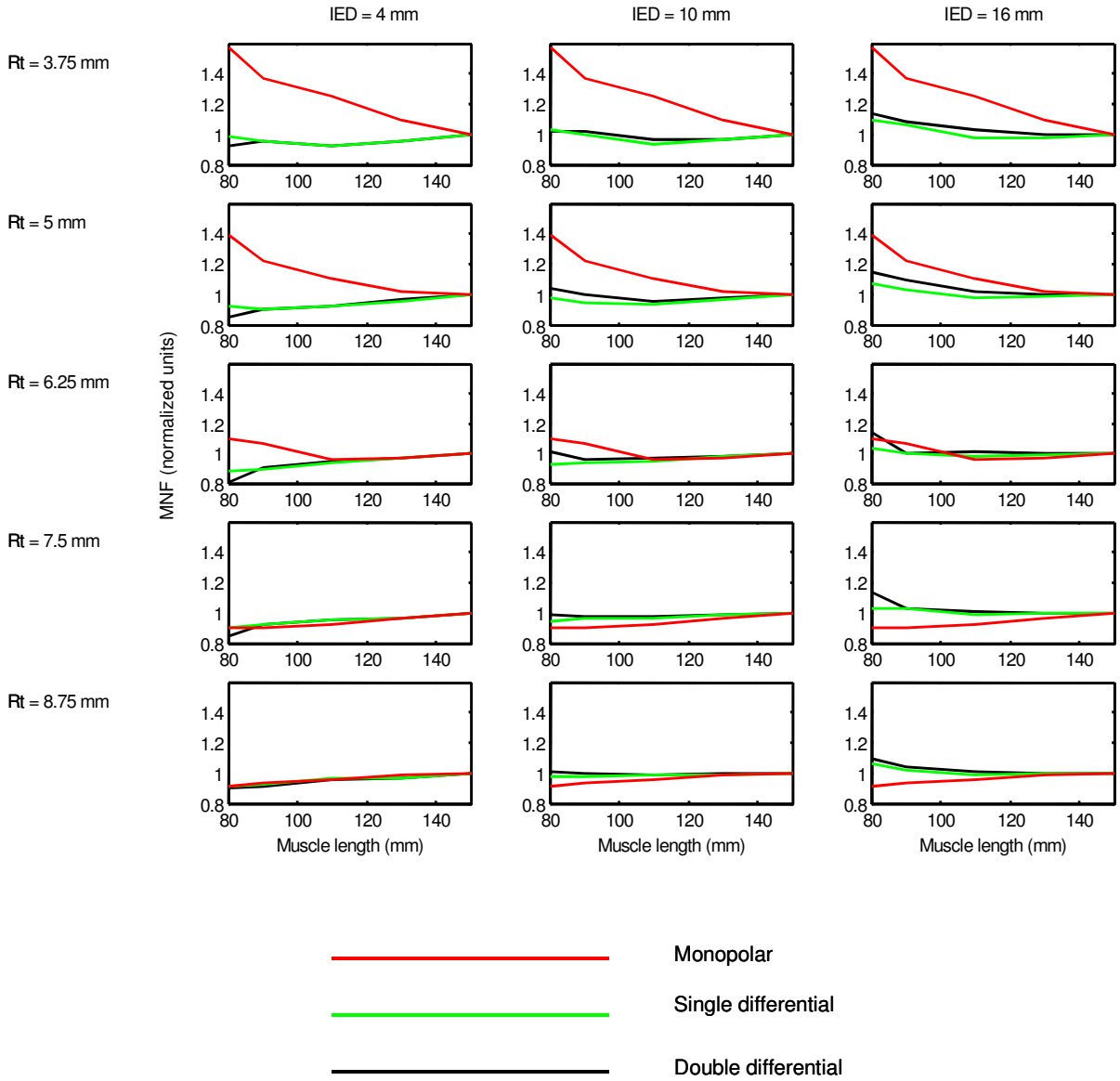

Figure 5.3. The influence if IED on all simulated muscle shortenings

Discussion

Figure 5.3 shows the effect of different IEDs on MNF. Both the SD and DD detection systems are shown with monopolar detection included as a reference condition.

From figure 5.3 it can be seen that the calculated values for MNF become slightly larger for larger IEDs. For the smaller IED, IED = 4 mm, it seems as if some information is lost at the most contracted position where the DD signal gives a very low MNF value. If a quick comparison is made between figures 5.2 and 5.3 it is worth mentioning that in both figures one has a monotone MNF when single and double detection is used at the most superficial fiber with an IED = 10 mm. From figure 5.3 it is evident that if the IED is increased to 16 mm, the MNF also increases, showing that for a larger IED more high frequency components are included. For deeper fibers the influence of IED on MNF becomes less pronounced.

Conclusion

IED is directly related to detection volume. Larger IEDs imply a larger ″pick-up volume″; if the IED is too large, non-propagating components generated at the innervation and tendon zones will have a greater influence on the EMG waveform (Merletti, Lo Conte, Avignone & Guglielminotti 1999a). Non-propagating components are high-frequency components that have no relation to the propagating part of the EMG signal. Schulte, Farina, Merletti, Rau and Disselhorst-Klug (2004) found that the MNF is least affected by shortening when using smaller IEDs. However, if the IED is too small the signal amplitude will decrease significantly and valuable information may be lost (Reucher, Silny & Rau 1987).

As can be seen in figure 5.3, large IEDs imply less variability. This is important to remember in dynamic conditions. Slight changes in electrode positioning or muscles sliding beneath electrodes effect the surface EMG less if the IED is larger (Farina, Cescon & Merletti 2002). MNF and CV are influenced in the same way by IED. However, figure 5.3 also shows that for a small IED, i.e. 4 mm, valuable information may be lost. For IED = 4 mm and R_t = 8.75 mm it seems as if the smaller IED rejects parts of the signal to such an extent that some of the spectral information is lost at the most contracted state. Both these effects are enhanced for deeper fibers. For deeper fibers the distance from the detection system to the fiber is similar to the distance from the detection system to the IZ or tendon ending. This implies that the resulting potential will have equal weight from the

propagating and non-propagating components of the EMG signal. This implies that an increase in fiber depth will enhance sensitivity to fiber shortening (Schulte, Farina, Merletti, Rau & Disselhorst-Klug 2004).

Mechanical, electrophysiological and MU control properties are different for different fiber lengths. The interpretation of results shown in this study indicates that the interpretation of MNF changes during movement may be unreliable, especially if the electrode position with respect to the muscle fibers is not monitored.

5.2.3. MNF measured at different angles

For the model used in this study the *biceps brachii* muscle was chosen. This particular muscle is well suited for sEMG analysis because of its long and parallel fibers with the main IZ often located at the muscle belly (Farina, Merletti & Fosci 2002). When sEMG is used in kinesiology studies the muscles under investigation do not always have the ideal parallel fibers. It is then very likely that the detection system may be misaligned with the fiber or in this case with the MU. Measuring MUAPs from different angles can give a representation of measurements taken from misaligned MUs and detection systems.

Although CV is not one of the parameters under discussion in this study it is worth mentioning that the CV of an MU is significantly affected by the angle between the array and the muscle fibers (Merletti, Roy, Kupa, Roatta & Granata 1999b). This effect is enhanced when the active fibers are not located symmetrically on the two sides of the electrode array and if the width of the active portion of the muscle is not sufficiently larger than the array projection in the direction transversal to the fibers.

Figures 5.4 and 5.5 are a representation of MNF values computed with the detection system placed at an angle α from the MU. Figure 5.4 represents both the SD and the DD detection systems. The values are not normalised. MNF is computed for two depths, R_t = 6.25 mm and R_t = 8.75 mm. Three different muscle lengths are shown. Figure 5.5 has the same conditions as figure 5.4, but shows the monopolar detection system with the SD detection system. The IED = 5 mm.

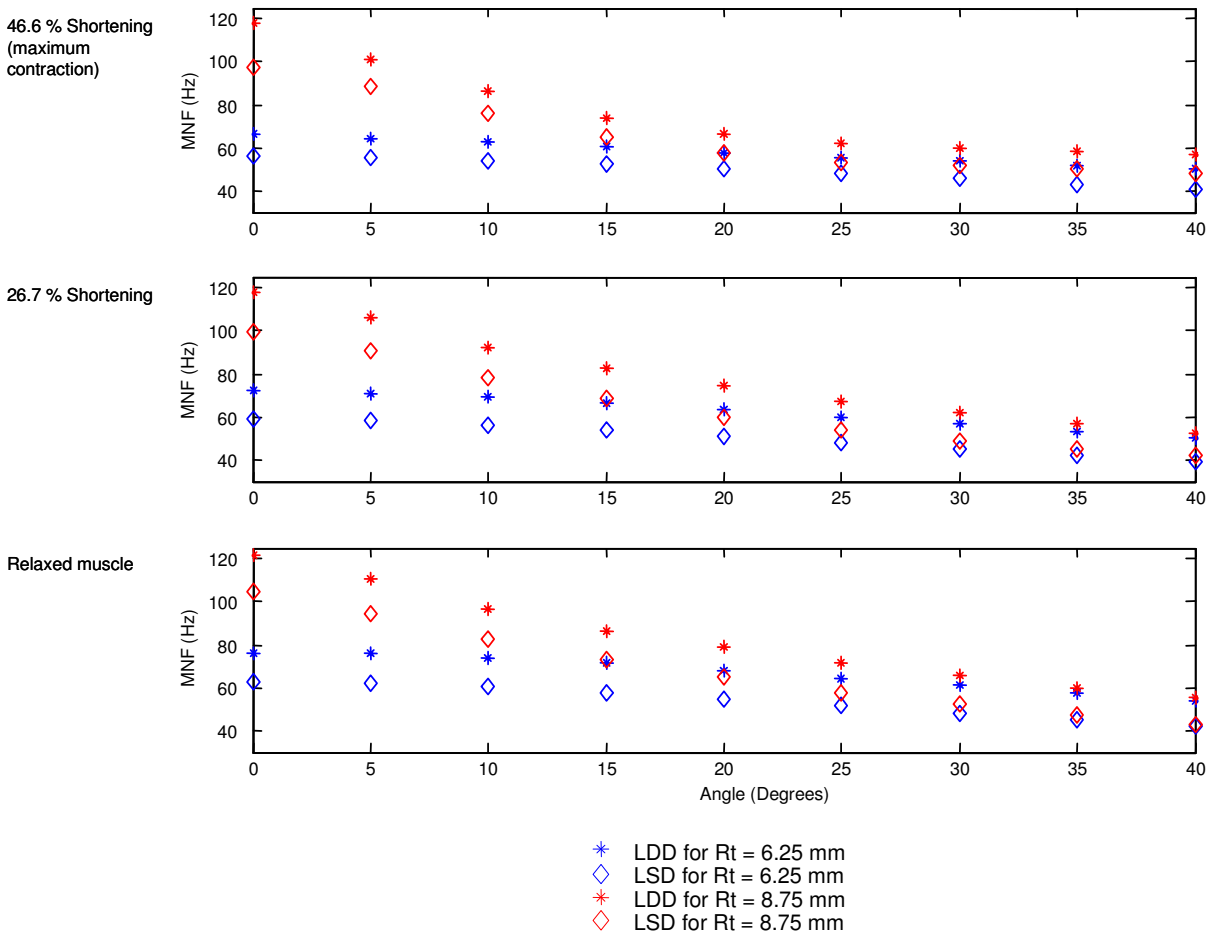

Figure 5.4. MNF values computed with the SD and DD detection systems placed at different angles from the MU

Discussion and conclusion

For both figure 5.4 and 5.5 the MNF decreases as the angle between the MU and the detection system increases; this was also found by Merletti, Lo Conte, Avignone and Guglielminotti (1999a) and Farina, Cescon and Merletti (2002). In Figure 5.4 the decrease for the superficial fibers is more exponential, whereas the decrease for the deeper MU is more monotonous. SD detection always has lower MNF values than the DD system, but higher values than the monopolar system. For all muscle lengths in figure 5.3, for the superficial fibers the difference in MNF values at different muscle lengths is very little. In figure 5.4 the difference for MNF values at different muscle lengths is more pronounced for the monopolar detection system. However, it seems that for angles larger than 20° the monopolar system maintains constant and equal values for both MU depths, implying a saturation point has been reached and no more valuable information can be obtained when the misalignment has reached these proportions.

The increased lateral distance between electrodes and MUs cause a widening and change of shape of the signals (Merletti, Lo Conte, Avignone & Guglielminotti 1999a). The shape of the AP is changed owing to the effect of tissue anisotropy. This may lead to an underestimation when CV value is computed (Merletti, Roy, Kupa, Roatta & Granata 1999b). Farina, Cescon and Merletti (2002) also showed that the effects of spatial filter, electrode size and fiber misalignment are minor, especially with respect to the ARV values obtained, as shown in the next section.

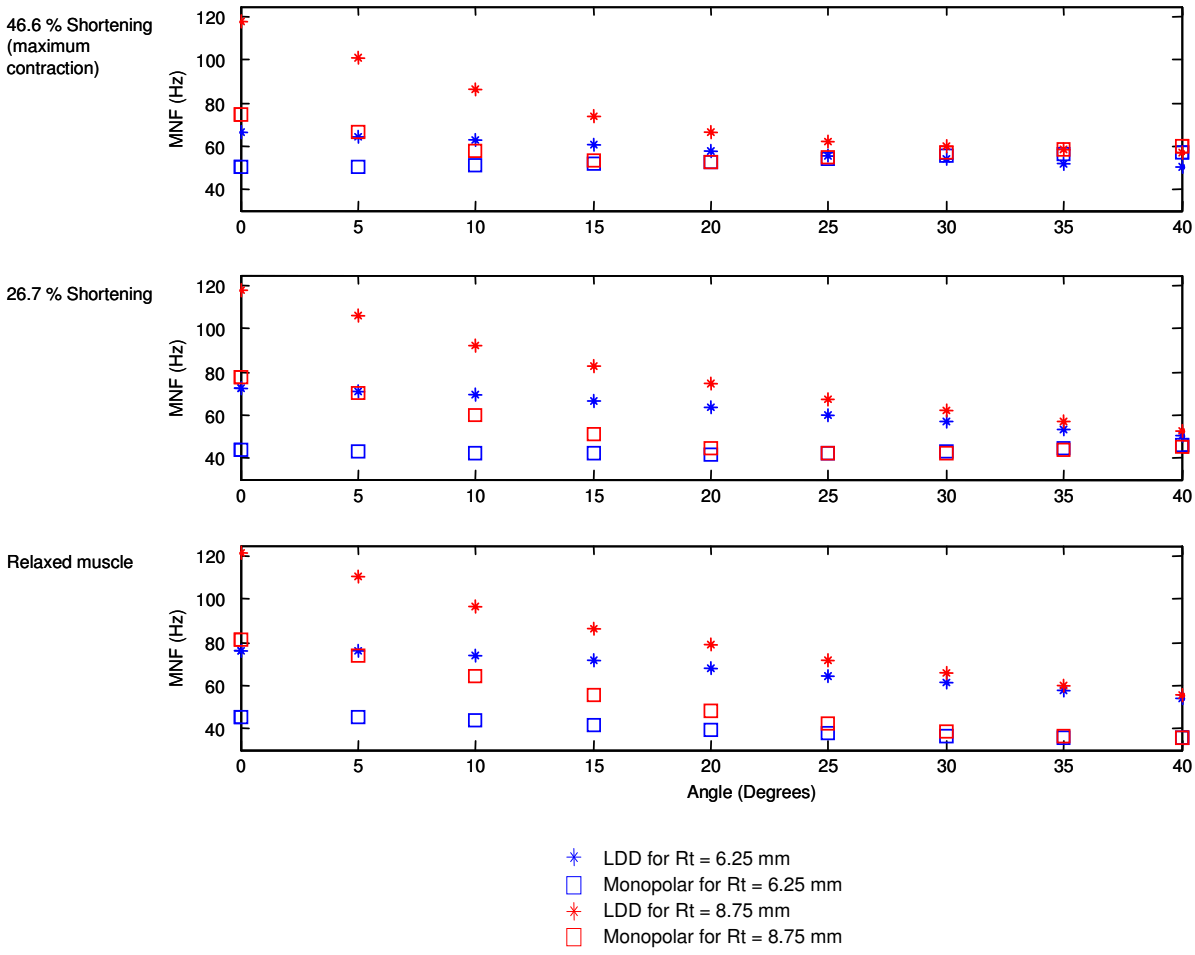

Figure 5.5. MNF values computed for the monopolar and SD detections systems placed at different angles from the MU

5.3. RESULTS WHEN USING ARV AS AN ESTIMATOR

When the joint angle of a limb changes the muscle will shorten. The volume of the muscle, however, remains constant, resulting in a change in diameter of the MUs. This implies that as the muscle contracts (or shortens) the diameter of the MUs will increase (Webster

1998). For sEMG this involves a change in the distance between the intracellular source and detection system, leading to differences in amplitude measurements. When using sEMG for force estimation in kinesiology studies, a change in geometry of the muscle may lead to incorrect measurements and incorrect force estimation (Merletti and Parker 2004).When modelling dynamic-like sEMG simulations it is important to include these geometrical artefacts in order to understand their influence on the resulting sEMG signal better.

SEMG amplitude measurements are used as an indication of force production of a muscle (Moritani & Muro 1987). An important and much investigated subject is the assessment of the contribution of single muscles to the total force exerted by the group (Merletti & Parker 2004). This also relates to the contribution of single MUs to the total force exerted by a single muscle (Roeleveld & Stegeman 2002). The relationship between EMG amplitude and force depends on a number of factors. SEMG amplitude depends strongly on electrode location. Placing electrodes near or on either the IZ or the end-plates will result in small noisy signals very sensitive to electrode movement (Merletti, Lo Conte, Avignone & Guglielminotti 1999a). The relationship between force and EMG may depend on subcutaneous fat layer thickness, inclination of fibers with respect to the detection system, distribution of CVs of the active MUs, IED, spatial filter applied, presence of crosstalk, and the degree of synchronisation of active MUs. In addition to all these limitations the relationship between EMG amplitude and force should be adapted to the muscle condition, including muscle length/joint angle, muscle temperature, fatigue and a number of other physiological factors. For example, in submaximal contractions the fatigued muscle generates EMG signals with larger amplitudes compared to the unfatigued condition although maintaining constant force (Masuda, Masuda, Sadoyama, Inaki & Katsuta 1999). EMG amplitude is a good indicator of muscle activation and a qualitative index of activation change with respect to a reference condition.

5.3.1. ARV measured at different shortenings and different fiber depths

Figure 5.6 is a combined representation of ARV computed at seven different MU depths, each graph representing a depth specified by the variable R_t. For a specific depth the ARV for five different muscle lengths is presented. ARV in each instance was computed using three different detection systems: monopolar, single and double. An IED of 10 mm was used and 0° angular displacement. The ARV values are normalised with respect to the values obtained at the longest muscle length.

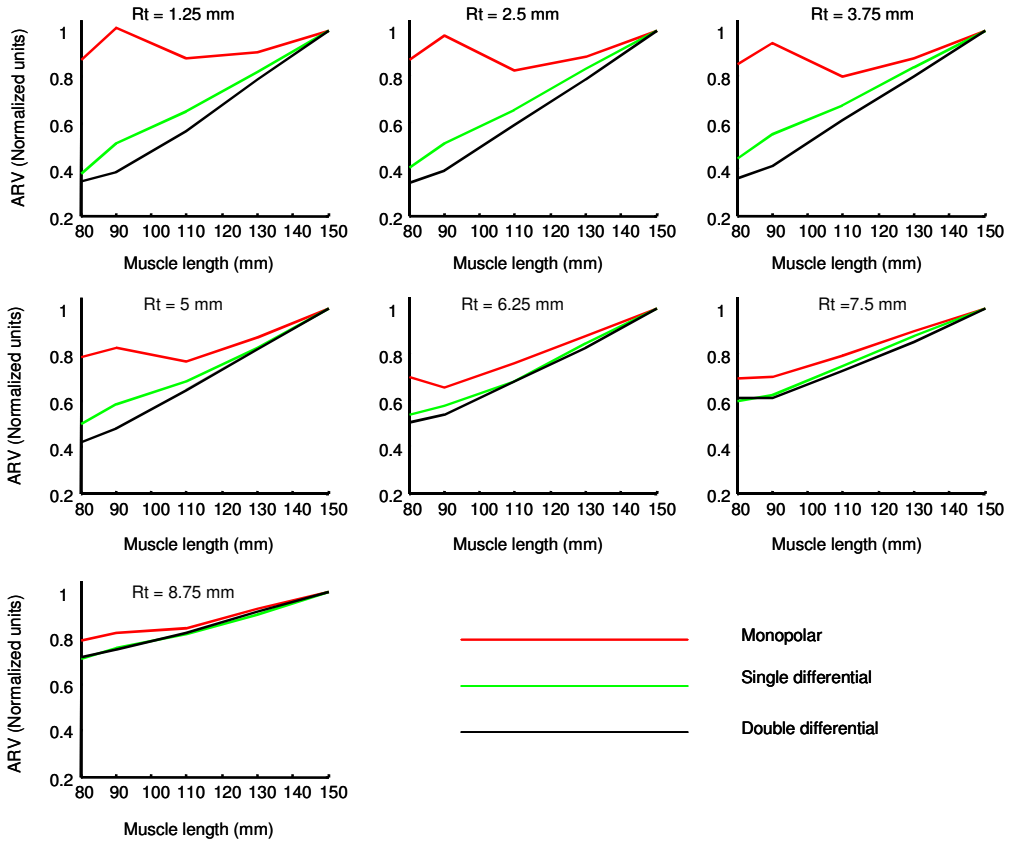

Figure 5.6. ARV values computed at five shortenings for seven different MU depths. Three detection systems were used: monopolar, SD and DD. ARV values are normalised with respect to values obtained for the relaxed muscle position.

From figure 5.6 it is evident that muscle shortening has a prominent effect on ARV. This was also determined in a number of models simulating joint angle changes (Rainoldi, Nazzaro, Merletti, Farina, Caruso & Gaudenti 2000; Lowery, Stoykov & Kuiken 2003; Lowery, Stoykov, Taflove & Kuiken 2002; Roeleveld, Blok, Stegeman & Van Oosterom 1997a; Farina, Merletti, Nazzaro & Caruso 2001; Maslaac, Parker, Scott, Englehart & Duffley 2001; Farina, Cescon & Merletti 2002). Moreover, it is clear that ARV decreases with a decrease in muscle length. For the DD detection system the decrease is more pronounced, while for more superficial fibers there is little difference between the detection systems used and the results obtained. For deeper fibers the monopolar detection system seems more monotonous.

Discussion

As was discussed for the MNF estimator, there are two main components contributing to the MUAP, the propagating and non-propagating components. Monopolar recordings of

the ARV seem less sensitive to the influence of shortening. This can be attributed to the fact that non-propagating components have a larger overall influence on monopolar recordings, whereas these components are rejected by the SD and DD detection systems. As the muscle contracts the MUs increase their diameter and the source moves further away from the electrodes, decreasing the amplitude of the propagating component. The end-plate and IZs move closer to the electrode, increasing the amplitude of the non-propagating component. Because monopolar recording does not reject the non-propagating component, the amplitudes of the propagating and non-propagating components counteract each other (Mesin, Joubert, Hanekom, Merletti & Farina 2006), presenting a less reliable result. The SD and DD detection systems reject the increasing non-propagating component and for the contracted muscle only leave the decreased propagating component to compute the ARV value with, resulting in the decrease seen in figure 5.6.

The effect of muscle shortening on ARV is less pronounced for superficial fibers. The detection system is always closer to the superficial fibers than to the deeper fibers. For this reason signals simulated from the deeper fibers will include more propagating components, especially as the muscle shortens and the fiber moves even further away from the detection system.

5.3.2. The effect of IED on ARV

Figure 5.7 presents the ARV computed for the five muscle lengths obtained with three different IED distances. Results were obtained for IED = 4 mm, IED = 10 mm and IED = 16 mm. Results are again shown for five different MU depths and for the three detection systems used before. The monopolar detection system is included as a reference, since the IED for this recording system cannot be changed. Results are normalised with respect to ARV computed at the most relaxed position.

Figure 5.8. presents ARV calculated at a range of different IEDs. Values are normalised with respect to the ARV values obtained for an IED = 4 mm.

Discussion and conclusion

Figure 5.7 shows that amplitude selectivity reduces with an increasing IED, as was found by Lowery, Stoykov and Kuiken (2003). Using a DD detection system also reduces amplitude selectivity (Farina, Cescon & Merletti 2002).

From figure 5.8 it is also evident that the more superficial fibers reach a peak value of ARV at a smaller IED than the deeper MUs. The deeper MUs have a steep incline towards larger IEDs. LDD for all MUs is more affected by IED than LSD.

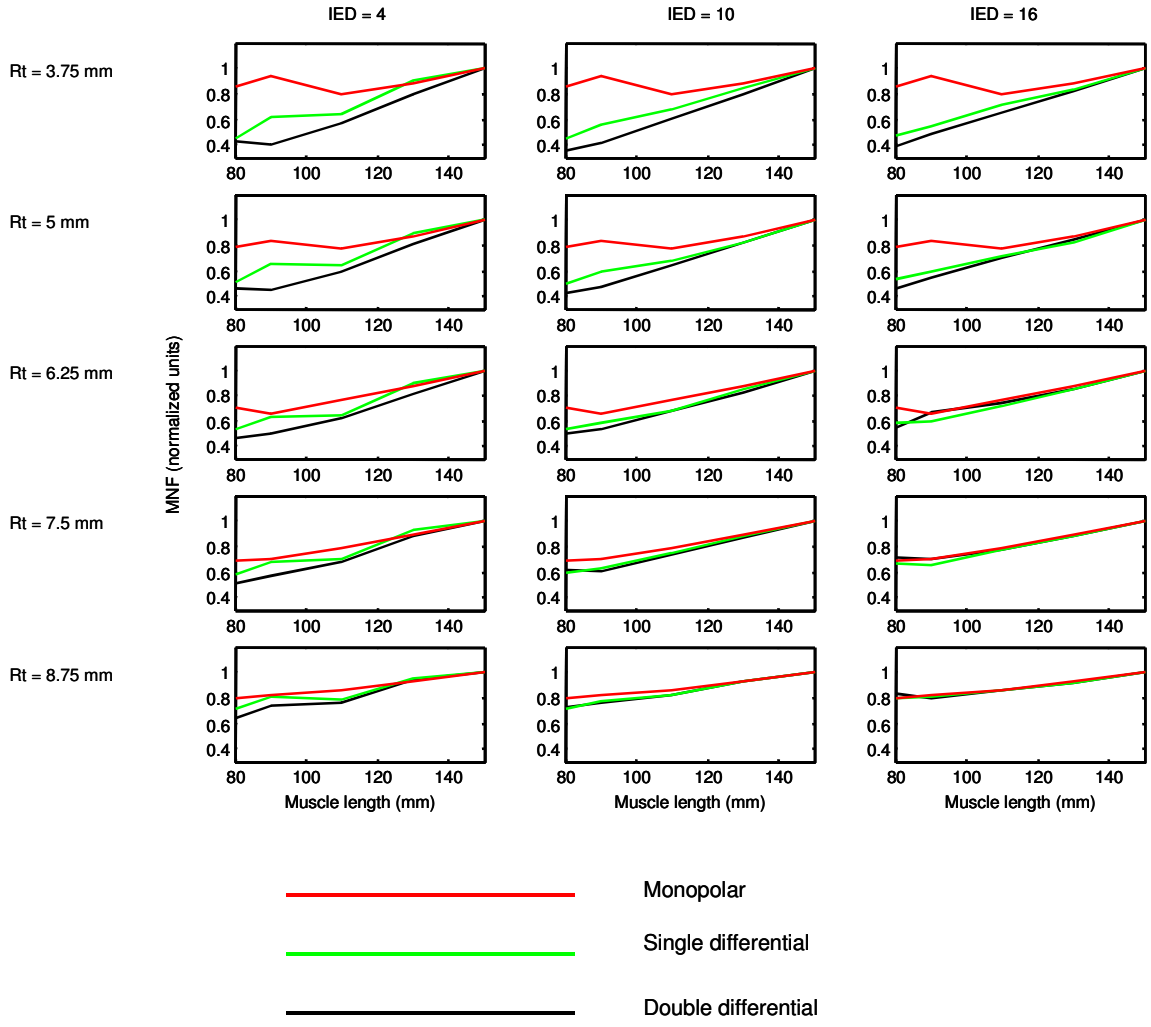

Figure 5.7. The influence of IED on the ARV estimator. Values are normalised with respect to ARV values obtained for the relaxed muscle position.

From figures 5.7 and 5.8 it is evident that different IEDs have a large influence on the ARV estimator. The influence of IED is more pronounced for the ARV estimator than for the MNF estimator. From figure 5.7 it can be deduced that the influence of muscle shortening on the ARV estimator seems less pronounced when a larger IED is used. This leads to the conclusion that large IEDs imply less variability of EMG amplitude in dynamic or dynamic-like conditions when electrodes are individually attached (Farina, Cescon & Merletti 2002). To maximise signal amplitude, larger IEDs are suggested up to 20 mm; however, it is important for the distance between the innervation and termination

zones to be greater than the IED to obtain meaningful estimates of the variable (Merletti, Lo Conte, Avignone & Guglielminotti 1999a).

For the relaxed muscle, changes in IED had a smaller effect than for the 26.7% shortening shown in figure 5.8.

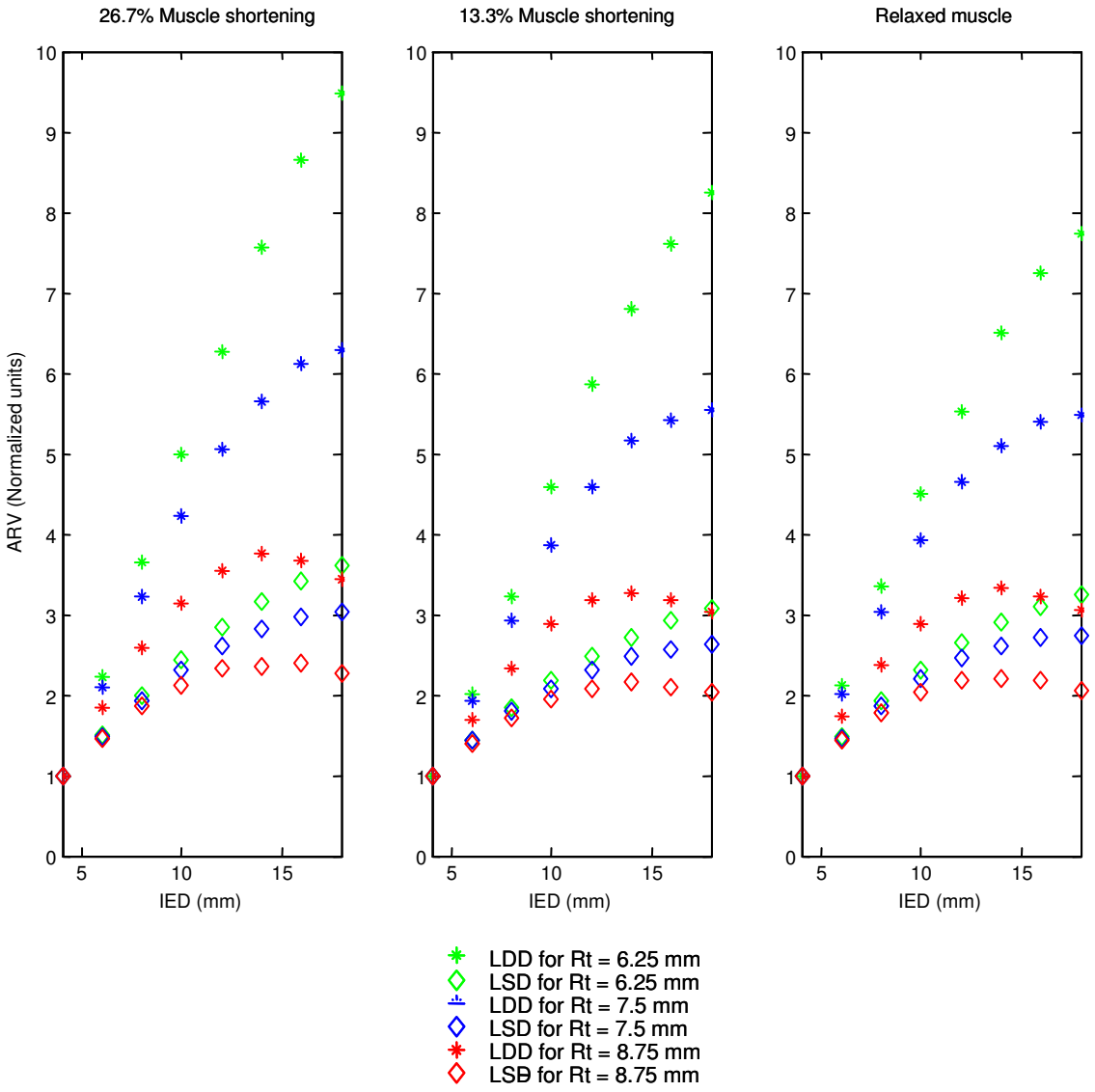

Figure 5.8. ARV vs. IED for SD and DD detection systems. Three MU depths are shown. Values are normalised with respect to the ARV value obtained for IED = 4 mm.

If the DD detection system is used the amplitude is even greater, since this detection system will attenuate the non-propagating component and include a larger part of the propagating component. Signal amplitude increases with larger IED, since more of the propagating part of the potential is included. However, as can be seen from the LSD values

in figure 5.8, the ARV does reach a peak at a certain IED value. The LSD reaches this peak first since it attenuates the non-propagating part less. This implies that there is a critical IED where the negative potential of the non-propagating component influences the total potential in such a way that the ARV will decrease from this point forward.

When the IED is smaller than the length of the MUAP or in the simulated model case smaller than the tripole length (6.9 mm), there is an overlap between opposite profiles under both electrodes. MUAPs of deeper fibers have longer durations and greater overlap. An increase in overlap increases the magnitude (Roeleveld, Stegeman, Vingerhoets & Van Oosterom 1997b).

5.3.3. ARV detected at different angles between source and electrode system

As mentioned for the MNF estimator, simulating a difference in angle between the MUAP source and the electrode detection system is a method of evaluating fiber misalignment in sEMG.

Figure 5.9 and 5.10 is a representation of ARV values computed with the detection system placed at an angle α from the MU. Figure 5.9 represents both the SD and the DD detection systems. The values are not normalised. ARV is computed for two depths, R_t = 6.25 mm and R_t = 8.75 mm. Three different muscle lengths are shown. Figure 5.10 has the same conditions as figure 5.9, but shows the monopolar detection system with the SD detection system. The IED = 5 mm.

Discussion and conclusion

Monopolar detection systems are isotropic, resulting in a transfer function that is close to being invariant to rotation. The isotropy of the detection system implies that the signal detected is independent of the orientation of muscle fibers. This was found by Farina, Cescon and Merletti (2002) and can clearly by seen from figure 5.10. The ARV measured with the monopolar electrode system has a larger ARV and decreases more monotonously than the ARV simulated with the DD detection system.

The overall effect is that the ARV decreases as the angle separating the electrode system from the source increases. This is the theoretically expected result. As with the MNF values, the shortening of the muscle fiber does not have a huge influence when simulations are done with the detection system placed at different angles. When the detection system is

moved transversally along the muscle, it is displaced in equal parts regarding the propagating and non-propagating components of the signal. This implies that both components of the

signal have little influence on the resulting surface potential as the detection systems move further away from the source.

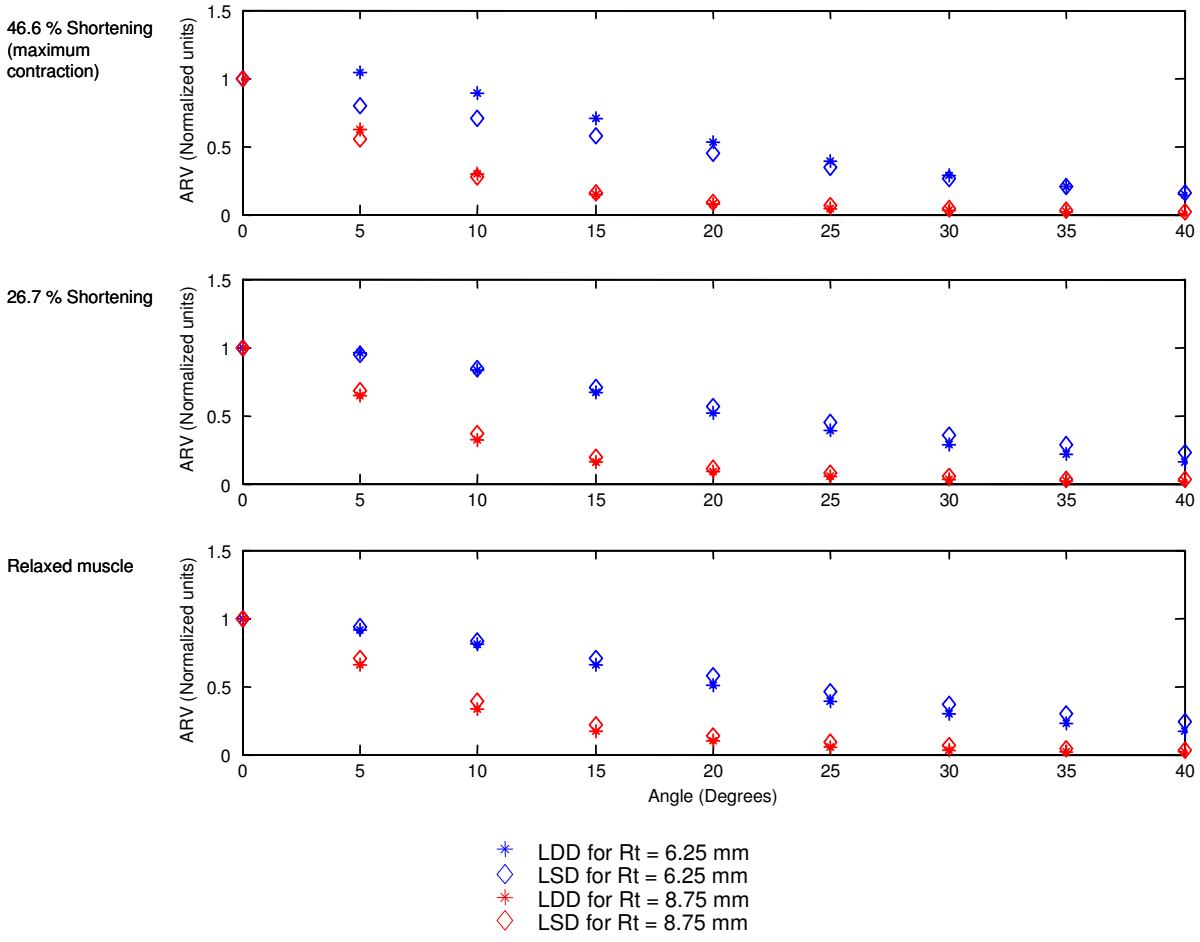

Figure 5.9. ARV values computed with the SD and DD detection systems placed at different angles from the MU

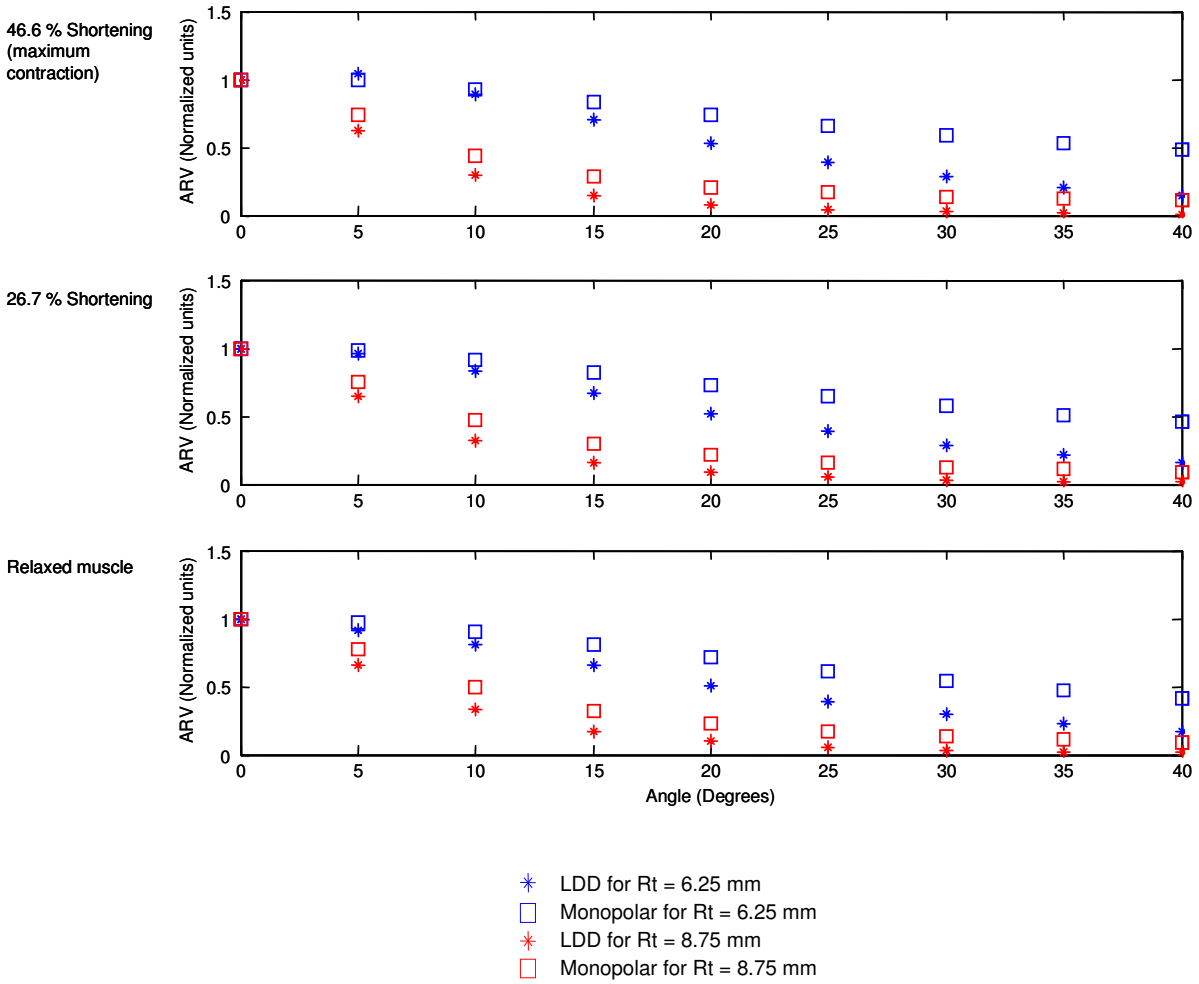

Figure 5.10. ARV values obtained at different electrode locations using DD and monopolar detection

5.4. INVESTIGATING MUSCLE SLIDING

Clinical gait analysis and isokinetic assessment are just some of the dynamic applications for which sEMG is used (Farina, Merletti, Nazzaro & Caruso 2001). Dynamic muscle contractions are those that involve changes in muscle force and joint angle as the contraction progresses (Maslaac, Parker, Scott, Englehart & Duffley 2001). Currently sEMG is the preferred technique to complement movement analysis (Merletti & Parker 2004). Although the model developed in this study does not include changes in force activation of the muscle, the data collected for MNF and ARV estimators at different joint angles are valuable information leading to better understanding of the geometrical artefacts influencing dynamic sEMG.

Electrode location and IED have a significant influence on sEMG estimators. Electrodes have to be located between the innervation and termination zones to obtain valid information. The distance between electrodes is also important, especially when muscle shortening is included to obtain the optimal amount of information without the non-propagating component dominating the data. One of the inconveniences of using sEMG in dynamic or dynamic-like conditions is the geometrical artefact of muscle sliding. With contraction or movement the muscle changes size and moves with respect to the electrodes located over the skin, altering the original electrode placement (Farina, Merletti, Nazzaro & Caruso 2001; Schulte, Farina, Merletti, Rau & Disselhorst-Klug 2004; Merletti & Parker 2004). Since the resulting sEMG is very sensitive to electrode placement, muscle sliding may have a major effect on the ARV and MNF estimators and could result in large geometrical artefacts and misinterpretation of sEMG when used in the determination of muscle activation level or in the investigation of muscle fatigue (Farina, Merletti, Nazzaro & Caruso 2001).

The object of this section of the chapter is to investigate the influence of muscle movement under the skin surface on ARV and MNF estimators.

5.4.1. Results for the geometrical effect of muscle sliding on MNF computations

Figures 5.11, 5.12 and 5.13 are representations of MNF computations along the length of the MU. MNF values are obtained for electrodes spaced at 5 mm intervals. These figures give an indication of the geometrical artefact that can be caused by muscle sliding. Figure 5.11 shows the *biceps brachii* muscle at three shortening conditions. The MNF is calculated with both the SD and DD detection systems. For figure 5.11 only two fiber depths (R_t = 3.75 mm and R_t = 2.5 mm) are shown. In figure 5.12 a more superficial depth (R_t = 7.5 mm) is included. It appears as if more superficial fibers are less influenced by this artefact than deeper fibers. As in figure 5.11, figure 5.12 also shows the MNF calculated with both the SD and DD detection systems, for every 5 mm. Figure 5.13 shows only one fiber depth (R_t = 3.75 mm) but includes the monopolar detection system. None of the representations are normalised.

Figures 5.11, 5.12 and 5.13 indicate what the effect could be if the muscle slides underneath the electrodes, leaving the detection system 5 mm from its original position.

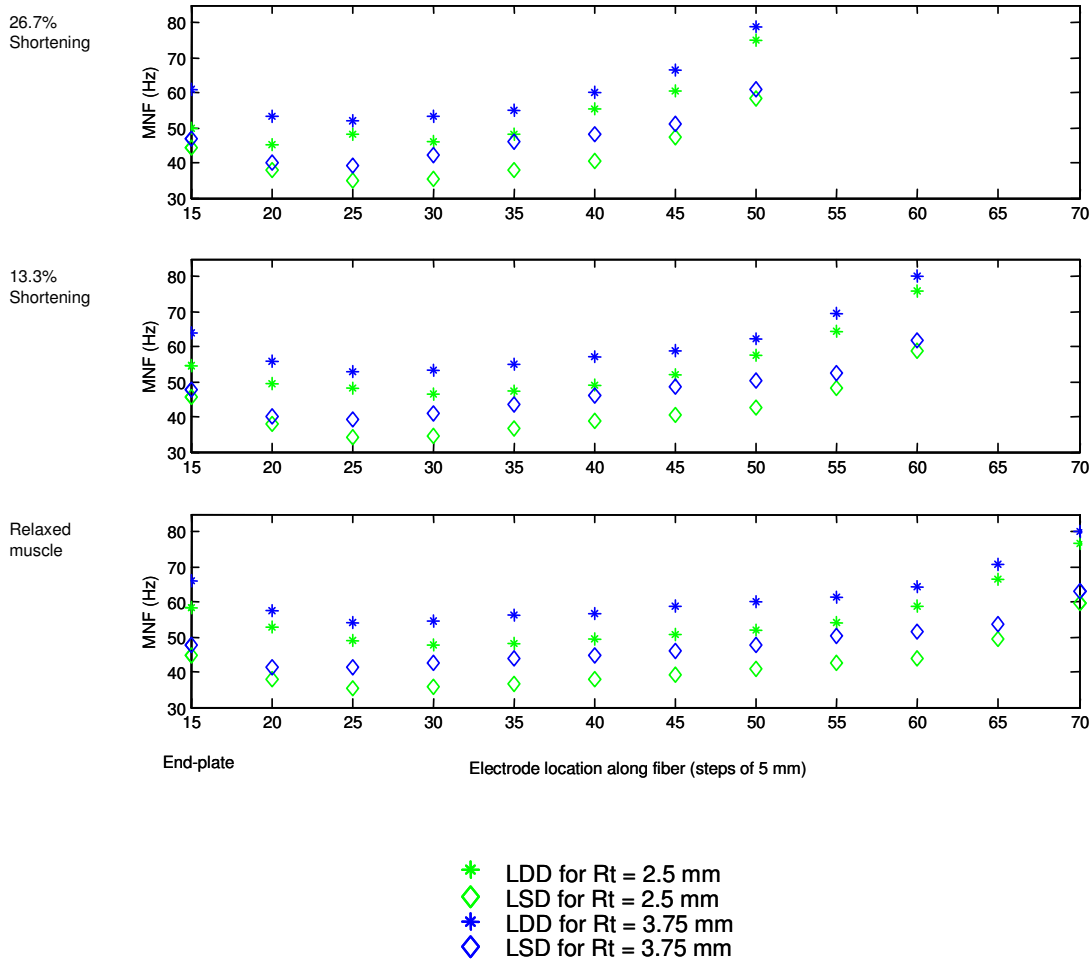

Figure 5.11. MNF measured at 5 mm intervals along the muscle fiber. Two fiber depths are shown, R_t = 2.5 mm and R_t = 3.75 mm. MNF was calculated with both the SD and DD detection systems. The *biceps brachii* muscle is shown in the relaxed position and for the 13.3% and 26.7% shortening conditions.

Discussion and conclusion

From figure 5.11 it is clear that the MNF tends to have a positive bias near the innervation and termination zones. This is attributed to the greater influence of high-frequency non-propagating components near the IZ and tendon region. It is obvious that for a more contracted muscle the space in which to place the electrode system becomes more confined than for a relaxed muscle. Even if electrodes are carefully placed between the innervation and tendon zones, they may shift as soon as the muscle contracts, resulting in higher values of MNF than expected. For the more contracted muscle the high-frequency components are clearly more prominent. The relaxed muscle allows for more variability in the placement of the electrode system. However, it is still clear that if the muscle allows for a shift in the

electrode placement larger than 5 mm the MNF will be erroneous. The relative shift of the muscle with respect to the skin during movement can be up to 3 cm, as has been seen in the semitendinosus muscle (Merletti & Parker 2004).

From figure 5.11 it is evident that not all locations along a muscle will give reliable estimation of the spectral variables (Farina, Merletti, Nazzaro & Caruso 2001). It is important to know the proper electrode location in order to reduce frequency and amplitude estimate variablility due to geometrical artefacts.

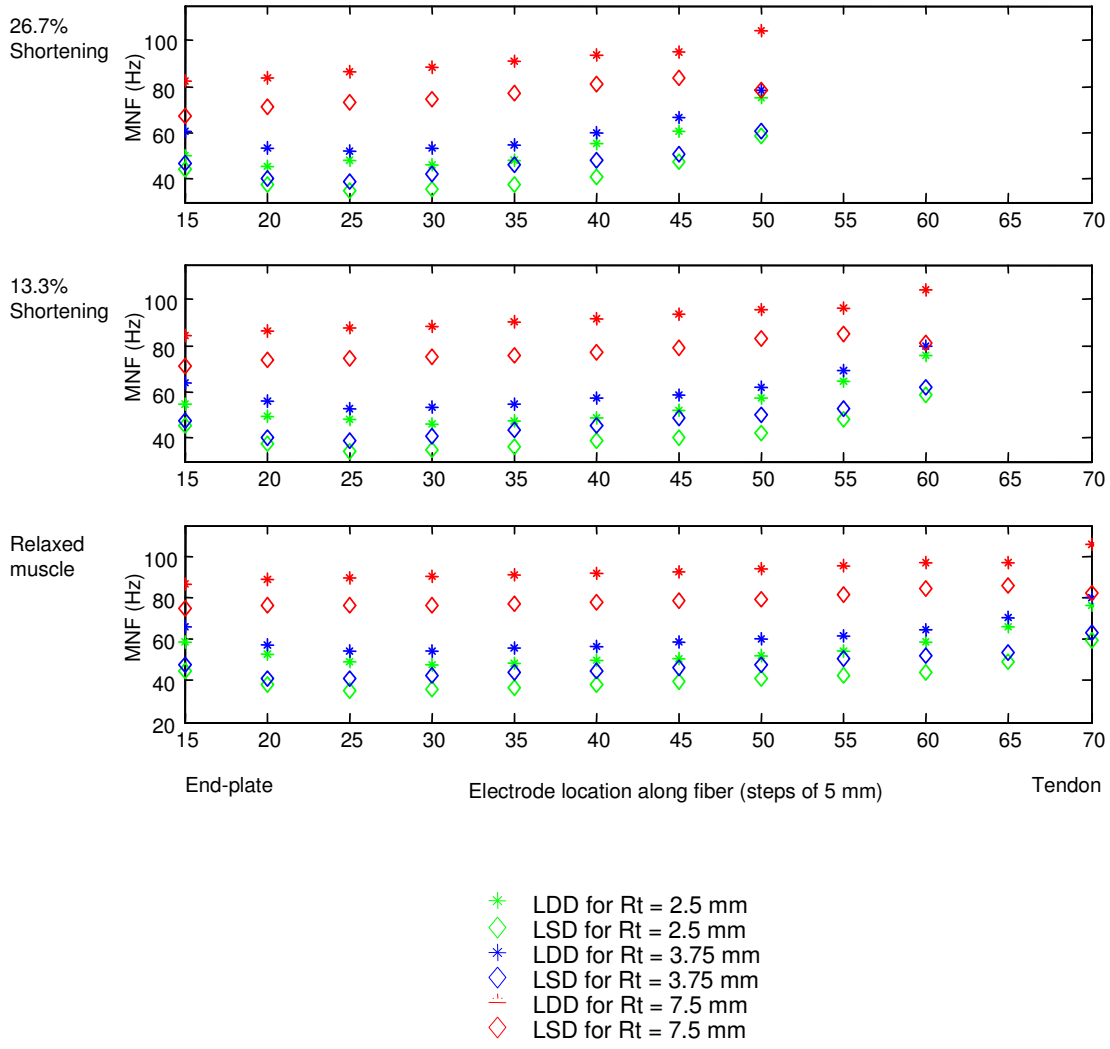

Figure 5.12. MNF measured at 5 mm intervals along the muscle fiber. Three fiber depths are shown, Rt = 2.5 mm and Rt = 3.75 mm and a more superficial fiber at Rt = 7.5 mm. MNF was calculated with both the SD and DD detection systems. The *biceps brachii* muscle is shown in the relaxed position and for the 13.3% and 26.7% shortening conditions.

From figure 5.12 it is clear that the superficial fiber is influenced least by the geometrical artefact of muscle sliding, especially when the muscle is relaxed. However, as the muscle contracts the influence at this depth also increases. Again the increase of MNF near the innervation and tendon zones can be seen clearly. Recently Martin and MacIsaac (2006) have shown experimentally that the total amount of IZ shift for the *brachial biceps* muscle of the arm over a range of joint angles is between 5 and 30 mm, depending on the patient. They showed that this artefact also significantly affects the calculation of the CV.

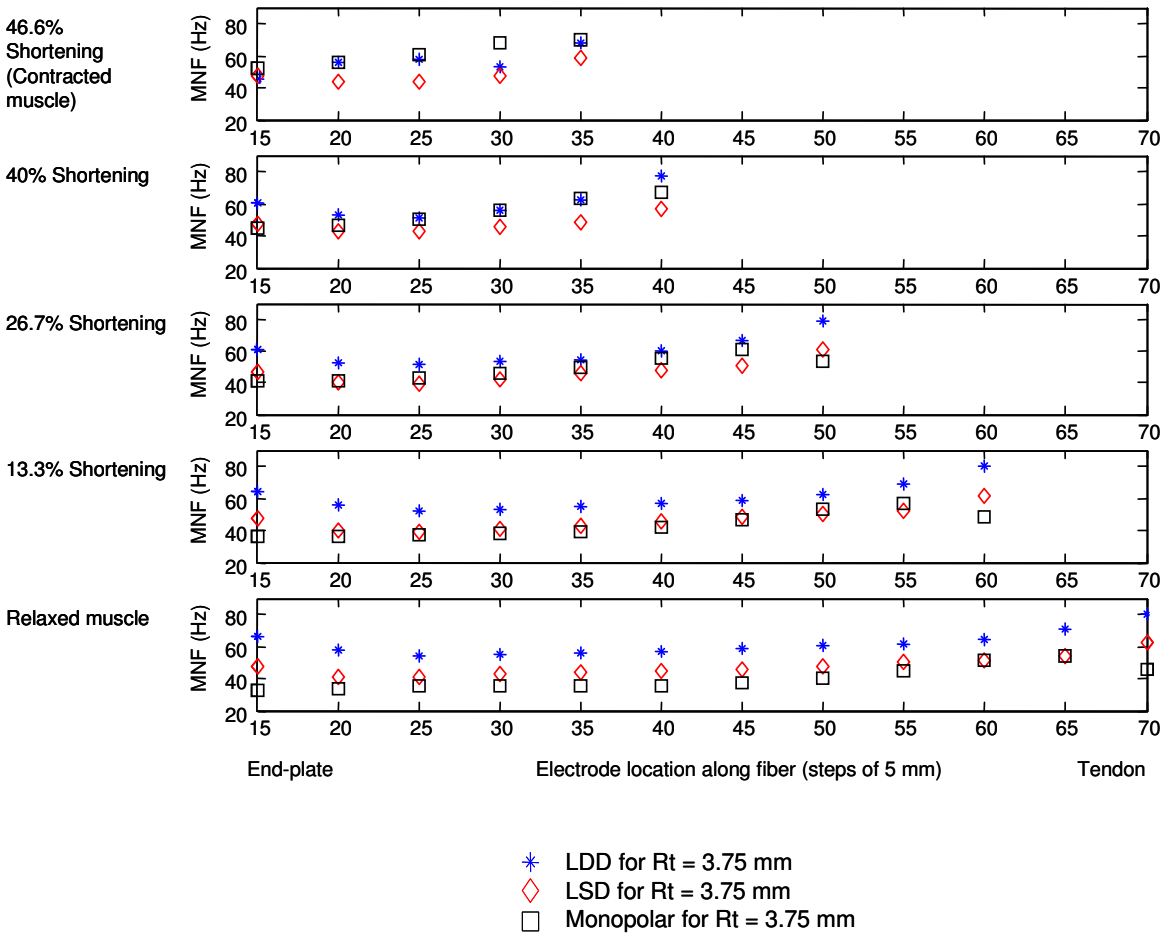

Figure 5.13. **MNF measured at 5 mm intervals along the muscle fiber. Only one fiber depth is shown, Rt = 3.75 mm. MNF was calculated with the monopolar, SD and DD detection systems. The *biceps brachii* muscle is shown in the relaxed position and for the 13.3%, 26.7%, 40% and 46.6% shortening conditions.**

Figure 5.13 shows the influence of muscle sliding beneath the skin on MNF calculations with the monopolar detection system. It appears as though the MNF calculated with the monopolar detection system is more erratic. For the relaxed muscle, the 13.3% and 26.7%

shortening the MNF calculated nearest to the tendon region is significantly smaller than the MNF calculated with the electrodes 5 mm to the left. As explained in chapter 4, the monopolar detection system is more susceptible to the non-propagating signal component. For the DD and SD detection systems the non-propagating components are differentiated and carry less weight than the propagating part of the signal. For the monopolar detection system the non-propagating signal is not differentiated and combines with the propagating part, resulting in a diminished MNF. When using the monopolar detection system it is evident that with the muscle shortened to 46.6% of its original length, even the slightest muscle shift will result in erroneous results. The use of linear electrode arrays when recording sEMG may, to some extent, counter the effect of muscle sliding (Merletti & Lo Conte 1997).

The general conclusion to this section is that muscle shortening has a significant influence on the measurable variables of the sEMG signal. As was found by Rainoldi, Nazzaro, Merletti, Farina, Caruso and Gaudenti (2000), changes in the sEMG waveform when muscle length is altered are due to a change in the distance of neuromusclular junctions from the electrodes. Geometrical changes including the shortening and lengthening of the muscle fibers and the sliding of the muscle underneath the skin, resulting in a transformed electrode position, change in the relative orientation of the muscle fibers with respect to the electrode detection system and variations in the muscle layer thickness add to the variation in spectral and amplitude measurements (Schulte, Farina, Merletti, Rau & Disselhorst-Klug 2004). It is difficult to distinguish between these variables when dissecting an sEMG signal. However, in all cases the influence of the non-propagating signal near the tendon and innervation zone is evident. It is clear that this influence increases with shortening, since these zones then move closer to the placement of the detection system. With muscle shortening or joint angle changes the placement of the electrode detection system is very important. The inclusion of a conductivity tensor, dependent on joint angle changes, in this sEMG model enhances the actual influence of the muscle shortening (Mesin, Joubert, Hanekom, Merletti & Farina 2006).

6. COMPARISON BETWEEN HOMOGENEOUS AND NON-HOMOGENEOUS FIBER PATHS

The sEMG model presented in this study describes a fusiform muscle with muscle fibers following a curvilinear fiber path. In previous studies the conductivity of this fiber path has been accepted as constant with only a difference in the axial and radial conductivities (Lowery, Stoykov, Taflove & Kuiken 2002). This is a basic assumption made to reduce the inherent complexity of the sEMG model. In order to simulate some practical situations, for instance tissue consisting of different conductivities or containing glands or vessels in different locations, a conductivity tensor needs to be introduced into the model (Farina, Mesin & Martina 2004). The analytically derived conductivity tensor of the muscle tissue should be matched with the fiber orientation and can be very complex. Making use of numerical techniques to describe the nonspace invariant volume conductor allows for the insertion of an analytically derived conductivity tensor.

The sEMG model is expanded by including joint angle changes. When the joint angle changes the muscle fiber shortens. With decreasing muscle length, fiber diameter increases. This implies that the shape of the muscle, as well as the direction of the fibers changes. Changes in fiber diameter lead to changes in the shape of the IAP. Including a conductivity tensor in the sEMG model simulates these variations in both the geometry of the volume conductor and the IAP shape changes.

In this chapter the influence of including a conductivity tensor as opposed to modelling a homogeneous volume conductor is briefly shown.

6.1. METHOD

In order to compare potentials obtained using homogeneous and non-homogeneous volume conductors accurately, the same sEMG model is used. Potentials were obtained with the monopolar and SD electrode configurations for R_t = 6.25 mm and for five joint angles. For the non-homogenous condition, the conductivity tensor of Equation 3.12 is used in the model simulations. For the homogeneous condition the conductivity in the radial direction is 0.1 S/m and in the transversal direction 0.5 S/m. These conductivities remain constant through the complete fiber length and do not change as the joint angle changes. As before, the tendon ending was considered isotropic with a conductivity of 0.3 S/m for both the homogeneous and the non-homogeneous simulations.

6.2. RESULTS

Figure 6.1 shows the results for the homogeneous and non-homogeneous potentials obtained using a monopolar electrode configuration. Figure 6.2 shows the same simulations for an SD electrode configuration. Simulations are shown for five joint angles. The distance from the z axis to the fiber is R_t = 6.25 mm. Electrodes are placed in the middle of the fiber between the end-plate and tendon with the fiber located directly under the electrodes. For the SD simulations the IED is 10 mm.

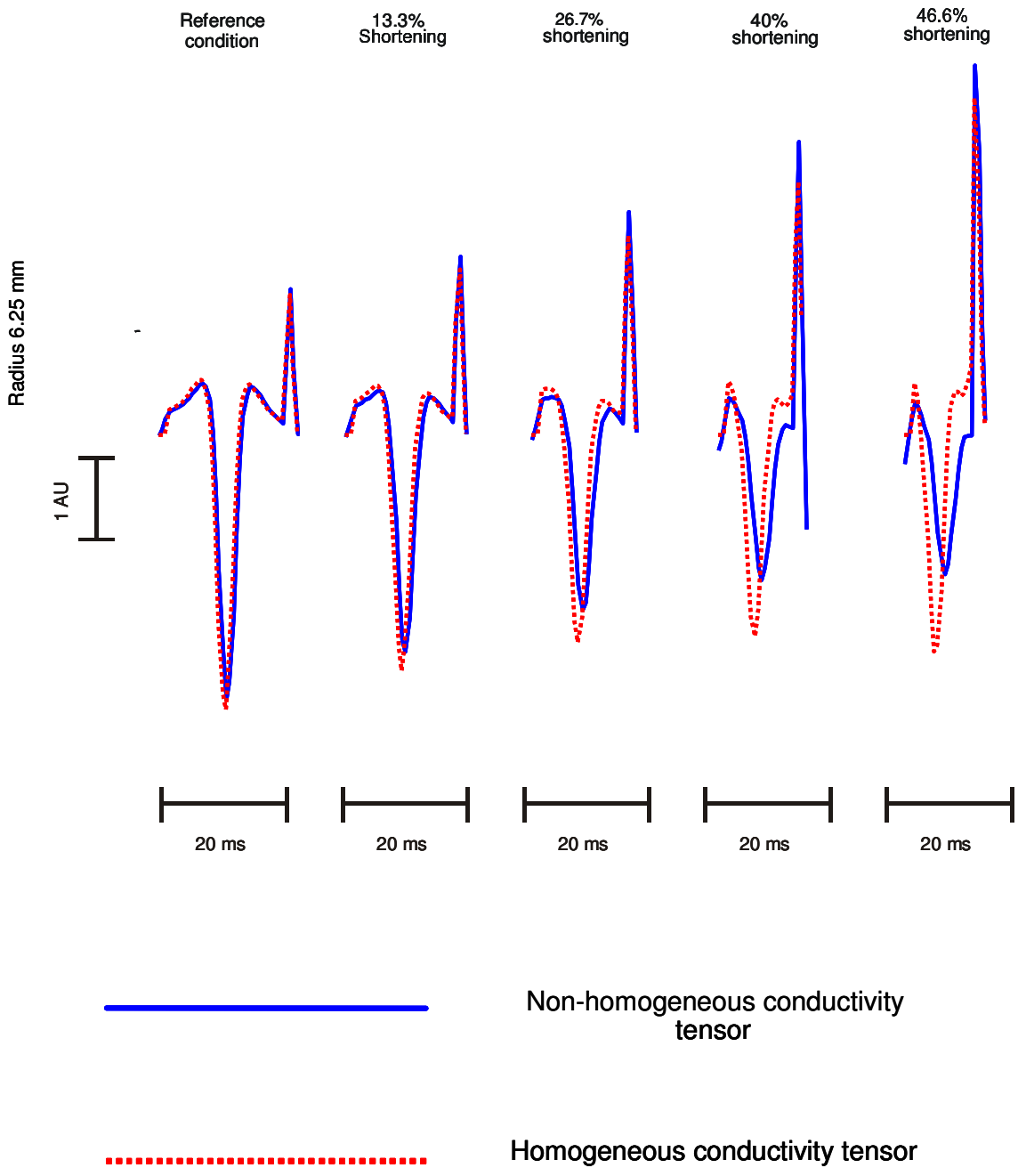

Figure 6.1. Surface potentials simulated using homogeneous and non-homogeneous conductivity tensors respectively. The solid blue line represents the non-homogeneous conductivity tensor and the dashed red line represents the homogenous conductivity tensor. The potentials are simulated for five joint angles using a monopolar electrode configuration. The distance from the fiber to the z-axis is Rt = 6.25 mm.

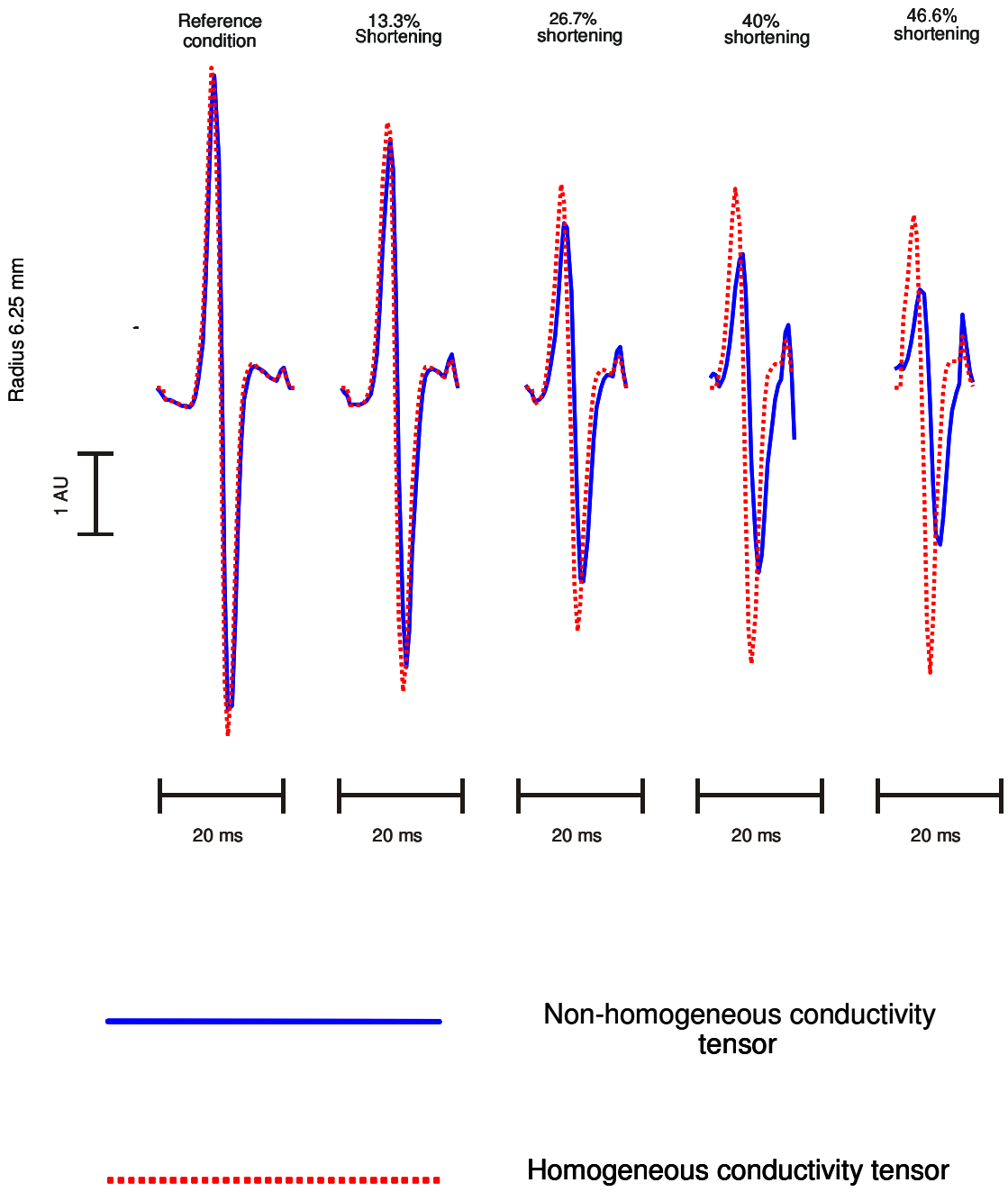

Figure 6.2. Surface potentials simulated using homogeneous and non-homogeneous conductivity tensors respectively. The solid blue line represents the non-homogeneous conductivity tensor and the dashed red line represents the homogenous conductivity tensor. The potentials are simulated for five joint angles using an SD electrode configuration. The distance form the fiber to the z-axis is Rt = 6.25 mm.

6.3. DISCUSSION AND CONCLUSION

For the relaxed muscle condition the potentials obtained from the different simulations are very similar. For this condition the homogeneous conductivity and the conductivity tensor are basically the same. As the joint angle decreases both of the potentials (with regard to the propagating component of the potentials) become smaller although the non-homogeneous potentials seem to reduce more significantly. Note, however, that the non-propagating part of the potentials becomes larger in equal parts for both the homogeneous and non-homogenous simulations. When the joint angle is at its smallest and the muscle is 46.6% contracted, the potentials from the different simulations become very diverse. It also seems as if for the homogeneous condition the potentials at the smallest joint angle have increased.

Since the homogeneous and non-homogeneous simulations are similar for the relaxed muscle condition it can be accepted that the fiber path resembles a rectilinear fiber path and that the conductivity tensor of Equation 3.12 approximates a homogeneous conductivity. As the joint angle decreases, the geometry of the muscle changes. The fiber diameter increases giving rise to an IAP shape change. These geometrical changes are much more noticeable in the simulation for the non-homogeneous conductivity tensor, since the conductivity tensor is calculated to reflect these changes. The changes in potential shape for the homogenous condition are more subdued, since the conductivity remains constant and does not reflect the geometrical changes as much.

Modelling the conductivity tensor of the muscle tissue has been neglected in the literature on sEMG simulation even in the case of sources propagating along a general curvilinear path. The non-constant conductivity tensor introduces an inhomogeneity in the volume conductor in the direction of source propagation, in addition to the inhomogeneity due to geometry. This implies that the surface potentials simulated with the conductivity tensor are affected by variations in the conductive properties of muscle tissue as well as by the relative source-electrode distance, which changes with muscle shortening. The simulation of only a geometrical change in the volume conductor leads to a different effect with respect to the inclusion of variations in both geometry and conductivity tensor (Mesin, Joubert, Hanekom, Merletti & Farina 2006).

The availability of numerical methods for describing complex geometries and conductivty tensors underlines the need of estimating the conductivty properties and geometrical features of the system under study, which may be a critical aspect for EMG simulation (Farina, Mesin & Martina 2004).

7. CONCLUSION

7.1. BRIEF SUMMARY

In this study an FE model for the generation of SFAPs in a muscle undergoing various degrees of fiber shortening is developed. The model includes a precise analytical calculation of a conductivity tensor included at each point in the fusiform muscle. The conductivity of the muscle depends point-by-point on the direction of its fibers. The non-constant conductivity tensor introduces an inhomogeneity in the volume conductor in the direction of source propagation in addition to the inhomogeneity due to changes in the geometry (Mesin, Joubert, Hanekom, Merletti & Farina 2006).

There are very few sEMG models in the literature that simulate changes in muscle geometry. This model was developed to answer some of the questions which arise when the sEMG technique is applied for dynamic contractions. Dynamic conditions coincide with joint angle changes and muscle shortening. In chapter 5 the influence of muscle shortening and changes in the conductivity of the muscle on the amplitude and spectral content of the MUAP are investigated. The MUAP is investigated for simulations done at different angles and for different IEDs. The well-known effect of muscle sliding is also investigated. For joint angle changes the muscle can shift underneath the skin, changing the relative orientation of the muscle fibers with respect to the detection system. This effect adds unwanted signal components to the recorded sEMG signal and is difficult to remove or predict (Kiryu et al. 1988).

In chapter 6 it is shown that the simulation of only a geometrical change in the volume conductor leads to a different effect with respect to the inclusion of variations in both the geometry and the conductivity tensor.

The propagating and non-propgating signals are the two main components contributing to the surface EMG potentials. The propagating part of the signal is generated as the signal source propagates along the muscle fibers. The non-propagating part is generated when the

signal is generated at the IZ and extinguished at the tendon zone. With geometrical changes such as muscle shortening, the tendon and innervation zones move closer to each other and also closer to the detection system. Also, the electrical and geometrical properties of the tissue separating the source and electrodes change. These changes affect the surface-detected potential in a way that is dependent on the detection system.

The representative results on SFAPs and MUAPs presented in this study underline that amplitude and spectral content of the signal may change significantly owing to changes in muscle length, independently of the intensity of muscle activation or the population of active MUs. The specific muscle shape and the way to simulate shortening are not a constraint of the proposed model. By deriving the Cartesian representation of the conductivity tensor, starting from the analytical description of the fiber orientation, the concepts proposed in this study can be applied to generic muscle shapes and fiber orientations. The model is innovative with respect to previous approaches since it provides, for the first time, the description of the muscle conductivity tensor according to the orientation of the muscle fibers during shortening. This model constitutes an important tool for interpreting surface EMG signal features in dynamic tasks (Mesin, Joubert, Hanekom, Merletti & Farina 2006).

7.2. CRITICAL REVIEW

The model developed in this study includes both a conductivity tensor and joint angle changes. These are two effects that have not been simulated together in earlier models. The model was first validated on an SF level and then extended in order to include MUs. In order to validate the model it was compared to other sEMG models in the literature, also by investigating experimental sEMG recordings.

When a muscle shortens as a consequence of joint angle change, geometrical artefacts arise and the MNF and ARV estimators of the sEMG signal are influenced significantly. The ARV of SFAPs may be reduced up to approximately one third of its initial value when muscle length is reduced to approximately 50% and the signals are detected with a bipolar system (Mesin, Joubert, Hanekom, Merletti & Farina 2006). In chapter 4, it was shown that as the muscle shortens the ARV decrease. This was also found by Farina, Merletti, Nazzaro and Caruso (2001), although they reported variable behaviour for different electrode locations. Farina (2006) shows experimental results also describing a decrease in ARV with shortening. The MNF of the simulated signal increases with shortening. This

was also reported by Maslaac, Parker, Scott, Englehart and Duffley (2001) and Schulte, Farina, Merletti, Rau and Disselhorst-Klug (2004). The accepted explanations for these findings are that with muscle shortening the relative electrode-source distance changes. For ARV this means that the source moves away from the electrodes as the muscle shortens, decreasing the amplitude. For MNF the electrodes move away from the source but closer to the IZ and tendon endings, including more high-frequency components in the signal, resulting in an increased MNF.

In chapter 5 the influence of IED and fiber misalignment (signals measured from different angles) on ARV and MNF estimators for MUAPs are investigated. Both ARV and MNF estimators decrease as the electrode detection system is placed at larger angles from the source. This is expected, since the source and the non-propagating components move away from the detection system. For a larger IED less variability was found when calculating the estimators for different joint angles. Larger IED does, however, include more non-propagating components and the IED should be chosen with care. A smaller IED may leave out important signal information. Farina, Cescon and Merletti (2002) also investigated the influence of detection system parameters on sEMG and obtained the same data as reported in chapter 5.

Some exceptions to the above-mentioned results were found. The geometrical artefact of muscle shortening, different fiber depths and different detection systems all had a significant effect on the results. Most of the trends seen are smaller for superficial than for deeper fibers, since the distance of superficial fibers from the electrodes changes less with shortening than that of the deep fibers. Since most of the surface EMG signal power is due to the activity of superficial fibers, the changes in ARV of the interference EMG signal are more limited than those obtained for deep single fibers. The effect on ARV depends on the detection system. While single and double differential systems lead to similar sensitivities to muscle shortening, monopolar recordings are much less sensitive to it. This is due to the relative weight of non-propagating potentials, which is larger for monopolar than for differential recordings. As the muscle shortens, the fibers increase their distance from the detection point but the end-plate and tendon endings approach the electrodes, thus the propagating component decreases and the non-propagating one increases in amplitude, counteracting each other. This effect is less evident for single and double differential systems, since these systems largely reduce the nonpropagating components. As for ARV, the effect of shortening on MNF depends on the depth of the fiber and on the detection

system. The action potentials generated by superficial fibers are less affected by shortening than those from deep fibers, as discussed for ARV (Mesin, Joubert, Hanekom, Merletti & Farina 2006).

The comparison of these results with those obtained in experimental conditions in previous studies is difficult, since in experimental studies the activation strategies of the MUs at different joint angles cannot be controlled. It is also important to note that the non-physiological factors that influence amplitude or frequency content of the surface EMG signal during dynamic contractions affect different subjects differently (Beck et al. 2006). Rainoldi, Nazzaro, Merletti, Farina, Caruso and Gaudenti (2000) reported significant changes in surface EMG amplitude with muscle shortening, depending on the location of the recording electrodes. These changes were probably due to the concomitant effect of the relative shift of the skin with respect to the electrodes. This effect is also shown in chapter 5 and reported by Martin and MacIsaac (2006) and Farina (2006).

Farina (2006) reports that the changes in conductivity properties of the tissue separating electrodes and muscle fibers are one of the paradigms that separate static contractions from dynamic contractions. In Chapter 6 the difference between the inclusion of a conductivity tensor and simulating with static conductivities are shown. Other sEMG models including the conductivity tensor are those of Farina, Mesin and Martina (2004) and Mesin, Farina and Martina (2004). For dynamic contraction the inclusion of a conductivity tensor should be studied extensively, since the conductivity of muscle tissue changes when muscle shortening causes changes in muscle fiber diameter, length and orientation (Farina 2006).

7.3. FURTHER WORK

The model developed in this study makes use of anatomical data in order to model the *biceps brachi* muscle accurately. For this study only the muscle layer was modelled. It would be informative to include some subcutaneous layers as well, for example the fat and skin layers. The influence of subcutaneous layers, such as skin and fat layers, is important , since they perform low pass filtering on the signals. These layers can easily be included in the numerical model.

The detection systems used in the study are the SD, DD and monopolar detection systems. Simulations with NDD and IB^2 could be included in the model. If would be instructive to

see if these filters could better reject the influence of the non-propagating component with muscle shortening.

The model already includes simulations for SFAPs and for MUAPs and it would be useful to simulate the activity of a number of MUs in order to create an interference pattern.

For this study a constant CV was implemented for the source propagation. However, as muscles shorten, the fibers increase in thickness and in practical situations this would also mean an increase in CV. Incorporating CV changes when simulating muscle shortening would give a more accurate picture of the influence of muscle shortening in surface EMG potentials.

However, the proposed model provides a more accurate description of the volume conductor with respect to past approaches when the muscle shortens. In particular, the variation in conductivity tensor owing to the variation in geometry is accounted for in the present approach. It has been shown that the accurate description of the conductivity tensor is relevant for the generation of the surface action potentials. While previous approaches considered only the relative shift of end-plates and tendon endings with fiber shortening (Schulte, Farina, Merletti, Rau & Disselhorst-Klug 2004), this study indicates that there are additional factors that affect the signal properties when the muscle shortens. In particular, it is shown that not only the non-propagating components but also the propagating ones change with shortening (Mesin, Joubert, Hanekom, Merletti & Farina 2006).

8. REFERENCES

Tense about tensors. http://home.pacbell.net/bbowen/tensors.htm. Last accessed in May 2004.

Beck, T. W., Housh, T. J., Johnson, G. O., Cramer, J. T., Weir, J. P., Coburn, J. W. & Malek, M. H. 2006, "Electromyographic instantaneous amplitude and instantaneous mean power frequency patterns across a range of motion during a concentric isokinetic muscle action of the biceps brachii", *Journal of Electromyography and Kinesiology*, vol. 16, pp. 531-539.

Bottinelli, R., Pellegrino, M. A., Canepari, M., Rossi, R. & Reggiani, C. 1999, "Specific contributions of various muscle fibre types to human muscle performance: an in vitro study", *Journal of Electromyography and Kinesiology*, vol. 9, pp. 97-95.

Christensen, H., Sogaard, K., Jensen, B. R., Finsen, L. & Sjogaard, G. 1995, "Intramuscular and surface EMG power spectrum from dynamic and static contractions", *Journal of Electromyography and Kinesiology*, vol. 5, no. 1, pp. 27-36.

Clancy, E. A., Bouchard, S. & Rancourt, D. 2001, "Estimation and application of EMG amplitude during dynamic contractions", *IEEE engineering in medicine and biology* pp. 47-54.

De la Barrera, E. J. & Milner, T. E. 1994, "The effects of skinfold thickness on the selectivity of surface EMG", *Electroencephalography and clinical neurophysiology. Evoked potential section*, vol. 93, no. 2, pp. 91-99.

De Luca, J. C. 2002, *Surface electromyography: Detection and recording*, Delsys Inc.

Devasahayam, S. R. 2000, "Modeling Myoelectric activity," in *Signals and systems in Biomedical Engineering*, pp. 267-289.

Dimitrov, G. V. & Dimitrova, N. A. 1998, "Precise and fast calculation of the motor unit potentials detected by a point and rectangular plate electrode", *Medical Engineering & Physics*, vol. 20, pp. 374-381.

Dimitrova, N. A. & Dimitrov, G. V. 2003, "Interpretation of EMG changes with fatigue: facts, pitfalls, and fallacies", *Journal of Electromyography and Kinesiology*, vol. 13, no. 1, pp. 13-36.

Disselhorst-Klug, C., Silny, J. & Rau, G. 1997, "Improvement of spatial resolution in surface-EMG: A theoretical and experimental comparison of different spatial filters", *IEEE Transactions on Biomedical Engineering*, vol. 44, no. 7, pp. 567-574.

Duchêne, J. & Hogrel, J. 2000, "A model of EMG generation", *IEEE Transactions on Biomedical Engineering*, vol. 47, no. 2, pp. 192-201.

Farina, D. 2006, "Interpretation of the Surface Electromyogram in Dynamic Contractions", *Exercise and sport science reviews*, vol. 34, no. 3, pp. 121-127.

Farina, D., Cescon, C. & Merletti, R. 2002, "Influence of anatomical, physical, and detection-system parameters on surface EMG", *Biological Cybernetics*, vol. 86, pp. 445-456.

Farina, D., Gaudenti, S., Merletti, R. & Nazzaro, M. 2004a, "Surface EMG during dynamic contractions of limb muscles", *Muscles, Ligaments and Tendons*.

Farina, D. & Merletti, R. 2000, "Comparison of algorithms for estimation of EMG variables during voluntary isometric contractions", *Journal of Electromyography and Kinesiology*, vol. 10, no. 5, pp. 337-349.

Farina, D. & Merletti, R. 2001, "A novel approach for precise simulation of the EMG signal detected by surface electrodes", *IEEE Transactions on Biomedical Engineering*, vol. 48, no. 6, pp. 637-646.

Farina, D., Merletti, R. & Fosci, M. 2002, "Motor unit recruitment strategies investigated by surface EMG variables", *Journal of Applied Physiology*, vol. 92, pp. 235-247.

Farina, D., Merletti, R., Indino, B., Nazzaro, M. & Pozzo, M. 2002, "Surface emg crosstalk between knee extensor muscles: Experimental and model results", M*uscle and Nerve*, vol. 26, pp. 681-695.

Farina, D., Merletti, R., Nazzaro, M. & Caruso, I. 2001, "Effect of joint angle on EMG variables in leg and thigh muscle", *IEEE engineering in medicine and biology* pp. 62-71.

Farina, D., Mesin, L. & Martina, S. 2004, "Advances in surface electromyographic signal simulation with analytical and numerical descriptions of the volume conductor", *Medical and Biological Engineering and Computing*, vol. 42, no. 7, pp. 467-476.

Farina, D., Mesin, L., Martina, S. & Merletti, R. 2004b, "A Surface EMG generation model with multilayer cylindrical description of the volume conductor", *IEEE Transactions on Biomedical Engineering*, vol. 51, no. 3, pp. 415-426.

Farina, D., Pozzo, M., Merlo, E., Bottin, A. & Merletti, R. 2004c, "Assessment of average muscle fiber conduction velocity from surface EMG signals during fatiguing dynamic contractions", *IEEE Transactions on Biomedical Engineering*, vol. 51, no. 8, pp. 1383-1393.

Gabriel, C. & Gabriel, S. Compilation of the dielectric properties of body tissues at RF and microwave frequencies.
http://www.brooks.af.mil/AFRL/HED/hedr/reports/dielectric/Report/Report.html.
Last accessed on 5 May 2004.

Garner, B. A. & Pandy, M. G. 2003, "Estimation of musculotendon properties in the human upper limb", *Annals of biomedical engineering*, vol. 31, pp. 207-220.

Griep, P., Gielen, F., Boon, K., Hoogenstraten, L., Pool, C. & Wallinga de Jjonge, W. 1982, "Calculation and registration of the same motor unit action potential", *Electroencephalography and clinical neurophysiology*, vol. 53, pp. 388-404.

Kiryu, T., Suzuki, M., Saitoh, Y. & Ishioka, K. "Analysis of EMG signals during dynamic movements", in *IEEE Engineering in Medicine and Biology society 10th annual international conference*, pp. 1190-1191.

Kuiken, T. A., Stoykov, N. S., Popovic, M., Lowery, M. M. & Taflove, A. 2001, "Finite element modeling of electromagnetic signal propagation in a phantom arm", *IEEE transactions on neural systems and rehabilitation engineering*, vol. 9, no. 4, pp. 346-354.

Lapatki, B. G., Stegeman, D. F. & Jonas, I. E. 2004, "A surface EMG electrode for the simultaneous observation of multiple facial muscles", *Journal of Neuroscience Methods*, vol. 123, pp. 117-128.

Lowery, M. M., Stoykov, N. S., Dewald, J. P. A. & Kuiken, T. A. 2004, "Volume conduction in an anatomically based surface EMG model.", *IEEE Transactions on Biomedical Engineering*, vol. 51, no. 12, pp. 2138-2146.

Lowery, M. M., Stoykov, N. S. & Kuiken, T. A. 2003, "Independance of myoelectric control signals examined using a surface EMG model", *IEEE Transactions on Biomedical Engineering*, vol. 50, no. 6, pp. 789-793.

Lowery, M. M., Stoykov, N. S., Taflove, A. & Kuiken, T. A. 2002, "A multiple-layer finite element model of the surface EMG signal", *IEEE Transactions on Biomedical Engineering*, vol. 49, no. 5, pp. 446-454.

Marieb, E. 1995, *Human Anatomy and Physiology*, 3rd edn, The Benjamin/Cummings Publishing Company, Inc., California.

Martin, S. & MacIsaac, D. 2006, "Innervation zone shift with changes in joint angle in the brachial biceps", *Journal of Electromyography and Kinesiology*, vol. 16, pp. 144-148.

Maslaac, D. T., Parker, P. A., Scott, R. N., Englehart, K. B. & Duffley, C. 2001, "Influence of dynamic factors on myoelectric parameters", *IEEE engineering in medicine and biology* pp. 82-89.

Masuda, K., Masuda, T., Sadoyama, T., Inaki, M. & Katsuta, S. 1999, "Changes in surface EMG parameters during static and dynamic fatiguing contractions", *Journal of Electromyography and Kinesiology*, vol. 9, pp. 39-46.

Mcgill, K. C. & Huynh, A. "A model of the surface-recorded motor-unit action potential", in *IEEE engineering in medicine and biology society 10th annual international conference*, pp. 1697-1699.

Merletti, R. Standards for Reporting EMG Data. III-IV. 2004.
Ref Type: Pamphlet

Merletti, R., Farina, D. & Gazzoni, M. 2002, "The linear electrode array: a useful tool with many applications", *Journal of Electromyography and Kinesiology*, vol. 13, no. 1, pp. 37-47.

Merletti, R., Farina, D., Gazzoni, M. & Schieroni, M. P. 2002, "Effect of age on muscle functions investigated with surface electromyography", M*uscle and Nerve*, vol. 25, pp. 65-76.

Merletti, R., Lo Conte, L., Avignone, E. & Guglielminotti, P. 1999a, "Modeling of Surface Myoelectric Signals - Part 1: Model Implementation", *IEEE Transactions on Biomedical Engineering*, vol. 46, no. 7, pp. 810-820.

Merletti, R. & Lo Conte, L. R. 1997, "Surface EMG signal processing during isometric contractions", *Journal of Electromyography and Kinesiology*, vol. 7, no. 4, pp. 241-250.

Merletti, R. & Parker, P. 1994, *Wiley encyclopedia of electrical and electronics engineering,* John Wiley and sons, Inc., New York.

Merletti, R. & Parker, P. A. 2004, *Electromyography - Physiology, Engineering, and Noninvasive Applications*, 1st edn, John Wiley & Sons, Inc.

Merletti, R., Rainoldi, A. & Farina, D. 2001, "Surface electromyography for noninvasive characterization of muscle", *Exercise and sport science reviews*, vol. 29, no. 1, pp. 20-25.

Merletti, R., Roy, S. H., Kupa, E., Roatta, S. & Granata, A. 1999b, "Modeling of Surface Myoelectric Signals - Part 2: Model-based signal interpretation", *IEEE Transactions on Biomedical Engineering*, vol. 46, no. 7, pp. 821-829.

Mesin, L., Farina, D. & Martina, S. 2004, "Simulation of surface EMG signals generated by muscle tissues with in-homogeneity due to fiber pinnation", *IEEE Transactions on Biomedical Engineering*, vol. 51, no. 1521, p. 1529.

Mesin, L., Joubert, M., Hanekom, T., Merletti, R. & Farina, D. 2006, "A Finite element model for describing the effect of muscle shortening on surface EMG", *IEEE Transactions on Biomedical Engineering*, vol. 53, no. 4, pp. 593-600.

Moritani, T. & Muro, M. 1987, "Motor unit activity and surface electromyogram power spectrum during increasing force of contraction", *European journal of applied physiology and occupational physiology*, vol. 56, pp. 260-265.

Perry, J., Schmidt, E. C. & Antonelli, D. J. 1981, "Surface versus intramuscular electrodes for elecromyography of superficial and deep muscles", *Physical Therapy*, vol. 61, pp. 7-15.

Plonsey, R. & Barr, R. C. 2000, *Bioelectricity - A Quantitative Approach*, 2nd edn, Kluwer Academic/Plenum, New York.

Potvin, J. R. & Bent, L. R. 1997, "A validation of techniques using surface EMG signals from dynamic contractions to quantify muscle fatique during repetitive tasks", *Journal of Electromyography and Kinesiology*, vol. 7, no. 2, pp. 131-139.

Rainoldi, A., Nazzaro, M., Merletti, R., Farina, D., Caruso, I. & Gaudenti, S. 2000, "Geometrical factors in surface EMG of the vastus medialis and lateralis muscles", *Journal of Electromyography and Kinesiology*, vol. 10, no. 5, pp. 327-336.

Rattay, F. 1990, *Electrical Nerve Stimulation - Theory, Experiments and Applications* Springer-Verlag Wien, New York.

Rau, G., Disselhorst-Klug, C. & Silny, J. 1997, "Noninvasive approach to motor unit characterization: muscle structure, membrane dynamics and neuronal control", *Journal of Biomechanics*, vol. 30, no. 5, pp. 441-446.

Rau, G., Schulte, E. & Disselhorst-Klug, C. 2004, "From cell to movement: to what answers does EMG really contribute?", *Journal of Electromyography and Kinesiology* pp. 1-7.

Reucher, H., Silny, J. & Rau, G. 1987, "Spatial Filtering of Noninvasive Multielectrode EMG: Part II - Filter Performance in Theory and Modeling", *IEEE Transactions on Biomedical Engineering*, vol. BME-34, no. 2, pp. 106-113.

Roeleveld, K., Blok, J. H. Stegeman, D. F. & Van Oosterom, A. 1997a, "Volume Conduction Models for Surface EMG; Confrontation with Measurements", *Journal of Electromyography and Kinesiology*, vol. 7, no. 4, pp. 221-232.

Roeleveld, K. & Stegeman, D. F. 2002, "What do we learn from motor unit action potentials in surface myography?", *Muscle and Nerve supplement*, vol. 11, pp. 92-97.

Roeleveld, K., Stegeman, D. F., Vingerhoets, H. M. & Van Oosterom, A. 1997b, "Motor unit potential contribution to surface electromyography", *Acta physiologica scandinavica*, vol. 160, no. 175, p. 183.

Rosenfalck, P. 1969, "Intra and extracellular fields of active nerve and muscle fibers. A physico-mathematical analysis of different models", *Acta physiologica scandinavica*, vol. 321, pp. 1-49.

Roy, S. H., De Luca, C. J. & Schneider, J. 1986, "Effects of electrode location on myoelectric conduction velocity and median frequency estimates", *Journal of Applied Physiology*, vol. 61, no. 4, pp. 1510-1517.

Schneider, J., Silny, J. & Rau, G. 1991, "Influence of tissue inhomogeneities on noninvasive muscle fiber conduction velocity measurements - Investigated by physical and numerical modeling", *IEEE Transactions on Biomedical Engineering*, vol. 38, no. 9, pp. 851-860.

Schulte, E., Dimitrova, N. A., Dimitrov, G. V. Rau, G. & Disselhorst-Klug, C. 2005, "Estimation of the muscle fiber semi-length under varying joint positions on the basis of non-invasively extracted motor unit potentials", *Journal of Electromyography and Kinesiology*, vol. 15, pp. 290-299.

Schulte, E., Farina, D., Merletti, R., Rau, G. & Disselhorst-Klug, C. 2004, "Influence of muscle fibre shortening on estimates of conduction velocity and spectral frequencies from surface electromyographic signals", *Medical and Biological Engineering and computing*, vol. 42, pp. 477-486.

Silvester, P. P. & Ferrari, R. L. 1983, *Finite elements for electrical engineers*, 3rd edn, Cambridge University Press, Cambridge.

Stashuk, D. W. 1999, "Detecting single fiber contributions to motor unit action potentials", *Muscle and Nerve*, vol. 22, pp. 218-229.

Stegeman, D. F., Blok, J. H., Hermens, H. J. & Roeleveld, K. 2000, "Surface EMG models: properties and applications", *Journal of Electromyography and Kinesiology*, vol. 10, pp. 313-326.

Stegeman, D. F., Roeleveld, K., Dumitru, D. & King, J. C. 1997, "Near- and Far-fields: Source characteristics and the conducting medium in neurophysiology", *American clinical neurophysiology society*, vol. 14, no. 5, pp. 429-442.

Viljoen, S. 2005, *Analysis of crosstalk signals in a cylindrical layered volume conductor - Influence of the anatomy, detection system and physical properties of the tissues,* Master of Engineering (Bio-Engineering), University of Pretoria.

Webster, J. G. 1998, *Medical Instrumentation. Application and Design*, 3rd edn, Wiley & Sons, Inc., New York.

Wood, A. M., Jarret, J. A., Barker, A. T. & Brown, B. H. 2001, "Surface electromyography using electrode arrays: a study of motor neuron disease", *muscle and nerve*, vol. 24, no. 2, pp. 223-230.

Zhang, M., Mak, A. F. T. & Roberts, V. C. 1998, "Finite element modelling of a residual lower-limb in a prosthetic socket: a survey of the development in the first decade", *Medical Engineering and Physics*, vol. 20, pp. 360-373.

Zwarts, M. J., Drost, G. & Stegeman, D. F. 2000, "Recent progress in the diagnostic use of surface EMG for neurological diseases", *Journal of Electromyography and Kinesiology*, vol. 10, pp. 287-291.

Zwarts, M. J. & Stegeman, D. F. 2003, "Multichannel surface EMG: Basic aspects and clinical utility", *Muscle and Nerve*, vol. 28, no. 1, pp. 1-17.